CHARAKTERISIERUNG VON KOPF-HALS-TUMOREN MITTELS MALDI-MS IMAGING

Dissertation

zur Erlangung des wissenschaftlichen Grades

Doctor rerum naturalium (Dr. rer. nat)

Vorgelegt dem Rat der Medizinischen Fakultät

der Friedrich-Schiller-Universität Jena

Von Franziska Hoffmann

Geboren am 13.04.1988 **in** Nordhausen

Gutachter:

1. Prof. Dr. Ferdinand von Eggeling, Jena

2. Prof. Dr. Jürgen Popp, Jena

3. Prof. Dr. Timo Gemoll, Lübeck

Tag der öffentlichen Verteidigung: 18.12.2018

Inhalt

1. Abkürzungsverzeichnis

3D	Dreidimensional
CD31	Cluster of Differentiation 31
Da	Dalton
DHB	2,5-Dihydroxybenzoesäure
EGFR	Epidermal growth factor receptor
FFPE	Formalin-fixiert-Paraffin-eingebettet
FT-ICR	Fourier-Tranformation-Ionenzyklotronresonanz-Analysator
H&E	Hämatoxylin-Eosin-Färbung
CHCA	α-Cyanohydroxyzimtsäure
IHC	Immunhistochemie
LC	Liquid Chromatography
m/z	Masse-zu-Ladungsverhältnis
MALDI-MSI	Matrix-assisted laser desorption/ionization - mass spectrometry Imaging
MS	Massenspektrometrie
MS/MS	Tandem-Massenspektrometrie
PGAM1	Phosphoglyceratmutase 1
SA	Sinapinsäure
TOF	Time-of-flight
TORS	TranOral Robotic Surgery

2. Zusammenfassung der Arbeit

Trotz zahlreicher neuer Therapie- und Diagnosemöglichkeiten hat sich in den letzten Jahrzehnten die Gesamtüberlebensrate von Patienten mit Kopf-Hals-Tumoren nicht verbessert. Die detailliertere Aufklärung der molekularen Mechanismen, welche der Tumorentstehung- und Progression zugrunde liegen, kann zu einer Verbesserung beitragen. Eine Methode, welche dafür genutzt werden kann, ist das neue molekulare bildgebende Verfahren MALDI-MS (*matrix-assisted laser desorption/ionization-mass spectrometry*) Imaging. Hierbei können zahlreiche Biomoleküle gleichzeigt und ohne *a priori*-Wissen direkt am Gewebe detektiert und analysiert werden. In Intensitätsmappen kann die räumliche Verteilung der Moleküle dargestellt werden. Durch die anschließende Korrelation mit klassischen (Immun-) histochemischen Methoden können die molekularen Informationen mit den histologischen Eigenschaften kombiniert werden.

Das übergeordnete Ziel der Promotion war es die neue Methode MALDI-MS Imaging für eine umfassende molekulare Charakterisierung von Kopf-Hals-Tumoren zu nutzen. Die Komplexität der Methode machte es notwendig, die Probenvorbereitung, die MALDI-MSI-Messungen sowie die Datenauswertung und –interpretation, für jede die konkrete Fragestellung zu optimieren. Final sollte dieser Ansatz in dem Auffinden neuer potentieller Marker für die Tumorbereiche im Plattenepithelkarzinom genutzt werden. Dafür wurde das bildgebende Verfahren mit bereits in der Klinik etablierten Methoden wie der Immunhistochemie, der Histochemie, der LC-MS/MS und der Elektronenmikroskopie kombiniert.

Die vorliegende Arbeit umfasst im Wesentlichen drei Publikationen, welche sich auf unterschiedliche Weise mit der Fragestellung beschäftigen. Bei Lotz und Hoffmann et al. wurde ein molekulares 3D-Modell eines Oralen Plattenepithelkarzinoms erstellt. Dieses Modell zeigt die Heterogenität des Tumors auf Proteinebene, indem Segmentierungskarten basierend auf spektrale Eigenschaften mit morphologischen Informationen vereint wurden. Dafür wurden die MALDI-MSI-Daten mit H&E- sowie IHC-Färbungen korreliert. Es entstand ein interaktives Werkzeug, welches frei drehbar ist und virtuelles Schneiden erlaubt und somit neue Einblicke in die Tumorgröße,- form und –begrenzung gibt.

Neben der Proteinanalyse wurde bei Krasny et al. (Kapitel 5.2) das Tumorlipidom untersucht. Dafür wurde ein MALDI-FT-ICR-System genutzt, welches eine hohe Massenauflösung und -genauigkeit ermöglicht. Es konnte gezeigt werden, dass sich

auch auf der metabolischen Ebene die Tumorheterogenität wiederspiegelt. Insbesondere der Anteil an Phosphatidylcholinen war in den epithelialen Tumorbereichen erhöht.

In der letzten Publikation (Kapitel 5.3/Hoffmann et al.) wurde ein Protokoll etabliert, in welchem erstmalig FFPE-Gewebe von Oralen Plattenepithelkarzinomen für die Proteomanalyse mittels MALDI-MSI genutzt wurde. In Kombination mit LC-MS/MS konnten neue potentielle Marker, welche für die Tumorregion charakteristisch sind, identifiziert werden und gleichzeitig mit bereits genutzten Markern visualisiert werden.

In ihrer Gesamtheit konnte die vorliegende Arbeit dazu beitragen, MALDI-MS Imaging im Bereich der Tumorforschung weiter zu etablieren und neue Erkenntnisse zu den molekularen Eigenschaften von Kopf-Hals-Tumoren zu gewinnen.

3. Einleitung

In den letzten Jahren konnten neuste Fortschritte auf dem Gebiet der Massenspektrometrie dazu beitragen Methoden mit Hilfe derer eine markierungsfreie und gleichzeitige Detektion von Molekülen im Gewebeverband möglich ist, zu entwickeln. An jedem Messpunkt werden Massenspektren generiert, welche in Intensitätsmappen die Verteilung der Moleküle visualisiert. Je nach Fragestellung können somit kleine Moleküle, Lipide, Proteine oder Peptide unter Beibehaltung ihrer Lokalisation auch in komplexen Gewebsstrukturen untersucht werden. Diese Eigenschaften bieten insbesondere für die translationale Tumorforschung neue Möglichkeiten für den Weg zur personalisierten Medizin. Speziell bei Tumoren aus dem Kopf-Hals-Bereich besteht eine große Notwendigkeit die noch wenig aufgeklärten molekularen Mechanismen, welche der Pathogenese zu Grund liegen, weiter aufzuklären.

3.1 Klinische Aspekte von Kopf-Hals-Tumoren

Als Kopf-Hals-Tumore werden Malignome aus dem Bereich der Mundhöhle, des Rachens sowie des Kehlkopfes bezeichnet. Dabei handelt sich zu 90% um Plattenepithelkarzinome. Die jährliche Inzidenz beträgt 600.000 Fälle weltweit und die Mortalität liegt bei 40-50 % (Ferlay et al. 2015).

Die Standardbehandlung ist die operative Entfernung des Tumors mit postoperativer Radio-Chemotherapie (Grégoire et al. 2010). In den letzten Jahren gab es trotz neuer Operationstechniken wie *TransOral Robotic Surgery* (TORS) (Friedrich et al. 2017) und neuer Therapiemöglichkeiten wie dem Verabreichen von *epidermal growth factor receptor* (EGFR)-spezifischer Antikörper (Bonner et al. 2006) oder von Immuncheckpointinhibitoren (Moskovitz et al. 2018) keine signifikanten Verbesserungen hinsichtlich der Gesamtüberlebensraten (Braakhuis et al. 2014). Daraus ergeben sich zahlreiche klinische Herausforderungen.

Eine Herausforderung ist die komplette Entfernung des Tumorgewebes (R0-Resektion). In 7,5% bis 10% der Fälle erfolgt eine R1-Resektion, wobei 50% eine anschließende Re-Operation und/oder Radiotherapie benötigen (Weijers et al. 2002). Die übrigen 50% sind unerkannte R1-Resektionen, von denen 75% ein Rezidiv innerhalb der folgenden 2 Jahre entwickeln.

Eine weitere Herausforderung ist die Personalisierung der Therapie. Um dies zu gewährleisten ist die Aufklärung der molekularen Mechanismen, welche in die Tumorentstehung und Progression involviert sind, notwendig. Auf dieser Basis ist das Etablieren von Biomarkern, die eine Prognose des Therapieansprechens gestatten, möglich. Hierbei stellt insbesondere die Heterogenität des Tumorgewebes ein Problem dar.

Um den oben genannten Problemen nachzukommen, müssen die bisher genutzten Methoden mit neuen technischen Entwicklungen erweitert werden. Eine dieser Methoden ist MALDI-Imaging, welche in dieser Arbeit zur molekularen Charakterisierung von Kopf-Hals-Tumoren genutzt wurde. In dem folgenden Kapitel 3.2 wird das Prinzip von MALDI-Imaging genauer erläutert.

3.2 MALDI-MS Imaging

Matrix-assisted Laser Desorption/Ionisation (MALDI)-Imaging gehört zu den neuen molekularen bildgebenden Verfahren, welches erstmalig 1997 vorgestellt wurde (Caprioli et al. 1997). Es erlaubt die markierungsfreie und gleichzeitige Detektion zahlreicher Moleküle in-vitro, wobei ihr histologischer Kontext erhalten bleibt. Somit kann die räumliche Verteilung von kleinen Molekülen, Lipiden, Proteinen, Peptiden, Kohlenhydraten und DNA-Segmenten direkt am Gewebeschnitt analysiert und visualisiert werden.

3.2.1 Das Prinzip von MALDI-MS Imaging

Der schematische Ablauf eines MALDI-MS Imaging-Experiments ist in Abbildung 1 dargestellt. In Vorbereitung auf die MALDI-MS Imaging Messung wird der Gewebeschnitt mit einer homogenen Matrix-Schicht bedeckt. Die Matrix bildet Kokristalle mit den in der Probe vorhandenen Analyten aus.

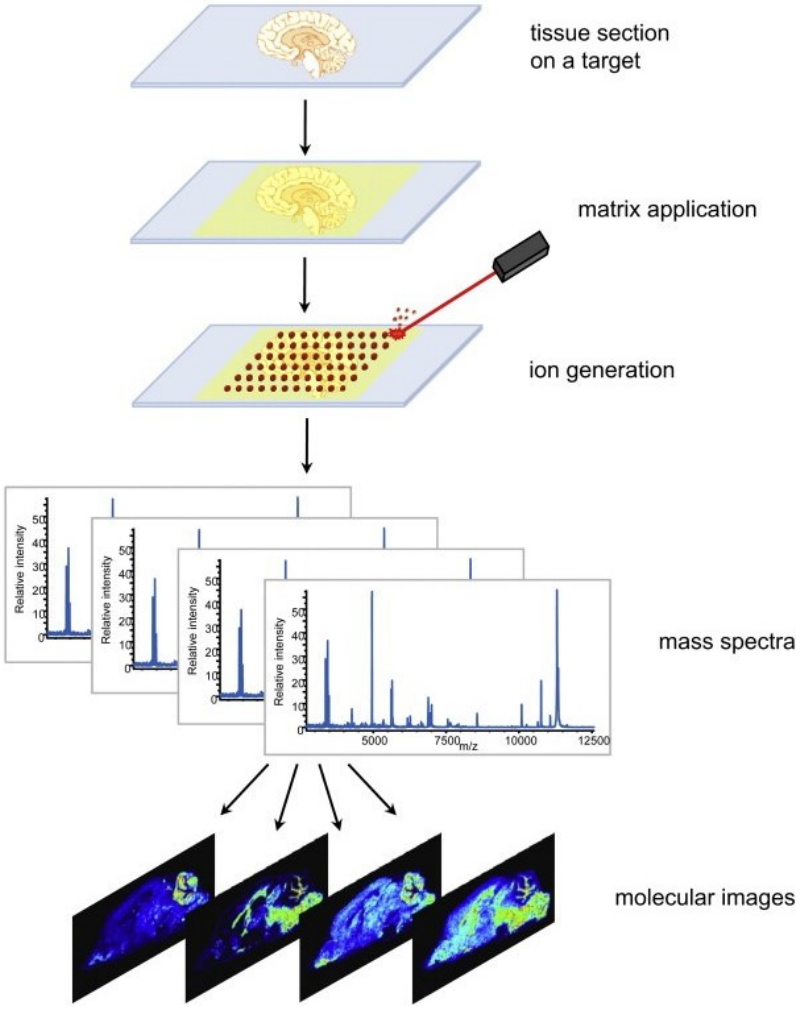

Abbildung 1: Schematische Darstellung eines MALDI-Imaging-Experiments (Schwamborn und Caprioli 2010).

Als Bestandteile der Matrix werden Stoffe genutzt welche die Energie der entsprechenden Wellenlänge des später eingesetzten Lasers absorbieren. Standardmäßig sind dies organische Substanzen wie α-Cyanohydroxyzimtsäure (CHCA), Sinapinsäure (SA) oder 2,5-Dihydroxybenzoesäure (DHB). Zusätzlich wird die Wahl der Matrix durch die Analyten bestimmt, welche detektiert werden sollen. Für die massenspektrometrische Messung wird der Gewebeschnitt mit einem Laserstrahl pixelweise beschossen. Dadurch werden an jeder x,y-Koordinate

Massenspektren generiert. Durch den Laserbeschuss kommt es zur Desorption und zur Ionisation der Matrix-Analyt-Kokristalle.

Anschließend durchqueren die Ionen den Massenanalysator in dem sie getrennt werden. Abschließend erreichen sie den Detektor, wobei die Signale in Spektren umgewandelt werden. In diesen werden die Signalintensitäten gegen die Masse-zu-Ladungsverhältnisse (*m/z*) dargestellt.

Es gibt verschiedene Typen von Analysatoren, welche sich hinsichtlich des physikalischen Prinzips der Trennung unterscheiden. Im Folgenden werden kurz die zwei Typen vorgestellt, welche in den Publikationen genutzt wurden: der Flugzeitanalysator (*time of flight*; TOF; Abb. 2a) und der Fourier-Transform-Ionenzyklotronresonanz-Analysator (FT-ICR; Abb. 2b). Beim TOF-Analysator werden die Ionen nach ihrer Flugzeit getrennt, welche von dem *m/z* abhängt. Leichtere Ionen erreichen den Detektor früher als schwerere. Beim FT-ICR-Analysator werden die Ionen zunächst in einem Magnetfeld eingefangen. Dort werden sie durch die Lorentz-Kraft in eine Kreisbahn gezwungen, deren Frequenz vom *m/z* abhängt. In Kombination mit einem elektrischen Wechselfeld nimmt der Radius der Kreisbahn spiralförmig zu. Leichtere Ionen erreichen denselben Radius wie schwere Ionen nach weniger Zyklen. Detektiert werden dann die Veränderungen der Zyklonenradien. Durch die Anwendung der Fourier-Transformation werden die zeitabhängigen Signale in frequenzabhängige Daten umgewandelt, wodurch eine zusätzliche Steigerung der Frequenzauflösung erreicht wird.

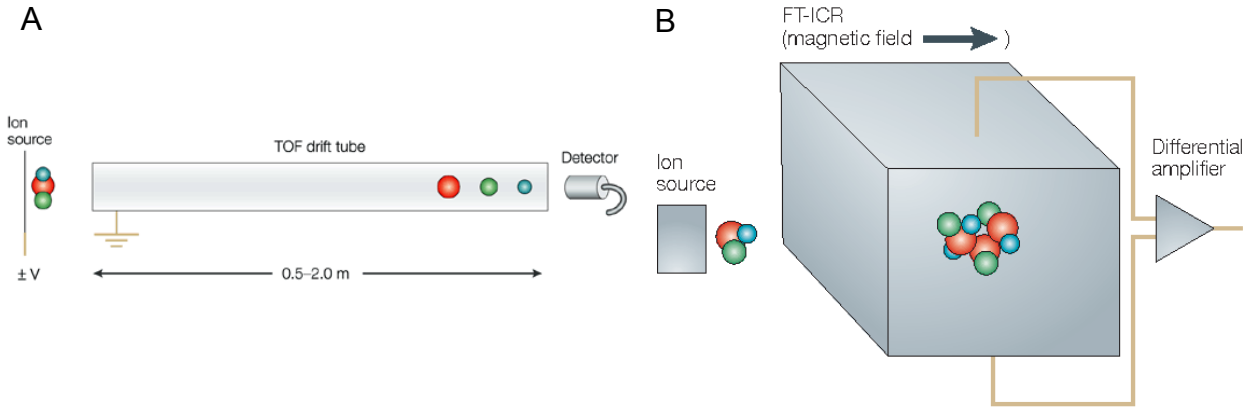

Abbildung 2: Schematische Darstellung der für die Publikationen genutzten Analysatoren. A) TOF-Analysator, B) FT-ICR-Analysator (Glish und Vachet 2003).

Der Vorteil von TOF-Analysatoren ist zum einen ein breiter Massenbereich, welcher analysiert werden kann, so dass sowohl Proteine als auch Peptide detektiert werden können. Zudem ist es eine schnelle und sehr sensitive Methode. Allerdings ist die

Massengenauigkeit nicht hoch genug um eine direkte Identifikation zu ermöglichen, wodurch weitere Methoden wie die LC-MS/MS eingesetzt werden. Die Massenauflösung welche bei FT-ICR-Geräten erreicht wird ist hingegen so hoch, dass hier eine direkte Identifizierung der detektierten Massen möglich ist. Jedoch dauern die Messungen länger als mit dem TOF-Analysator. (Trim und Snel 2016)
Entscheidend für die räumliche Auflösung ist die Größe des Laserfokus. Je nach Fragestellung werden standardmäßig 50 bis 200 µm eingesetzt. Die Pixelgröße wird durch den Abstand bestimmt, welche die Probe zwischen zwei Laserschusseinheiten zurücklegt. Dabei ist die Schrittgröße nicht kleiner als der Laserstrahldurchmesser, um ein Überlappen der Messpunkte zu vermeiden.

3.2.2 Daten- und Bildauswertung

Jede x,y-Koordinate des Messareals wird durch ein MALDI-Spektrum charakterisiert. Durch das Plotten dieser Signale gegenüber ihrer Position im Gewebeschnitt können Bilder generiert werden. Da während der Messungen die Gewebeschnitte intakt bleiben, können nach Entfernung der Matrix die Schnitte für (immun-)histochemische Färbungen genutzt werden. Somit ist direkte Korrelation der spektralen Daten mit histologischen und/oder pathologischen Merkmalen möglich.
Es gibt verschiedene Möglichkeiten die räumliche Verteilung der Moleküle im Gewebe zu visualisieren. Eine Variante ist die Darstellung eines einzelnen Moleküls. Hierbei werden die Intensitäten eines distinkten *m/z*-Wertes in Falschfarben gezeigt. Dies kann für jeden beliebigen *m/z*-Wert der aufgenommen Spektren durchgeführt werden, wobei der *m/z*-Wert einem Molekül entspricht. Zusätzlich sind statistische Auswertungen der komplexen Datensätze möglich. Dabei können grundlegend zwei Ansätze unterschieden werden: zum einen die überwachte Methode, bei der mindestens zwei bereits bekannte und somit vorgegebene Regionen analysiert und verglichen werden. Dies wird beispielsweise genutzt um Peaks zu finden, welche in einer bestimmten Region hohe Intensitäten aufweisen und in der anderen Region nicht.
Zum anderen können unüberwachte Methoden angewandt werden. Dies sind zum Beispiel die Segmentierung und die Probabilistische latente semantische Analyse (pLSA), welche auch in den Publikationen verwendet wurden. Dabei wird lediglich die zu analysierende Region festgelegt, innerhalb derer die Spektraldaten analysiert

werden sollen. Die Algorithmen suchen nach Unterschieden und Gemeinsamkeiten in den spektralen Informationen. Das Ergebnis ist eine Einfärbung der Spots entsprechend der Zugehörigkeit nach einer der gefundenen Datenklassen.
Weiterhin können durch die Einführung einer virtuellen z-Ebene und *volume rendering* die zweidimensional aufgenommen Datensätze zu einem 3D-Datensatz erweitert werden.
Für die Daten- und Bildanalyse in den Publikationen wurden die kommerziell verfügbare Softwares SCiLS Lab und flexImaging genutzt.

3.3 MALDI-Imaging als Werkzeug in der Tumorforschung

Wie in 3.2 erwähnt, kann mittels MALDI-Imaging jedes Molekül, welches desorbiert und ionisiert wurde, in seinem histologischen Kontext dargestellt werden. Dieses Molekül muss im Vorfeld nicht bekannt sein. Zusätzlich können zahlreiche Moleküle gleichzeitig innerhalb einer Messung detektiert werden. Dies sind die bedeutenden Vorteile gegenüber den klassischen histopathologischen Methoden. So ist es für die immunhistochemische Färbung notwendig, das Zielprotein zu kennen und einen geeigneten Antikörper zu haben. Weiterhin können nur zwei bis drei Antikörper gleichzeitig an demselben Gewebeschnitt genutzt werden.
Diese Limitierungen sind mit MALDI-Imaging nicht vorhanden, so dass es ein geeignetes Werkzeug sowohl für die Tumorforschung als auch für die klinische Anwendung darstellt. Dies konnte durch zahlreiche Publikationen bereits gezeigt werden, was durch (Kriegsmann et al. 2015) umfassend dargestellt wird.
Zum einen kann MALDI-Imaging für die Entdeckung neuer Biomarker eingesetzt werden. Hierbei ist es auf Grund der gleichzeitigen Detektion mehrerer Proteine oder Peptide möglich, komplette molekulare Signaturen zu erhalten, welche auch bereits etablierte Biomarker mit einschließen können. Dies eröffnet die Möglichkeit eines detaillierteren Verständnisses der Entstehung und Progression von Tumoren. Insbesondere für die Untersuchung der molekularen Tumorheterogenität ist MALDI-Imaging geeignet (Alberts et al. 2018).
Ebenso kann MALDI-Imaging für diagnostische Studien genutzt werden, in denen diverse Gewebetypen, bspw. Tumor und Nicht-Tumor, oder prekanzeröse Stadien unterschieden werden. Darüber hinaus wurde MALDI-Imaging bereits für prognostische Studien eingesetzt, bei denen Protein-Signaturen mit Überlebensraten

korreliert werden konnten. Ein anderes Anwendungsgebiet ist die Voraussage von Therapieansprechen bzw. möglichen Resistenzen gegenüber Chemotherapeutika (Bauer et al. 2010).
Dies zeigt, dass MALDI-Imaging in Kombination mit den bereits etablierten Diagnose- und Therapietechniken zukünftig Pathologen und Kliniker zur Verfügung stehen kann. Demnach stellt es einen weiteren Schritt in Richtung personalisierter Medizin dar.

3.4 übergeordnete wissenschaftliche Fragestellung

Die übergeordnete Fragestellung aller im Rahmen der Promotion veröffentlichten Publikationen hatte die Aufklärung der komplexen molekularen Tumorstruktur humaner Plattenepithelkarzinome aus dem Kopf-Hals-Bereich im Fokus. Dabei sollte insbesondere die Anwendung und die damit verbundene Etablierung von MALDI-Imaging für die Tumorforschung vorangebracht werden.
Somit reiht sich die vorliegende Arbeit in die Forschungsprojekte der Arbeitsgruppe MALDI-Imaging von Prof. Dr. Ferdinand von Eggeling ein, welche sich mit der Identifizierung von proteomischen Biomarkern und der Charakterisierung von humanem Tumorgewebe mittels verschiedener massenspektrometrischer Verfahren beschäftigen. Diese Arbeit baut auf den bisherigen Publikationen der Arbeitsgruppe, in denen MALDI-Imaging zur Untersuchung der Tumorheterogenität in neuroendokrinen Tumoren, Larynxkarzinomen und pleomorphen Adenomen genutzt wurde, auf (Ernst et al. 2015, Alexandrov et al. 2013).

4. Zielstellung der Arbeit

Ziel dieser Arbeit war es das neue molekulare bildgebende Verfahren MALDI-Imaging für die umfassende molekulare Charakterisierung von Kopf-Hals-Tumoren zu nutzen. Dabei sollte gezeigt werden, dass dies auf verschiedenen Ebenen möglich ist, welche sowohl das Lipidom als auch das Proteom umfassen sowie Kryo- und FFPE-Gewebe einschließen. Letztendlich sollte dieses Verfahren in dem Auffinden von neuen Markern, welche charakteristisch für das Tumorgewebe sind, resultieren und somit die Tumorforschung entscheidend unterstützen.

Dafür stand zunächst die Methodenetablierung und –optimierung im Vordergrund. Darüber hinaus war die Korrelation mit anderen Methoden wie der (Immun-) Histochemie und LC-MS/MS Bestandteil der Arbeit.

I) Ein erster Teilaspekt bestand in der Etablierung von MALDI FT-ICR Imaging für das Untersuchen des Tumor-Lipidoms. Es sollte erstmalig gezeigt werden, dass die räumliche Segmentierung von molekularen Daten auch im Bereich höchster Massenauflösung angewandt werden kann und somit zur Aufklärung der funktionalen Lipidorganisation im Tumor beitragen kann.

II) Ein weiteres Teilziel der Arbeit war die molekulare 3D-Darstellung eines Kopf-Hals-Tumors, welcher aus den 2D-Messungen rekonstruiert wurde. Weiterhin sollten diese Daten in den histologischen Kontext in Form von hochauflösenden Scans der bereits für die MALDI-MS Imaging-Messungen genutzten und anschließend H&E gefärbten sowie konsekutiven IHC-gefärbten (anti-CD31) Gewebeschnitten eingebunden werden. Hierbei war insbesondere die Standardisierung der Probenbearbeitung und Messung von Interesse. Zudem sollten Methoden entwickelt werden, welche die Erstellung und Bearbeitung solcher komplexen multimodalen Datensätze ermöglichen. Das konkrete Ziel war hier, ein effektives und interaktives Werkzeug für die diagnostische Tumorforschung zu entwickeln.

III) Schließlich sollte MALDI-Imaging eingesetzt werden, um proteomische Marker zu finden, welche die Tumorheterogenität charakterisieren. Dies sollte die erste Studie sein, welche dies an FFPE-Gewebe durchführt, um zusätzlich das Potential der in großen pathologischen Archiven vorhandenen FFPE-Gewebe auch für MALDI-Imaging zu nutzen.

Als wissenschaftliche Kooperationen sind insbesondere das Fraunhofer-Institut für Bildgestützte Medizin sowie die Firma SCiLS GmbH für die Datenverarbeitung zu nennen. Für die Identifizierung mittels LC-MS/MS fand eine Kooperation mit dem

Leibniz-Institut für Naturforschung statt. Die Standardisierung der Aufbereitung von FFPE-Gewebe für MALDI-Imaging wird gemeinsam mit der Firma SunChrom im Rahmen eines AIF-Projektes bearbeitet.

5. Publikationen

5.1 **Integration of 3D multimodal imaging data of a head and neck cancer and advanced feature recognition**

Lotz, J. M. and Hoffmann F, Lotz J, Heldmann S, Trede D, Oetjen J, Becker M, Ernst G, Maas P, Alexandrov T, Guntinas-Lichius O, Thiele H, von Eggeling F, Biochim Biophys Acta., 1856(7): 946-956, 2016.

Biochimica et Biophysica Acta 1865 (2017) 946–956

Contents lists available at ScienceDirect

Biochimica et Biophysica Acta

journal homepage: www.elsevier.com/locate/bbapap

Integration of 3D multimodal imaging data of a head and neck cancer and advanced feature recognition☆

Judith M. Lotz [e,1], Franziska Hoffmann [a,b,1], Johannes Lotz [e], Stefan Heldmann [e], Dennis Trede [g], Janina Oetjen [h], Michael Becker [i], Günther Ernst [a,b,2], Peter Maas [f], Theodore Alexandrov [g,h,j], Orlando Guntinas-Lichius [b], Herbert Thiele [e,3], Ferdinand von Eggeling [a,b,c,d,*,3]

[a] Institute of Physical Chemistry, Friedrich Schiller University, Jena, Germany
[b] ENT Department, University Hospital Jena, Germany
[c] Leibniz Institute of Photonic Technology (IPHT), Jena, Germany
[d] Jena Center for Soft Matter (JCSM), Friedrich Schiller University Jena, Jena, Germany
[e] Fraunhofer Institute for Image Computing MEVIS, Lübeck, Germany
[f] Center for Industrial Mathematics, University of Bremen, Bremen, Germany
[g] SCiLS GmbH, Bremen, Germany
[h] MALDI Imaging Lab, University of Bremen, Bremen, Germany
[i] Bruker Daltonik, Bremen, Germany
[j] European Molecular Biology Laboratory, Heidelberg, Germany

ARTICLE INFO

Article history:
Received 5 April 2016
Received in revised form 3 August 2016
Accepted 27 August 2016
Available online 1 September 2016

Keywords:
MALDI imaging
3D
Head and Neck Cancer
OSCC
immunohistochemistry
multimodality
image registration

ABSTRACT

In the last years, matrix-assisted laser desorption/ionization mass spectrometry imaging (MALDI MSI) became an imaging technique which has the potential to characterize complex tumor tissue. The combination with other modalities and with standard histology techniques was achieved by the use of image registration methods and enhances analysis possibilities.
We analyzed an oral squamous cell carcinoma with up to 162 consecutive sections with MALDI MSI, hematoxylin and eosin (H&E) staining and immunohistochemistry (IHC) against CD31.
Spatial segmentation maps of the MALDI MSI data were generated by similarity-based clustering of spectra. Next, the maps were overlaid with the H&E microscopy images and the results were interpreted by an experienced pathologist. Image registration was used to fuse both modalities and to build a three-dimensional (3D) model. To visualize structures below resolution of MALDI MSI, IHC was carried out for CD31 and results were embedded additionally.
The integration of 3D MALDI MSI data with H&E and IHC images allows a correlation between histological and molecular information leading to a better understanding of the functional heterogeneity of tumors.
This article is part of a Special Issue entitled: MALDI Imaging, edited by Dr. Corinna Henkel and Prof. Peter Hoffmann.

1. Introduction

For several decades, conventional histological staining and immunohistochemistry (IHC) have been the main tools to visualize and understand tissue morphology. In a clinical setting, histological changes are graded according to commonly accepted guidelines. In most cases, these guidelines represent the main method for the assessment of tumors or tumor-suspicious tissue regions and are the basis of diagnostically or therapeutically relevant decisions. However, IHC is a targeted method and a specific antibody is required for each protein. Multiplexing capabilities are, however, limited to not more than two or three proteins simultaneously. Therefore, it does not provide a

☆ This article is part of a Special Issue entitled: MALDI Imaging, edited by Dr. Corinna Henkel and Prof. Peter Hoffmann.

* Corresponding author at: Institut für Physikalische Chemie, FSU Jena, Klinik für Hals-, Nasen- und Ohrenheilkunde, UKJ, Leibniz-Institut für Photonische Technologien (IPHT), Stoystrasse 3, 07743 Jena, Germany.
E-mail addresses: F.v.Eggeling@uni-jena.de, feggeling@med.uni-jena.de (F. von Eggeling).

[1] JL and FH contributed equally.
[2] GE experienced pathologist.
[3] HT and FvE contributed equally.

http://dx.doi.org/10.1016/j.bbapap.2016.08.018
1570-9639/

global proteomic view of the tissue nor is it suited for the discovery of new biomarkers.

Molecular genomic- and proteomic-based attempts to refine or facilitate these histopathological analyses have been successful only to a minor degree [1]. Large-scale differential studies, both on the transcript and protein level, are generally prone to oversimplification as the complex morphology of tissue biopsies is not accounted for. As a consequence, the generated expression profiles typically represent an average across multiple morphological features and cell types. This limitation can be partially overcome by laser-based tissue microdissection as it allows a more precise sample preparation for further molecular analysis [2]. However, tissue microdissection is a time consuming technique and highly sensitive downstream analyses are needed [2–4], due to the limited number of samples.

Mass spectrometry-based imaging techniques capable of elucidating molecular profiles directly from tissue are becoming increasingly popular. Matrix-assisted laser desorption/ionization (MALDI) mass spectrometry imaging (MSI), MALDI imaging in short, is at the moment the most popular MS-based technique for proteomic application, and allows to obtain proteomic profiles and identification of markers directly from thin tissue sections [5,6]. MALDI imaging is a label-free technique and can visualize the distribution of hundreds of molecular compounds in a single, pixel wise measurement while maintaining the morphological and molecular integrity of the tissue and therefore allowing a subsequent histological staining of the same tissue section [7,8].

We and others have used MALDI imaging for the pathological analysis of various tissue types [9–12]. A typical MALDI imaging data set includes several thousand individual mass spectra (depending on the analyzed sample size and the resolution), with several thousand intensity values each (depending on the mass resolution of the instrument). Although the superimposition of individual m/z-images with microscopic images can provide valuable insight it cannot be performed manually for a large MALDI imaging data set. Especially, if multiple measurements are involved in 2D or a three-dimensional (3D) model is analyzed. Moreover, this common approach of selecting m/z-values of interest can result in overlooking a compound present only at a small portion of data points. To overcome this, one of the computational methods proposed for MALDI imaging data mining is the spatial segmentation. The individual spectra of a data set are grouped (e.g. by a clustering method) according to their spectral similarity and groups of similar spectra are highlighted on the tissue in a common color [11,13]. However, MALDI imaging data exhibits strong pixel-to-pixel variation which complicates both visual examination and computational analysis. We have recently proposed a computational method significantly reducing the pixel-to-pixel variation leading to clear, noiseless, and smooth segmentation maps revealing a complex and detailed histological structure [13,14] with a proof-of-principle application in histology. Later, we proposed improved peak picking for MALDI imaging data which leads to more sensitive results [14]. Whereas the first publication [13] was the proof-of-principle application of segmentation to MALDI imaging data with only limited histological insight (tumor tissue was discriminated from non-tumor), in a subsequent study we were able to show the potential of the segmentation approach in histological evaluation [10,15]. The acquired segmentation maps are a result of the correlation of proteomic images and detailed tissue topology that is important for new diagnostic strategies and for the biological understanding of tumors.

To analyze several consecutive tissue sections at a time we generated a 3D MALDI imaging and a 3D high resolution histological image model respectively [16,17]. The simultaneous analysis should give us a more complex insight into cancer tissue. For building up 3D models from consecutive sections, image registration techniques are needed. Registration of serial sections is not new and various methods already exist, see e.g. [18–22]. The goal of image registration is to establish spatial correspondence between neighboring sections by dealing with several local and global distortions because the sectioning process introduces for example local cracks, tissue folding, or missing parts in slices.

In general, our image registration techniques compute a deformation that maps one image to a second and aim to make them similar. The deformation can either be a global rigid (or affine) transformation which includes translation and rotation (or additionally scaling and shearing) of the image or a nonlinear deformation which also allows local deformations. Rigid and affine registration can be considered as well-established technologies which are already used in state-of-the-art medical imaging software. This, however, is not the case for nonlinear registration of microscopic images. In this case we deal with severe computational challenges, nonlinear registration can produce complex local deformations and validation of results is difficult [18,23–27].

In the present study we have to deal with several nonlinear registration tasks (see Fig. 1) First, we need to perform a monomodal registration aligning neighboring sections which are unstained and scanned with a low resolution. Those images used to create the 3D MALDI data set are acquired prior to MALDI imaging. The second task is the 3D reconstruction of the now differently stained and with high resolution digitized slide images by multimodal nonlinear registration. The third task is to fuse or co-register the 3D MALDI imaging data with the reconstructed 3D data set from the high resolution histological images. In our setting, images have sizes in the range of gigabytes that require special numerical solutions. Although these problems have already been addressed in the past, no off-the-shelf solutions are available and developed methods are tailored to a particular data set. This is also reflected in the fact that digital pathology is a quite new and quickly emerging field. The current situation in digital pathology can be compared to the time when radiology became digital with emerging computational power 20 years ago. However, with this study we aim to develop methods that can handle multimodal series of large 2D images as 3D data sets. Our goal is not only to support and enable diagnostics for cancer research but to create a general technology and tools that are suitable for the efficient and interactive handling of such data. The integration of image data with a non-targeted approach like MALDI imaging is the next logical step to receive new molecular insight in cancer and explains the innovative nature of this method.

2. Materials and methods

2.1. Sample preparation and MALDI imaging

A tissue sample from a 68 years old male patient with a primary oral squamous cell carcinoma (OSCC; pharynx carcinoma) was obtained from the Department of Otorhinolaryngology of the Jena University Hospital. All necessary approval was obtained from the local Ethics Committee, approval No.3008–12/10. The tissue sample was cut in 162 cryo-sections with a thickness of 12 μm. 65 samples could be used for MALDI MSI and subsequent H&E staining, 21 for IHC (see below). The sections were mounted on indium-tin-oxide coated conductive glass slides (Bruker Daltonics) and stored at −80 °C until use. After drying under vacuum for 15 min, the slides were washed two times for 2 min each in 70% ethanol and thereafter for 2 more minutes in 99% ethanol. We applied sinapinic acid as a matrix using the Bruker ImagePrep™. MALDI MSI was performed on an Autoflex speed™ mass spectrometer (Bruker Daltonics) in linear positive mode. Spectra were acquired in a mass range of 2000–20,000 m/z with a deflection set to 1500 m/z. Each spectrum is a sum of 200 laser shots and the random walk option was set to 25 shots per position. A medium size laser diameter was selected for the chosen lateral resolution of 60 μm. In total, the data set comprises of 828,558 spectra with 7680 data points per spectrum. The complete data set has been published recently [28]. The spectra were preprocessed during acquisition by application of Gaussian spectral smoothing with a width of 2 within 4 cycles as well as baseline reduction with the Top Hat algorithm.

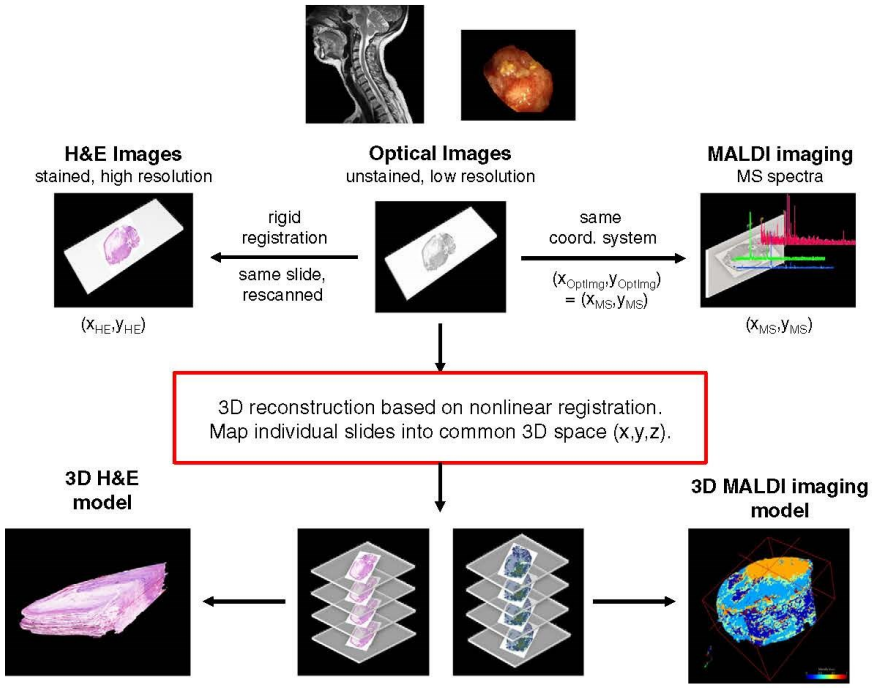

Fig. 1. On each cryo-section MALDI-TOF MSI measurement was performed followed by H&E staining. Different modalities produce 2D data coordinates ($x_{H\&E}$,$y_{H\&E}$ and x_{MS},y_{MS}). The 3D processing of the tumor sample is based on image registration: H&E images are high resolution stained versions of the optical images, rigid registration is needed for alignment. MALDI spectra and optical images have the same coordinate system, thus nonlinear automatic registration of the optical images yields a 3D model of the MALDI imaging data. Via nonlinear registration a 3D H&E model is generated.

The spectral data of all sections were imported into the software SCiLS Lab (SCiLS, Bremen, Germany), version 2015b and also, along with the image data, into the software MeVisLab (MeVis Medical Solutions AG, Bremen).

2.2. Image registration pipeline

First of all, we give a short definition of image registration as we understand it and afterwards describe the deployed registration pipeline.

The goal of image registration is to find a transformation such that, applied to a so-called template or moving image, this image becomes similar to a so-called reference or fixed image. The aim is to reestablish spatial correspondence – in our case between neighboring sections – with the goal to, for example, reconstruct a 3D volume from serial tissue sections or integrate the different information of two images into one by creating a digital double-stained image, e.g. from two IHC stains.

Image registration has been performed according to [29]. We deployed the registration in two steps: First a linear rigid registration followed by a second, nonlinear or deformable registration.

As a first step, a global linear transformation t is computed depending on only few parameters. It can be written as $t(x) = Ax$, where x is an image point and A a 3-by-3 transformation matrix allowing translation and rotation of the image where x belongs to. It serves very well as an initial alignment of the images. But the histological sectioning process introduces forces which result in more complex deformations than the ones covered by the rigid deformation model. Hence, we extent our registration pipeline to get a physically more plausible deformation model and use a nonlinear registration as refinement in a second step. According to the variational approach presented in [29], this is realized by computing a deformation y that maps points of the reference image R onto points of the template image T. This is achieved by minimizing a functional $J[y] = D[T,R,y] + S[y]$ with respect to y, where D is a distance term to measure image similarity and S is a regularizer which controls the behavior and smoothness of the deformation in y.

To be able to register multimodal images, i.e. differently stained sections (unstained/H&E-stained/IHC-stained images), we chose the Normalized Gradient Field (NGF) [27] as distance term, which writes as follows:

$$D[T,R,y] = NGF[T,R,y] = \int_\Omega 1 - \left(\frac{\nabla T(y(x))^T \nabla R(x)}{\|\nabla T(y(x))\|_\epsilon \|\nabla R(x)\|_\epsilon} \right)^2 dx.$$

The functional incorporating the NGF-term becomes minimal if image edges are aligned. Thus deformations aligning edges, like tissue structures for example, are preferred by the algorithm. To ensure the resulting deformation is still plausible in terms of deformability of tissue, we additionally incorporate the elastic regularizer into our functional J which aims to align neighboring sections such that they are as similar as possible while keeping the elastic energy small at the same time.

The elastic regularizer is defined as: $S[y] = \frac{\alpha}{2} \int_\Omega \mu \langle \nabla y, \nabla y \rangle + (\lambda + \mu)(\nabla \cdot y)^2 dx$.

The stiffness of the deformation can be modified by changing elasticity parameters λ and μ. The parameter α models the tradeoff

between image similarity (distance term) and deformation smoothness (regularizer). Ω denotes the image domain. For more information on elasticity and elastic registration, respectively, see [23,24,29–31].

When reconstructing a 3D volume from several serial sections, we deploy our methods consecutively to map all images in one reference spatial domain.

After explaining the image registration methods used, we describe the registration pipeline; for a scheme see also Fig. 1. Digital 3D reconstruction of the OSCC sample forms the basis of the study. Therefore, the whole unstained image stack needs to be registered in such a way that neighboring sections become aligned, i.e. we need to apply serial registration. This is not an easy task, even if slices are very thin and we expect morphological changes to be small. Typically, the images include various artifacts such as tearing, folding, or loss of tissue due to preparation of tissue sections, in particular due to the mechanical sectioning process. To correct these distortions, an elastic deformation is applied as described above.

Upfront MALDI MSI data acquisition low resolution images of the unstained tissue sections (we call them optical images) were taken in order to record the exact locations of the MALDI measurements, i.e. the spot coordinates $(x_{MS},y_{MS}) = (x_{Optimg},y_{Optimg})$. Hence, when an alignment of the optical images is computed, we also get an alignment of the spots.

Before starting with the actual registration we perform initial stacking of the images such that all have the same orientation. This is an important preprocessing step because each tissue section is put manually on a glass slide for MALDI data acquisition and position and orientation on the sections may differ largely. Subsequent registration yields a more accurate alignment but strongly depends on a reasonable so-called initial guess. Literature suggests several ways to come to an initial alignment. Among these are simple manual inspection and manual registration or so-called moment based methods such as principle component analysis (PCA) [20,32], which is used in this study. See [33] for a detailed description.

The two-step approach explained above is applied to the initially stacked images. Spatial correspondence between sections is reestablished and MALDI spot coordinates are transformed accordingly. Using the optical images for computing the alignment, i.e. the 3D MALDI imaging model, instead of spectra has several advantages. First of all, the spatial resolution of the optical images is much higher than the spatial resolution of the MALDI imaging data and image registration is based on pixel information (gray values, image gradients (edges)). Since we are interested in a spatial alignment we expect optical images to yield a more accurate alignment than directly using MALDI spots. Furthermore, with optical images we only have to deal with a fraction of the amount of data compared to spectral data. This is important and makes even quite complex and elaborated methods computationally traceable. Finally, we can make straightforward use of existing methods for serial registration that are based on image data [20–22].

Subsequent to MALDI imaging the sections were stained with H&E and high resolution digital microscopy images were generated. Deploying the same registration pipeline (initial stacking, rigid, and nonlinear registration) a 3D H&E-stained model is computed. This is not limited to H&E-stained sections. Our multimodal registration approach also deals with IHC stains.

Since the spatial location of the 3D optical image model is known, after co-registration between both 3D models we will be able to incorporate the MALDI MSI information and the H&E-stained sections into one multimodal image. Eventually, we obtain an enhanced 3D model that includes all available imaging modalities for this head and neck cancer data set and allows easy correlation of histology with molecular information. For an overview of the processing pipeline see also Fig. 1.

2.3. Data processing

With the SCiLS Lab software (SCiLS, Bremen, Germany), version 2015b for the entire data set, we applied the spatial segmentation method as proposed in [14] which has been generalized for 3D MALDI imaging in [34,35]. In short, we performed peak picking, applied edge-preserving de-noising to the m/z-images of detected peaks, and clustered the reduced and processed spectra by their similarity. As clustering method, we have used the bisecting k-means algorithm for faster processing which is a hierarchical top-down clustering method that iteratively divides a set of spectra into two sets that are maximally different, see [14,34]. The segmentation results are presented as a segmentation map and a corresponding hierarchical dendrogram, with pseudo-colors assigned to pixels. We explored the generated segmentation maps and dendrograms with different numbers of clusters. They were also visually analysed by an experienced pathologist (GE). After segmentation, we determined individual m/z-values co-localized with the segments of the spatial map corresponding to each cluster by calculating the Pearson correlation between the cluster spatial mask (an image equal to 1 at the pixels of the cluster and 0 otherwise) and each m/z-image. Significantly correlated ($p < 0.05$) m/z-values with high correlation coefficients were selected and aligned to the peaks of the mean spectrum as done after peak picking. The peak alignment reduces the number of co-localized m/z-values by omitting redundant m/z-values and selecting only one m/z-value per peak thus simplifying interpretation.

For creation and visualization of the 3D MALDI imaging data the commercially available software SCiLS Lab 3D, version 2015b has been used. Generation of the 3D MALDI MS model from consecutive sections has been done based on co-registered optical images. Optical images for all sections have been manually and rigidly aligned. The same transformation has been applied to the MALDI MS data to obtain the 3D MALDI MS imaging model.

2.4. IHC staining

The deep frozen sections (12 μm) for IHC that were consecutive to the MALDI measured tissue sections were dried at 37 C° overnight and then fixed in ice-cold acetone for 10 min. The avidin–biotin blocking was done with Dako Biotin Blocking System according to the manufacturer's instructions (Dako; Glostrup, Denmark). IHC staining was performed with Dako REAL Detections System, Alkaline Phosphatase/RED, Rabbit/Mouse (Dako; Glostrup, Denmark) following the manufacturer's instructions. Specific antibodies against the human CD31 (Monoclonal, Mouse Anti-Human CD31, Endothelial Cell, Clone JC70A; Dako; Glostrup, Denmark) was used as primary antibody at a dilution of 1:700.

2.5. Multimodal 3D-visualization of reconstructed histological tissue

Our aim is to incorporate all available imaging modalities into one 3D model to facilitate analysis and interpretation of very different kinds of information. We reconstructed the 3D MALDI imaging model with nonlinear automatic image registration methods available in MeVisLab and further deployed those techniques, to a) automatically reconstruct a 3D model based on the H&E-stained and high resolution digitized images, b) fuse both the 3D MALDI imaging and the 3D H&E model, and c) to reconstruct a 3D model based on the H&E- and CD31-stained high resolution digitized images.

We developed a processing pipeline to make use of the multimodal 3D information and to deal with and explore complex samples (e.g. head and neck cancer) in 3D. Furthermore, our pipeline offers advanced visualization possibilities, like arbitrary cross-sections and visualization of extracted macroscopic 3D structures like an artery and its molecular composition.

The MeVisLab-based tools and pipelines developed in this context are not open source, thus not freely available. However, if you are interested in our registration methods or viewing concepts you are very welcome to contact JL. We could provide the software in research cooperation contexts.

3. Results and discussion

MALDI imaging (MALDI MSI) can visualize the distribution of hundreds of molecular compounds in a single, pixel wise measurement while maintaining the morphological and molecular integrity of the tissue allowing a subsequent histological stain of the same tissue section. This constitutes an ideal basis for multimodality. Data and images generated by MALDI imaging can be naturally combined with the corresponding H&E stained sections. Further imaging modalities, like immunohistochemical stains, can be added to gain additional functional information on analyzed tissue.

Multimodality and 3D models based on appropriate image registration methods for serial sections open the chance to gain new insight into the functional-structural connection of tissues in general and the genesis and progression of cancer in particular. Further it will support digital pathology. Especially for head and neck squamous cell carcinoma (HNSCC) the spatial molecular characterization is crucial to improve individualized therapy.

In this study a complex larynx carcinoma specimen containing normal squamous epithelium, different stages of dysplasia, invasive well differentiated and dissociated growing tumor parts with highly irregular cell and tissue architecture and surrounding stroma was used as an example to demonstrate the abilities of 3D multimodal imaging. The processing of the tissue sample is depicted in the flowchart (Fig. 1). After cutting the sample into 162 cryo-sections the different modalities were generated by applying several imaging techniques (MALDI MSI, H&E, and IHC). Image registration was used to create a 3D model of each modality and to fuse them into one multimodal data set.

3.1. 3D reconstruction of unstained sections

Before MALDI imaging, all native unstained tissue sections of the tumor sample were scanned on low resolution, we call them optical images. As described in 2.2 we applied a rigid and afterwards a nonlinear registration.

Fig. 2 illustrates the differences between both registration results. The comparison clearly shows that nonlinear registration produces significantly better reconstructions with smooth recovery of structures scattered over different slices.

Serial sections often show artifacts and distortions. To model this uncertainty at the edges, we developed a new method that focuses only on regions, where the tissue of two sections is overlapping. We only measure image similarity in the overlapping region and also allow more deformation inside the tissue, where we believe that corresponding structures are located. Outside the overlapping region, a stiffer deformation is enforced. In suppl. Fig. S1 a simple nonlinear registration and nonlinear registration with our "overlap constraint" are compared. In the latter method edges receive less attention while inner structures gain importance.

3.2. Evaluation of the registration

A nonlinear registration has a complex set of parameters and a visually convincing alignment of the images is not a sufficient evaluation criterion. There should also be an analysis of the deformation field, which is the result of a nonlinear registration [36].

Often a visual inspection of the deformed image is useful, yet the problem is that the deformation field is not a scalar but a vector field. Hence a simple gray value image offers no suitable visualization. Popular methods for deformation field inspection include arrow representations or color coding for the movement of registered image points. Another way is the depiction of the deformation field applied to a regular grid. Grid points are transformed by the deformation and since neighboring points are connected via lines valuable additional information can be obtained from the deformed grid. Three neighboring points of the (undeformed) grid should be in the same order after application of the deformation field. Otherwise it contains a discontinuity which is a mathematically unwanted result, because the function is not invertible and for the image it means a flip of pixels (and neighborhood relation of grid points), visible as a folding in the regular grid. Such a result is improper because it models an unrealistic behavior in medical imaging. A grid visualization is shown in Fig. 3 as a red overlay to the registered image. We restrict the description to 2D but similar ideas are extendable to higher

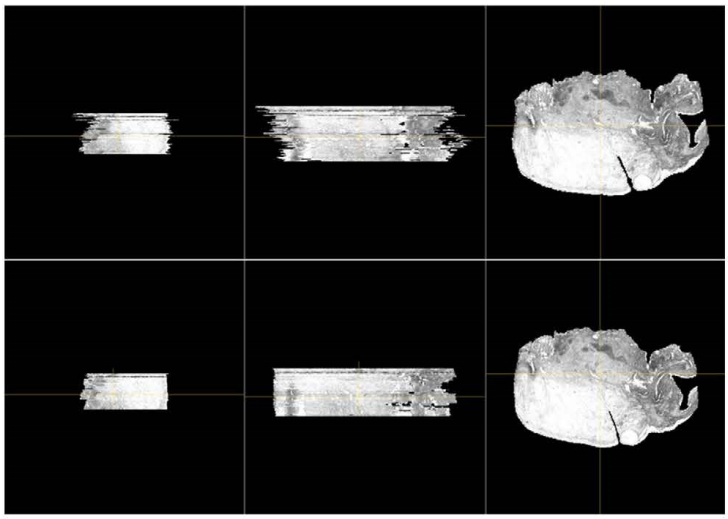

Fig. 2. Comparison of 3D reconstruction based on rigid (top row) and nonlinear (bottom row) registration. Internal structures of the head and neck tumor sample are recognizably better aligned if nonlinear registration is applied. Visualized in MeVisLab are orthogonal sections, along the thin yellow lines, through the 3D reconstructions. Note that the data's z-dimension has been virtually thickened 50 times for visualization purposes.

dimensions. It is an indication for a realistic registration that there are no foldings visible in the grid depicted in Fig. 3.

Another indicator for an unrealistic deformation, which is nicely visualized by the deformed grid, is expansion or shrinkage of tissue areas [29]. In Fig. 3 there is no very large expansion or shrinkage observable. The biggest changes happened on the boundary of the section. Areas without major changes are easily identified by their regular pattern like in the white regions in the lower left of the section. In total it is very convenient for human observers to tell from this visualization how a deformed image approximately would look like and where movement occurred.

3.3. MALDI imaging and pathological annotation

MALDI imaging analysis of the 58 cryo-sections of the OSCC tumor sample resulted in evaluable spectra in the mass range of 2000–20,000 *m/z*. In total, the data set comprised 828,558 spectra with 7680 data points per spectrum. The complete 3D MSI data set was published recently [28]. The data for all sections were imported into the software SCiLS Lab, version 2015b. The resulting spectra were subjected to spatial segmentation in SCiLS Lab software. Thereafter, the tissue sections were stained with hematoxylin and eosin (H&E), histopathologically analyzed, annotated and scanned with high resolution. The segmentation map was interpreted for plausibility after its overlay with the H&E microscopy image. Histopathological annotation was performed by a pathologist (GE) for all sections (Fig. 4). Annotations were widely congruent to the segmentation done by SCILS Lab software.

For all 58 sections it could be shown that histological annotation and the segmentation maps are in good general accordance. This good correlation has been shown also in previous studies on head and neck tumors and pleomorphic adenomas [15,37].

3.4. 3D reconstruction of MALDI imaging

Additionally to 2D data inspection, the consecutive sections have been registered and a 3D MALDI imaging model has been constructed with SCiLS Lab 3D, version 2015b. For this, rigid image registration was performed by user-guided stacking and manual alignment by shifting and rotating of consecutive sections. This process is supported by several options of difference images which visualize the quality of the alignment of two consecutive sections. For 3D visualization, a slice thickness, or z-distance, of 60 μm was selected to produce voxels of 60 μm^3.

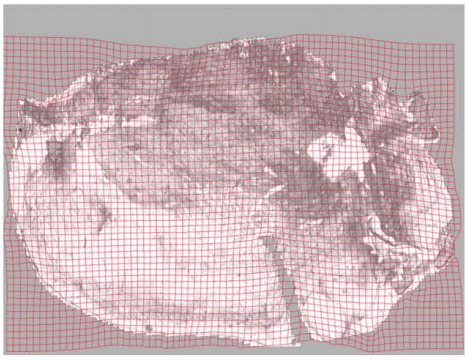

Fig. 3. Unstained tissue section superimposed by the nonlinear deformation field applied to a regular grid. No grid folds, mathematically speaking no discontinuities in the function, and no large expansions or contractions of the tissue are visible, which indicates a plausible registration.

Fig. 5 shows the result of the manual rigid registration. The 3D segmentation map demonstrates the overall consistent and acceptable alignment of the consecutive sections. Although in a more detailed view a misalignment can be seen due to local tissue deformations resulting from the cutting process. As a countermove, the manual rigid registration can be done quickly and easily in SCiLS Lab 3D.

3.5. 3D visualization of reconstructed histological tissue

With increasing availability of whole slide scanners, high resolution scans of histological samples contribute to the rapid increase of digital pathology related research. One opportunity unavailable to classic histology is 3D examination of tissue samples. During 3D reconstruction based on high resolution scans, several challenges have to be met. One of the most difficult is the large amount of memory consumed by these images, if stored uncompressed. We have to deal with high-resolution images suitable for digital microscopy, such that storage required for one image is not in the range of gigabytes anymore.

So far, we accomplish this by not using the image's highest magnification level for image registration. We create a 3D reconstruction at moderate image resolution above cellular level but meeting at least the resolution of MALDI imaging, that shows the morphology and in particular the vessel structure of the tumor sample.

The scanned H&E-stained sections were automatically nonlinearly registered to build a 3D model for a specific region of interest (Fig. 6) with relatively high resolution and later for the complete area (Fig. 7 and suppl. Movie S2) with moderate resolution.

In order to establish the spatial correspondence between the H&E-stained and the 3D model of optical images, we take advantage of the fact that they show the same sections. In order to map the H&E-coordinate system onto the one of the optical images, a nonlinear registration was performed.

Like any other volumetric data, reconstructed histological tissue can be either viewed as 3D rendering or within a combined view displaying the data in three orthogonal viewing directions.

In a 3D volume rendering one can pan and rotate around like in real world and section the model virtually. Although this is an intuitive way of interaction, this visualization is very complex to use for inspection purposes: One has to deal with covered areas inside the tissue and, to get an insight, one has to find a cutting plane which works best (suppl. Movie S3).

With the three orthogonal viewing directions one can inspect easily the inside of the tissue block. Through the cursor position the three views are linked together. Moving the cursor in one direction will also change its position within the other two related directions. Gathering information within one of the orthogonal sections is very intuitive. Spatial imagination can be complex to the untrained eye, but clinicians like pathologists are used to it.

Both visualizations can incorporate additional information as overlays to the original image. These overlays are only suitable on existing cutting planes or viewing directions. With adjustable transparency of the overlay one can get an idea of the related information.

We developed a tool based on MeVisLab to make use of the full 3D multimodal information and to deal and explore complex samples (e.g. tumors). Furthermore, we are able to compute arbitrary cross-sections and, in particular, visualize extracted macroscopic structure like an artery and its molecular composition (see 3.6 and 3.7).

3.6. 3D co-registration of MALDI imaging data and H&E-stained sections

After reconstruction of the H&E-stained 3D model and registration onto the optical images we also gained the co-registration with the 3D MALDI imaging data, since they share the coordinate system with the optical images. All image modalities are now fused and can be visualized and explored at the same time (Figs. 8 and 9), which facilitates the correlation of histology with molecular data.

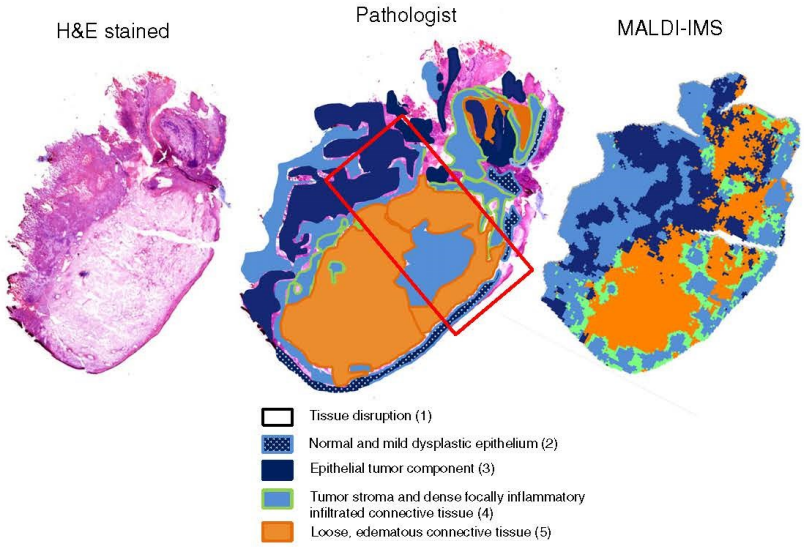

Fig. 4. Depiction of one exemplary H&E stained tumor section, the annotation of the pathologist and the segmentation map from MALDI imaging data. The histopathological annotation as well as the segmentation map displays the complex composition of the tumor sample. Areas with tissue disruption (1), normal and mild dysplastic epithelium (2), epithelial tumor components (3), tumor stroma and dense focally inflammatory and infiltrated connective (4) and loose, edematous connective tissue (5) are present. Numbers in brackets are used in the Figs. 4–9 to depict tissue areas.

Fig. 8 shows a visualization of our tool which allows synchronous scrolling through and exploration of the 3D H&E and 3D MALDI imaging model in different orthogonal orientations.

Another way to explore the co-registered 3D data sets is a volume rendering that displays both volumes next to each other as shown in Fig. 9. One cluster from the spatially segmented MALDI imaging data is projected in a transparent field. A clipping plane can be moved synchronous through both models. The supplemental Movie S3 shows another alternative where the 3D H&E-stained and the 3D MALDI imaging models are displayed as an overlay in one volume. The linkage of both modalities is very close there.

The tool links 3D volume rendering, orthogonal slicing in axial, coronal, and sagittal direction, and clipping along a free plane with arbitrary angle and offset. MALDI MSI cluster results representing defined regions of functional difference can in this way be rendered independently of the whole volume and allow a better understanding of tissue borders and the spatial context.

3.7. 3D reconstruction of immunohistochemically and H&E-stained sections

Immunohistochemical staining with CD31 reveals precisely present vessels in the tissue. Based on our registration pipeline, we reconstructed a 3D model from the alternating H&E- and CD31-stained sections and segmented an exemplary blood vessel, visualized in green color in Fig. 10. Our visualization tool allows to virtually section the 3D IHC-H&E model while leaving the segmented vessel untouched. This is just an example for possibilities to examine 3D structures and the surrounding tissue at one time. IHC seems to be an appropriate modality to visualize structures below resolution of MALDI MSI.

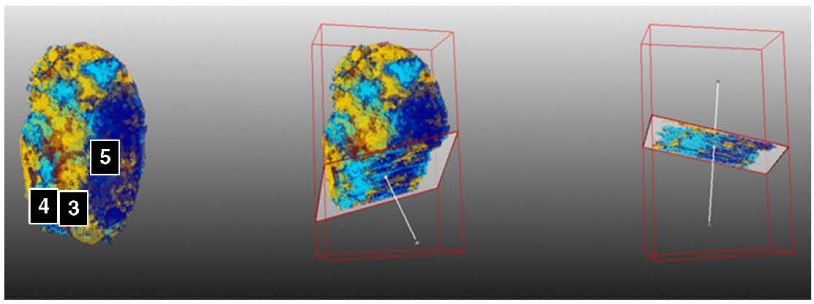

Fig. 5. 3D spatial segmentation map for four clusters. Left: entire data set. Middle: virtual sectioning of the data set. Right: One specific virtual section through the entire data set. Annotations by pathologist (compare also to Fig. 4): epithelium tumor components (3), tumor stroma and dense focally inflammatory and infiltrated connective tissue (4), loose, edematous connective tissue (5).

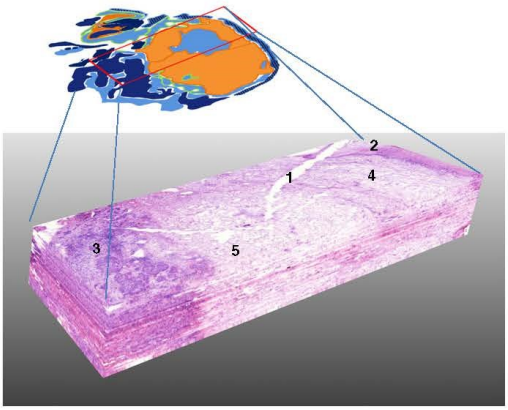

Fig. 6. 3D reconstruction based on high resolution scans of H&E-stained sections for a specific region of interest (red box marked in the 2D segmentation map). The functionally different regions of the tissue are tagged by numbers (annotated by pathologist): tissue disruption (1), normal and mild dysplastic epithelium (2), epithelial tumor component (3), tumor stroma and dense focally inflammatory infiltrated connective tissue (4), and connective tissue with edematous areas (5).

All kind of presented 3D visualizations have their advantages. Augmented reality (AR) which is already used during surgeries (e. g. displaying a virtual X-ray view on the patient) could also be an interesting tool for digital pathology. Superimposing classic H&E microscopy images with MALDI imaging and IHC data as digital double stained images can provide the pathologist with information, which are otherwise hidden or can be accessed only with large effort.

3.8. Clinical application and future perspectives

Due to enormous technical progress in terms of speed as well as spatial and mass resolution the introduction of MALDI MSI to clinical practice for diagnostic and prognostic purposes is certain in the field of cancer. Nevertheless, some problems have to be solved in order to apply MALDI MSI routinely.

In pathology it is inevitable to have standard protocols for the use of formalin fixed paraffin embedded (FFPE) tissue including deparaffinization, tryptic digestion, and matrix application [38–41]. The data processing pipeline with registration and segmentation tools has to be adapted for a specific diagnostic question as well.

In pathology MALDI MSI can be used as automated high-throughput technique for simple routine analysis, (e. g. localization of tumor cells or, tracing of pharmaceutical compound of interest [42]). This unburdens the diagnostic staff and copes with until now unmet diagnostic needs, e. g. stratification of responder and non-responder to chemotherapy.

Substantial requirements are to carry out identification and quantification directly from tissue sections [43] or to gain stable biomarker signature. For the latter, especially when carried out by analysis of complex biological samples with high spatial and mass resolution, computational power and memory are required in order to handle large MALDI MSI data sets. The complexity of the data has to be reduced for routine applications.

For the next years 3D MALDI MSI will not enter routine diagnostic because it is too time-consuming, even with fast instrumentation. But it will certainly have a high impact on preclinical cancer research since it gives insight into the molecular structure of a tumor and its biological behavior. 3D MALDI MSI will provide a more detailed view on the spatial distribution of biomarkers and the direction of progression. Maybe the development of MSI follows Moore's law in the way that speed, spatial resolution and mass resolution can be improved like computer power and needed size.

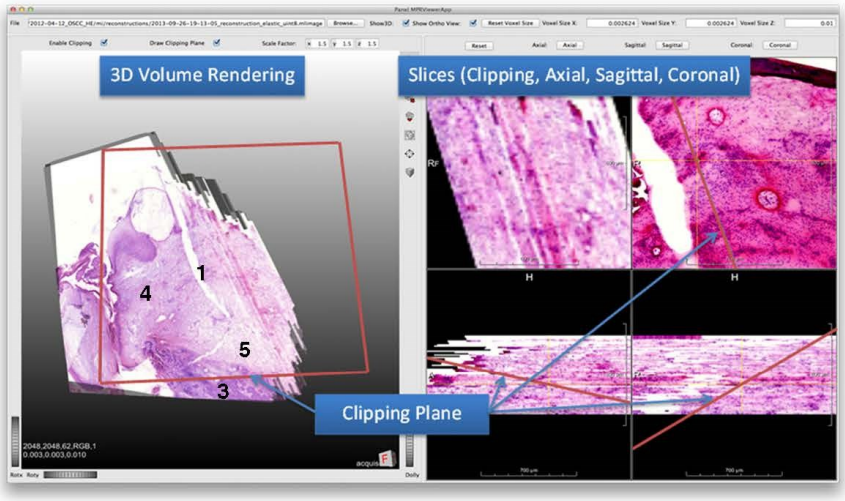

Fig. 7. Registration and 3D visualization based on high resolution scans of H&E-stained sections was performed in MeVisLab. A virtually sectioned (clipped) volume rendering of the 3D H&E model is shown on the left. The front part is clipped along a free positionable clipping plane (red rectangle). The according 2D views along orthogonal sections and the clipping plane are shown on the right. To see this viewer in action, see the movie in the supplemental data (S2). The functional different regions of the tissue are tagged corresponding to Fig. 6 by numbers (annotated by pathologist): tissue disruption (1), epithelial tumor component (3), tumor stroma and dense focally inflammatory infiltrated connective tissue (4), and connective tissue with edematous areas (5).

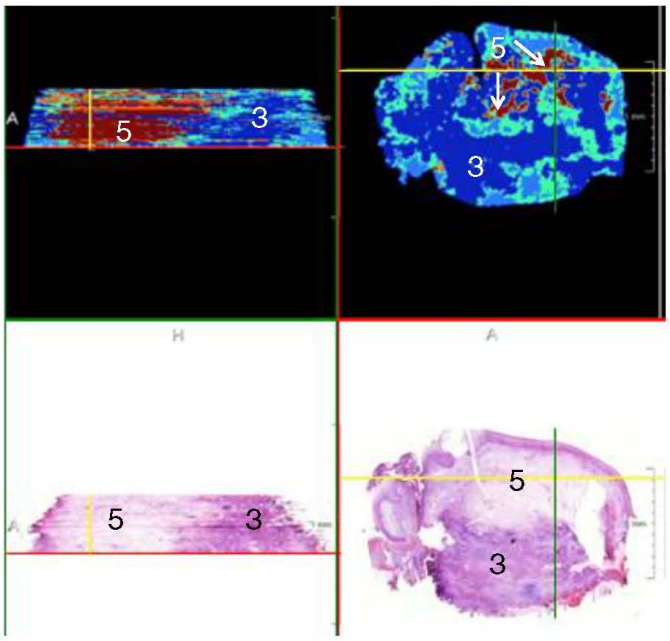

Fig. 8. We use image registration to get two 3D data sets (3D MALDI imaging and 3D H&E model) in one reference coordinate system. This allows simultaneous correlation of 3D histology and 3D molecular information, visualized in MeVisLab. Annotations by pathologist: epithelial tumor component (3), connective tissue with edematous areas (5).

In future multimodality in imaging will be extended. Other imaging modalities like Magnetic Resonance Imaging (MRI) [35] or Raman microscopy [44–47] can be included to get synergistic data for a better understanding of tumor development and as guidance during interventions. A physician could highly benefit from multimodal support for a therapeutic decision whereas it will be insignificant where the guiding image information comes from.

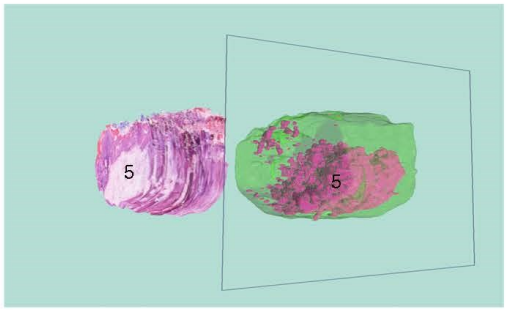

Fig. 9. Joint volume rendering in MeVisLab showing the 3D reconstructions of H&E-stained model (left) and MALDI imaging model (right). In the MALDI imaging data only one class is selected (loose, connective tissue with edematous areas (5)) to study its 3D expansion. The frame visible in the right is a virtual cutting plane and used to section the 3D volumes virtually.

4. Conclusions

The development of temporally and spatially resolved molecular analysis techniques to study biological processes relevant to human health is one of the most important fields of current clinical research. Compared to standard histological tools such as H&E or immunohistochemical stains, MALDI imaging segmentation (1) takes into account a large number of protein species at a time, (2) is not a targeted but a data-driven approach that finds regions of similar molecular composition, and (3) represents the tissue with several colors. Thus, segmentation maps represent functional proteomic topographies on a molecular level, which cannot be reached by other methods. Naturally, the interpretation of a segmentation map showing complex proteomic patterns in a single image and allocation of the derived segments to morphological features allows only a restricted view into the tumor sample, even if it is done for each of the 58 sections of the presented data set. To advance insight into tumor size, dimensions, shape and progression, a 3D model is computed which can be virtually sliced and examined. Correlating the MALDI-derived segmentation map with morphological features visible in the histological images is simplified by building two 3D data sets and co-registering them into one common reference coordinate system.

The 3D models were built from the MALDI MSI and H&E- and IHC-stained data sets using rigid and nonlinear registration.

The development of 3D MALDI imaging is still in its infancy but it offers high dimensional data that is important for understanding in general the complex spatial organization of tissues and in particular the genesis and progression of cancer.

As experiments take a long time (weeks to months) to complete and the resulting data is large (in excess of 100 GB per data set) opportunities for experts in bio-informatics to work on this type of data are limited.

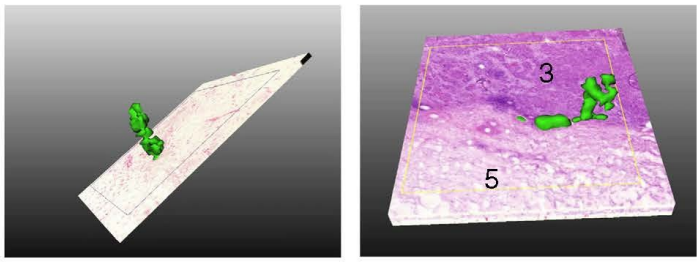

Fig. 10. Result of a joint 3D reconstruction of H&E- and CD31-stained sections. An additional segmentation of an altered swollen blood vessel in the tumor component is shown in green. The non-tumor part, in comparison, is interspersed with small vascular structures that exhibit clear ordered endothelial cells. Annotations by pathologist: Epithelial tumor component (3), connective tissue with edematous areas (5).

In this study we did not make use of the highest available magnification level of the digital microscopy images but one which exceeds the MALDI imaging resolution to create the 3D model. Using a medium magnification level we controled the computational load when registering the whole slide images. However, this is an active research field and as published in [33] we are able to base the registration on the full resolution scanned images by registering them patch-wise and achieve a more accurate alignment. Performance is an issue that needs to be addressed further.

The integration of 3D MALDI MSI data with H&E and IHC scans allows a correlation between histological and molecular information. Moreover, this model is open for additional image modalities which will further enhance the information content.

Therefore, the combination of MALDI imaging and automatic spatial segmentation is a useful approach in analyzing carcinoma tissue and provides a deeper insight into the functional proteomic organization of the respective tissue.

Supplementary data to this article can be found online at http://dx.doi.org/10.1016/j.bbapap.2016.08.018.

Conflict of Interest Statement

DT is the managing director, TA is the scientific director, and PM is on the Advisory Board of SCiLS GmbH, a company that develops and markets software for imaging mass spectrometry. MB was an employee of Bruker Daltonics GmbH, a vendor of mass spectrometry instrumentation.

Transparency document

The Transparency document associated with this article can be found, in the online version.

Acknowledgments

We acknowledge funding from BMBF 'MALDI-AMK', No. 01IB10004, the European Union's Horizon2020 and FP7 programs under the grant agreements No. 634402, 305259 and DFG funding EG 102/4-1 and EG102/5-1. We thank Jost Vehmeyer for building the u3d file displayed at the BBAPRO webpage.

References

[1] T.M. Rezende, M. de Souza Freire, O.L. Franco, Head and neck cancer: proteomic advances and biomarker achievements, Cancer 116 (2010) 4914–4925.
[2] F. von Eggeling, C. Melle, G. Ernst, Microdissecting the proteome, Proteomics 7 (2007) 2729–2737.
[3] N. Posorski, D. Kaemmerer, G. Ernst, P. Grabowski, D. Hoersch, M. Hommann, F. von Eggeling, Localization of sporadic neuroendocrine tumors by gene expression analysis of their metastases, Clin. Exp. Metastasis 28 (2011) 637–647.
[4] C. Melle, G. Ernst, B. Schimmel, A. Bleul, S. Koscielny, A. Wiesner, R. Bogumil, U. Moller, D. Osterloh, K.J. Halbhuber, F. von Eggeling, Biomarker Discovery and Identification in Laser Microdissected Head and Neck Squamous Cell Carcinoma with ProteinChip(R) Technology, Two-dimensional Gel Electrophoresis, Tandem Mass Spectrometry, and Immunohistochemistry, Mol. Cell. Proteomics 2 (2003) 443–452.
[5] P. Chaurand, M.E. Sanders, R.A. Jensen, R.M. Caprioli, Proteomics in diagnostic pathology: profiling and imaging proteins directly in tissue sections, Am. J. Pathol. 165 (2004) 1057–1068.
[6] H.C. Diehl, B. Beine, J. Elm, D. Trede, M. Ahrens, M. Eisenacher, K. Marcus, H.E. Meyer, C. Henkel, The challenge of on-tissue digestion for MALDI MSI- a comparison of different protocols to improve imaging experiments, Anal. Bioanal. Chem. 407 (2015) 2223–2243.
[7] M. Lagarrigue, M. Becker, R. Lavigne, S.O. Deininger, A. Walch, F. Aubry, D. Suckau, C. Pineau, Revisiting rat spermatogenesis with MALDI imaging at 20-microm resolution, Mol. Cell. Proteomics 10 (2011), M110 005991.
[8] A. Rompp, B. Spengler, Mass spectrometry imaging with high resolution in mass and space, Histochem. Cell Biol. 139 (2013) 759–783.
[9] L.H. Cazares, D.A. Troyer, B. Wang, R.R. Drake, O. John Semmes, MALDI tissue imaging: from biomarker discovery to clinical applications, Anal. Bioanal. Chem. 401 (2011) 17–27.
[10] L. Krasny, F. Hoffmann, G. Ernst, D. Trede, T. Alexandrov, V. Havlicek, O. Guntinas-Lichius, F. von Eggeling, A.C. Crecelius, Spatial Segmentation of MALDI FT-ICR MSI Data: A Powerful Tool to Explore the Head and Neck Tumor In Situ Lipidome, J. Am. Soc. Mass Spectrom. (2014).
[11] S.O. Deininger, M.P. Ebert, A. Futterer, M. Gerhard, C. Rocken, MALDI imaging combined with hierarchical clustering as a new tool for the interpretation of complex human cancers, J. Proteome Res. 7 (2008) 5230–5236.
[12] A. Walch, S. Rauser, S.O. Deininger, H. Hofler, MALDI imaging mass spectrometry for direct tissue analysis: a new frontier for molecular histology, Histochem. Cell Biol. 130 (2008) 421–434.
[13] T. Alexandrov, M. Becker, S.O. Deininger, G. Ernst, L. Wehder, M. Grasmair, F. von Eggeling, H. Thiele, P. Maass, Spatial segmentation of imaging mass spectrometry data with edge-preserving image denoising and clustering, J. Proteome Res. 9 (2010) 6535–6546.
[14] T. Alexandrov, J.H. Kobarg, Efficient spatial segmentation of large imaging mass spectrometry datasets with spatially aware clustering, Bioinformatics 27 (2011) i230–i238.
[15] G. Ernst, O. Guntinas-Lichius, L. Hauberg-Lotte, D. Trede, M. Becker, T. Alexandrov, F. von Eggeling, Histomolecular interpretation of pleomorphic adenomas of the salivary gland by matrix-assisted laser desorption ionization imaging and spatial segmentation, Head Neck (2014).
[16] A.D. Palmer, T. Alexandrov, Serial 3D imaging mass spectrometry at its tipping point, Anal. Chem. 87 (2015) 4055–4062.
[17] H. Thiele, S. Heldmann, D. Trede, J. Strehlow, S. Wirtz, W. Dreher, J. Berger, J. Oetjen, J.H. Kobarg, B. Fischer, P. Maass, 2D and 3D MALDI-imaging: conceptual strategies for visualization and data mining, Biochim. Biophys. Acta 1844 (2014) 117–137.
[18] P. Gremillet, M. Jourlin, C. Bron, J. Schüpbach, H.P. Gautschi, T. Bächi, Dedicated image analysis techniques for three-dimensional reconstruction from serial sections in electron microscopy, Mach. Vis. Appl. 4 (1991) 263–270.
[19] F. Maes, A. Collignon, D. Vandermeulen, G. Marchal, P. Suetens, Multimodality image registration by maximization of mutual information, IEEE Trans. Med. Imaging 16 (1997) 187–198.
[20] O. Schmitt, J. Modersitzki, S. Heldmann, S. Wirtz, B. Fischer, Image registration of sectioned brains, Int. J. Comput. Vis. 73 (2007) 5–39.
[21] A.W. Toga, P.K. Banerjee, Registration Revisited, J. Neurosci. Methods 48 (1993) 1–13.
[22] A.W. Toga, E.M. Santori, R. Hazani, K. Ambach, A 3d Digital Map of Rat-Brain, Brain Res. Bull. 38 (1995) 77–85.
[23] R. Bajcsy, R. Lieberson, M. Reivich, A Computerized System for the Elastic Matching of Deformed Radiographic Images to Idealized Atlas Images, J. Comput. Assist. Tomogr. 7 (1983).
[24] P.G. Ciarlet, Mathematical Elasticity, Elsevier Science Publishers B.V, 1988.
[25] J.P.W. Pluim, J.B.A. Maintz, M.A. Viergever, Mutual-information-based registration of medical images: A survey, IEEE Trans. Med. Imaging 22 (2003) 986–1004.

[26] P. Viola, W.M. Wells, Alignment by maximization of mutual information, Int. J. Comput. Vis. 24 (1997) 137–154.
[27] E. Haber, J. Modersitzki, Intensity gradient based registration and fusion of multi-modal images, Lect. Notes Comput. Sci 4191 (2006) 726–733.
[28] J. Oetjen, K. Veselkov, J. Watrous, J.S. McKenzie, M. Becker, L. Hauberg-Lotte, J.H. Kobarg, N. Strittmatter, A.K. Mroz, F. Hoffmann, D. Trede, A. Palmer, S. Schiffler, K. Steinhorst, M. Aichler, R. Goldin, O. Guntinas-Lichius, F. von Eggeling, H. Thiele, K. Maedler, A. Walch, P. Maass, P.C. Dorrestein, Z. Takats, T. Alexandrov, Benchmark datasets for 3D MALDI- and DESI-imaging mass spectrometry, GigaSci. 4 (2015) 20.
[29] J. Modersitzki, FAIR: Flexible Algorithms for Image Registration, SIAM, Philadelphia, 2003.
[30] J. Modersitzki, Numerical Methods for Image Registration, Oxford University Press, Oxford, 2003.
[31] C. Broit, Optimal Registration of Deformed Imagesvol. PhD University of Pennsylvania, Philadelphia, PA, USA, 1981.
[32] N.M. Alpert, J.F. Bradshaw, D. Kennedy, J.A. Correia, The principal axes transformation–a method for image registration, J. Nucl. Med. Off. Publ. Soc. Nucl. Med. 31 (1990) 1717–1722.
[33] J. Lotz, J. Olesch, B. Muller, T. Polzin, P. Galuschka, J. Lotz, S. Heldmann, K. Breuhahn, M. Gonzalez, B. Lahrmann, N. Grabe, H. Laue, O. Sedlaczek, A. Warth, J. Modersitzki, Patch-Based Nonlinear Image Registration for Gigapixel Whole Slide Images, IEEE Trans. Biomed. Eng. (2015).
[34] D. Trede, S. Schiffler, M. Becker, S. Wirtz, K. Steinhorst, J. Strehlow, M. Aichler, J.H. Kobarg, J. Oetjen, A. Dyatlov, S. Heldmann, A. Walch, H. Thiele, P. Maass, T. Alexandrov, Exploring three-dimensional matrix-assisted laser desorption/ionization imaging mass spectrometry data: three-dimensional spatial segmentation of mouse kidney, Anal. Chem. 84 (2012) 6079–6087.
[35] J. Oetjen, M. Aichler, D. Trede, J. Strehlow, J. Berger, S. Heldmann, M. Becker, M. Gottschalk, J.H. Kobarg, S. Wirtz, S. Schiffler, H. Thiele, A. Walch, P. Maass, T. Alexandrov, MRI-compatible pipeline for three-dimensional MALDI imaging mass spectrometry using PAXgene fixation, J. Proteome 90 (2013) 52–60.
[36] T. Rohlfing, Image similarity and tissue overlaps as surrogates for image registration accuracy: widely used but unreliable, IEEE Trans. Med. Imaging 31 (2012) 153–163.
[37] T. Alexandrov, M. Becker, O. Guntinas-Lichius, G. Ernst, F. von Eggeling, MALDI-imaging segmentation is a powerful tool for spatial functional proteomic analysis of human larynx carcinoma, J. Cancer Res. Clin. Oncol. 139 (2013) 85–95.
[38] R. Casadonte, R.M. Caprioli, Proteomic analysis of formalin-fixed paraffin-embedded tissue by MALDI imaging mass spectrometry, Nat. Protoc. 6 (2011) 1695–1709.
[39] B. Beine, H.C. Diehl, H.E. Meyer, C. Henkel, Tissue MALDI Mass Spectrometry Imaging (MALDI MSI) of Peptides, Methods Mol. Biol. 1394 (2016) 129–150.
[40] A. Buck, A. Ly, B. Balluff, N. Sun, K. Gorzolka, A. Feuchtinger, K.P. Janssen, P.J. Kuppen, C.J. van de Velde, G. Weirich, F. Erlmeier, R. Langer, M. Aubele, H. Zitzelsberger, M. Aichler, A. Walch, High-resolution MALDI-FT-ICR MS imaging for the analysis of metabolites from formalin-fixed, paraffin-embedded clinical tissue samples, J. Pathol. 237 (2015) 123–132.
[41] A.L. Bruinen, C. van Oevelen, G.B. Eijkel, M. Van Heerden, F. Cuyckens, R.M. Heeren, Mass Spectrometry Imaging of Drug Related Crystal-Like Structures in Formalin-Fixed Frozen and Paraffin-Embedded Rabbit Kidney Tissue Sections, J. Am. Soc. Mass Spectrom. 27 (2016) 117–123.
[42] B. Prideaux, M. Stoeckli, Mass spectrometry imaging for drug distribution studies, J. Proteome 75 (2012) 4999–5013.
[43] A. Buck, A. Walch, In situ drug and metabolite analysis [corrected] in biological and clinical research by MALDI MS imaging, Bioanalysis 6 (2014) 1241–1253.
[44] T. Meyer, O. Guntinas-Lichius, F. von Eggeling, G. Ernst, D. Akimov, M. Schmitt, B. Dietzek, J. Popp, Multimodal nonlinear microscopic investigations on head and neck squamous cell carcinoma: toward intraoperative imaging, Head Neck 35 (2013) E280–E287.
[45] T. Meyer, M. Chemnitz, M. Baumgartl, T. Gottschall, T. Pascher, C. Matthaus, B.F. Romeike, B.R. Brehm, J. Limpert, A. Tunnermann, M. Schmitt, B. Dietzek, J. Popp, Expanding multimodal microscopy by high spectral resolution coherent anti-Stokes Raman scattering imaging for clinical disease diagnostics, Anal. Chem. 85 (2013) 6703–6715.
[46] S. Heuke, O. Chernavskaia, T. Bocklitz, F.B. Legesse, T. Meyer, D. Akimov, O. Dirsch, G. Ernst, F. von Eggeling, I. Petersen, O. Guntinas-Lichius, M. Schmitt, J. Popp, Multimodal nonlinear microscopy of head and neck carcinoma - toward surgery assisting frozen section analysis, Head Neck (2016).
[47] T.W. Bocklitz, A.C. Crecelius, C. Matthaus, N. Tarcea, F. von Eggeling, M. Schmitt, U.S. Schubert, J. Popp, Deeper understanding of biological tissue: quantitative correlation of MALDI-TOF and Raman imaging, Anal. Chem. 85 (2013) 10829–10834.

5.2 Spatial Segmentation of MALDI FT-ICR MSI Data: A Powerful Tool to Explore the Head and Neck Tumor In Situ Lipidome

Krasny L, Hoffmann F, Ernst G, Trede D, Alexandrov T, Havlicek V, Guntinas-Lichius O, von Eggeling F, Crecelius AC., J. Am. Soc. Mass Spectrom. 26(1): 36-43, 2014.

J. Am. Soc. Mass Spectrom. (2015) 26:36–43
DOI: 10.1007/s13361-014-1018-5

RESEARCH ARTICLE

Spatial Segmentation of MALDI FT-ICR MSI Data: A Powerful Tool to Explore the Head and Neck Tumor In Situ Lipidome

Lukas Krasny,[1] Franziska Hoffmann,[2] Günther Ernst,[2] Dennis Trede,[3,4] Theodore Alexandrov,[3,4,5] Vladimir Havlicek,[1] Orlando Guntinas-Lichius,[6] Ferdinand von Eggeling,[2,6,7,8] Anna C. Crecelius[8,9]

[1]Institute of Microbiology, v.v.i., Videnska 1083, CZ 142 20, Prague 4, Czech Republic
[2]Institute of Physical Chemistry, Friedrich Schiller University Jena, Helmholtzweg 4, 07743, Jena, Germany
[3]SCiLS GmbH, Fahrenheitstraße 1, 28359, Bremen, Germany
[4]Steinbeis Innovation Center SCiLS Research, Fahrenheitstraße 1, 28359, Bremen, Germany
[5]Center for Industrial Mathematics, University of Bremen, Bibliothekstraße 1, 28359, Bremen, Germany
[6]Department of Otorhinolaryngology, Jena University Hospital, Lessingstraße 2, 07743, Jena, Germany
[7]Leibnitz Institute of Photonic Technology (IPHT), Albert-Einstein-Straße 9, 07745, Jena, Germany
[8]Jena Center for Soft Matter (JCSM), Friedrich Schiller University Jena, Philosophenweg 7, 07743, Jena, Germany
[9]Laboratory of Organic and Macromolecular Chemistry (IOMC), Friedrich Schiller University Jena, Humboldtstraße 10, 07743, Jena, Germany

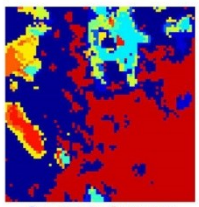

Abstract. Matrix-assisted laser desorption/ionization mass spectrometric imaging (MALDI MSI) is a well-established analytical technique for determining spatial localization of lipids in biological samples. The use of Fourier-transform ion cyclotron resonance (FT-ICR) mass spectrometers for the molecular imaging of endogenous compounds is gaining popularity, since the high mass accuracy and high mass resolving power enables accurate determination of exact masses and, consequently, a more confident identification of these molecules. The high mass resolution FT-ICR imaging datasets are typically large in size. In order to analyze them in an appropriate timeframe, the following approach has been employed: the FT-ICR imaging datasets were spatially segmented by clustering all spectra by their similarity. The resulted spatial segmentation maps were compared with the histologic annotation. This approach facilitates interpretation of the full datasets by providing spatial regions of interest. The application of this approach, which has originally been developed for MALDI-TOF MSI datasets, to the lipidomic analysis of head and neck tumor tissue revealed new insights into the metabolic organization of the carcinoma tissue.

Keywords: MALDI, MSI, FT-ICR, Head and neck, Cancer

Received: 23 May 2014/Revised: 8 October 2014/Accepted: 8 October 2014/Published online: 6 November 2014

Introduction

Matrix-assisted laser desorption/ionization mass spectrometric imaging (MALDI MSI) [1, 2] is a versatile technique, which has gained special interest in proteomics to discover the spatial distribution of proteins, mainly those below 20 kDa [3]. The spatial analysis of small molecules such as lipids by MALDI MSI is far more simple [4], since small molecules ionize easier by MALDI. In this respect, a high mass accuracy and resolution mass spectrometer can be employed such as Fourier-transform ion cyclotron resonance (FT-ICR) [5, 6], allowing to make hypotheses on chemical formulas directly from the exact masses of the detected peaks. However, because of the high mass resolving power and mass accuracy, FT-ICR MSI produces big datasets, especially when MSI is performed with a high spatial resolution that is

Electronic supplementary material The online version of this article (doi:10.1007/s13361-014-1018-5) contains supplementary material, which is available to authorized users.

Correspondence to: Anna C. Crecelius; *e-mail:* anna.crecelius@uni-jena.de

beneficial for many applications in biology and medicine. One possibility to reduce the datasets is to re-bin them, similar to that incorporated in the software package FlexImaging (Bruker Daltonics). The re-binning replaces the original measured values at a detailed *m/z* grid by a value of a larger *m/z*-interval. Nonetheless, the analysis of the raw data in a non-targeted, discovery manner by visualizing each single peak in the average spectrum in an extracted ion image with the corresponding co-registered hematoxylin and eosin (H&E) image is very time-consuming, considering that the dataset typically is comprised of millions of signals.

To overcome this challenge, we have utilized a workflow, previously developed for medium mass resolution MALDI-TOF MSI datasets [7], by spatially segmenting the MALDI FT-ICR MSI datasets. Precisely after the MSI run the serial tissue section is stained, histopathologically annotated, and finally superimposed onto the segmentation map, generated automatically from the imported raw dataset. The generated segmentation maps color regions of distinct molecular composition, facilitating significantly the data interpretation. The implementation of this approach to MALDI FT-ICR MSI data in order to determine the in situ lipidome of head and neck tumor revealed in most cases good agreement between histopathologically relevant features and certain molecular characteristics. The subsequent follow-up analysis of the lipid signals in certain clusters provided a way to obtain insights into the functional lipidomic organization of head and neck tumor.

Experimental

Materials and Reagents

HPLC grade acetonitrile, ethanol, water, and trifluoroacetic acid (TFA) were purchased from Thermo Fisher Scientific (Fair Lawn, NJ, USA). Alpha-cyano-4-hydroxycinnamic acid (CHCA) was obtained from Bruker Daltonics (Bremen, Germany).

Tissue Collection and Preparation

Four head and neck tissue samples (two cancer samples, one benign tumor, and a normal salivary gland tissue) were obtained after surgical resection at the Department of Otorhinolaryngology of the Jena University Hospital. After resection, the specimens were snap-frozen in liquid nitrogen, and stored at −80°C until further analysis. The tumor specimens were categorized according to the WHO classification [8]. Ethical approval was obtained from the Ethics Committee of the Jena University Hospital.

Each frozen clinical sample was attached with water on a cryostat steel plate and left for 1 h to adapt to the cryomicrotome cutting temperature of −20°C (Leica CM 1950; Leica Biosystems, Nussloch, Germany). Two 12 µm thick sections were thaw-mounted onto an indium-tin oxide (ITO) glass slide (Bruker Daltonics), and a third section on a regular glass slide for H&E staining. The two tissue sections on the ITO glass slide were subsequently desiccated for 30 min and immediately covered with CHCA at a concentration of 7 mg/mL in 50:50 (v/v) acetonitrile:TFA (0.2%) using the ImagePrep deposition device (Bruker Daltonics).

MALDI FT-ICR MSI Measurements

MALDI MSI was performed on a Solarix 12 T FT-ICR (dual ion source ESI, MALDI; Bruker Daltonics) mass spectrometer using a smart beam laser (1000 Hz). The spatial resolution was set to 50 µm and 20 laser shots per spectrum were used. The mass spectra were acquired in the positive ion mode with a *m/z* range of 350 to 1,500. The mass resolution at *m/z* 412.278 was 206,139.

Processing of MALDI FT-ICR MSI Datasets

The ion images were visualized either using FlexImaging (ver. 4.0; Bruker Daltonics) or SCiLS Lab (ver. 2014b; SCiLS GmbH, Bremen, Germany). The latter was used for processing the datasets as follows: Peak picking was performed on the mean spectra of the datasets, and 1000 peaks were selected by modeling the mean spectra as a sum of peaks of the Gaussian shape plus noise, as described by Alexandrov et al. [7].

Spatial Segmentation of MALDI FT-ICR MSI Datasets

For the unsupervised mining of the large MALDI FT-ICR MSI datasets, spatial segmentation was employed by clustering the spectra into distinct groups according to their similarities. For the clustering process, an efficient method called "bisecting k-means" was selected, which is optimized for hierarchical clustering of large MALDI MSI datasets in order to find hidden structures in the unlabeled data [9, 10]. The algorithm has the advantage that a prioiri the number of clusters need not be defined by the user, since it recursively partitions the data into two clusters at each step. Hence, the clustering process was conducted with the following parameters: for the cluster initialization, the farthest distance, and for the distance metric the correlation distance were used, respectively. The reduction of the spectrum-to-spectrum variation was accomplished by edge-preserving spatial denoising, which was performed prior to the segmentation. Note, all described steps were carried out within the "segmentation pipeline" of the SCiLS Lab software. Finally, the generated segmentation maps of two up to seven clusters were overlaid on the corresponding histologic images.

Tentative Lipid Assignments

To make hypotheses on detected lipid species, an average peak list from each dataset was created in the SCiLS Lab software, imported as a txt file in mMASS [11], and the peak centroids were manually queried against lipids monoisotopic molar masses by using the online database www.lipidmaps.org. The database was searched with a tolerance of 2 ppm.

Identification of Discrete Molecular Signals in Different Biological Compartments within the Tissue

The accordance between the histologic tissue regions of the tissue sample and the biochemical differences determined by clustering the FT-ICR MSI datasets was checked by an experienced pathologist, who finally decided the number of meaningful clusters. Afterwards, each tentative assigned lipid signal was attributed to a tissue region, which is defined by a cluster. Subsequently, the Pearson correlation coefficient (PCC) between each tentative assigned lipid specie in the dataset and the corresponding cluster was calculated using SCiLS Lab, on the basis of significant correlations (P-value <0.05). A PCC ≥0.5 was used as an indication that the specific lipid signal can be correlated with the cluster, below 0.5 the association between lipid signal and cluster was considered as not conclusive.

Results and Discussion

Head and neck cancer comprises malignant tumors located in the upper aerodigestive tract, for instance in the oral cavity or in the throat. The typical histology of head and neck tumor is squamous cell carcinoma (HNSCC), which is fatal without radical therapy. Nevertheless, half of the patients develops a

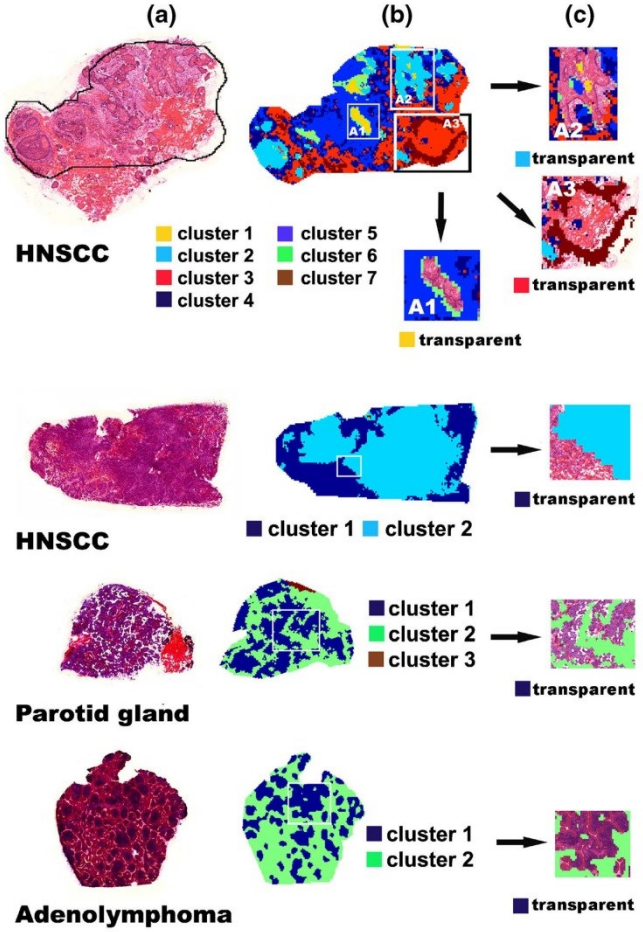

Figure 1. Digital histological analysis of the two considered head and neck carcinoma samples in comparison to normal parotid gland tissue, and a benign parotid tumor performed by means of spatial segmentation of MALDI FT-ICR MSI data: **(a)** Microscopic image taken from a serial section stained with H&E, **(b)** segmentation map generated from the MALDI FT-ICR MSI dataset, **(c)** zoom-in visualizing the associated histological features of one selected cluster, which was set transparent

locoregional recurrence in the next 2 years. Hence, the spatial molecular characterization is crucial to improve individualized therapy. The molecular imaging technique MALDI MSI that complements the histopathologic analysis and enables the simultaneous analysis of hundreds of molecular compounds in a single measurement has been applied to head and neck cancer to discover the spatial functional proteome [12, 13] as well as the lipidome [14]. Especially the lipidomic analysis of head and neck cancer is crucial for understanding the cellular physiology and pathology of this type of malignoma and, hence, has been selected for further examination. In the current study, a collection of four head and neck tissue samples were analyzed by MALDI FT-ICR MSI (see histologic images in Figure 1a). The challenges encountered during the FT-ICR MSI measurements were to handle the big datasets and to extract the important information. First, we performed the in-depth analysis of the lipidomic signatures by manually inspecting the spatial distribution of each individual signal in the dataset and its agreement with the corresponding H&E stain. Due to the fact that this tedious data analysis was lasting over 2 months for one sample, we decided to go for a computational approach, namely to represent the full dataset with a segmentation map by clustering mass spectra by their similarity and representing the clusters with different colors [7, 13]. This was performed with the commercially available SCiLS Lab software, which converts the datasets generated from any Bruker Daltonics mass spectrometer into an h5 file via a FlexImaging data importer. Since the current version is for MALDI-TOF MSI datasets, the following parameters have been modified to enable the analysis of high-resolution MSI datasets: the first two steps, including normalization to the total ion current (TIC) followed by the baseline correction of each spectrum were skipped, since it was not essential for the FT-ICR MSI datasets. Since, typically, FT-ICR mass spectra contain significantly more peaks than TOF mass spectra, the peak picking method was adapted by searching for a larger number of peaks, namely, 1000 in total. Edge-preserving spatial denoising and spectra clustering by means of "bisecting k-means" [9, 10] were done identical to the MALDI-TOF workflow. The segmentation maps generated accordinly for the four head and neck tissue samples are presented in Figure 1. The first HNSCC sample shows a complex morphologic structure as indicated in the H&E stain in Figure 1a, including tumor stroma, epithelial tumor components, and connective tissue. The automatic segmentation analysis resulted in up to seven clusters. Due to the assignment of a specific color to each cluster, the margins of each cluster within the investigated HNSCC sample are clearly visible (see Figure 1b). In order to present these findings, three clusters have been selected for a detailed examination. The first cluster, presented in yellow, consists of epithelial tumor components and central parts, as clearly observable in the area A1 when the cluster is set transparent and the co-registered H&E stain appears (see Figure 1c). The second cluster shown in light blue is defined by epithelial tumor cell components, as highlighted in the area A2, when the cluster is set transparent. The segmentation map is shifted to the right, since a consecutive section was chosen for the H&E stain. The third cluster shown in red includes preexisting connective (hyalinized) and fat tissue, which is obvious, when the cluster is set transparent and the H&E stain appears, as displayed in area A3. In the subsequent clustering of the three remaining tissue samples, the resulting segmentation maps were not always in perfect accordance with the histology, for which there are several explanations as follows. The quality of the tissue is very important. It relies on the biopsy area selected by the physician and the fast cooling of the specimen to avoid any degradation [15]. The second possible explanation is the selected spatial resolution for the acquisition of the MSI data. Ideally, the spatial resolution should be as small as possible to see all histologically relevant features. Currently, a spatial resolution of 5 to 10 μm in MALDI MSI is possible [16]; however, it prolongs the acquisition time very much and increases the dataset size enormously. We have

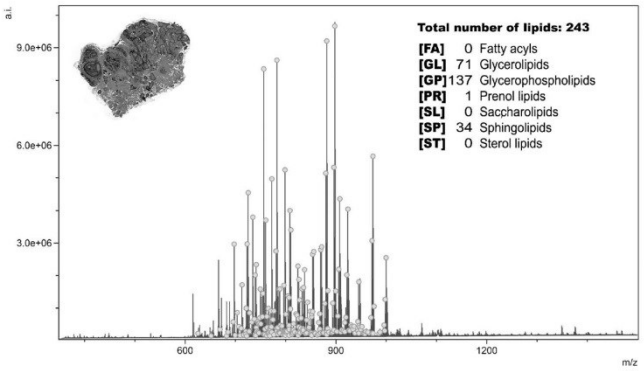

Figure 2. Average spectrum obtained by MALDI FT-ICR MSI in a HNSCC tissue section (first section in Figure 1). Peaks matched to monoisotopic molecular masses of + H, +Na, and + K ions of lipids from the database LIPID MAPS are annotated with grey dots. The list of the tentative lipid assignments can be found in the Supplementary Material

chosen a spatial resolution of 50 µm, causing on one hand some difficulties to visualize very small tissue compartments but, on the other hand, the experiments could be performed overnight resulting in datasets in the size of 100 gigabytes. The third explanation for this not "ideal" correspondence between molecular distribution and histologic features could be the use of a consecutive section for H&E staining, as shown earlier, which was necessary because the hydrophobic character of the ITO-glass slides led to the disruption of the tissue during matrix removal. Consequently, only meaningful data could be generated by choosing the segmentation maps with two clusters in the three remaining tissue samples (second HNSCC tissue sample, parotid gland, and adenolymphoma), as presented in Figure 1. Additionally, the clusters were typically not as clearly

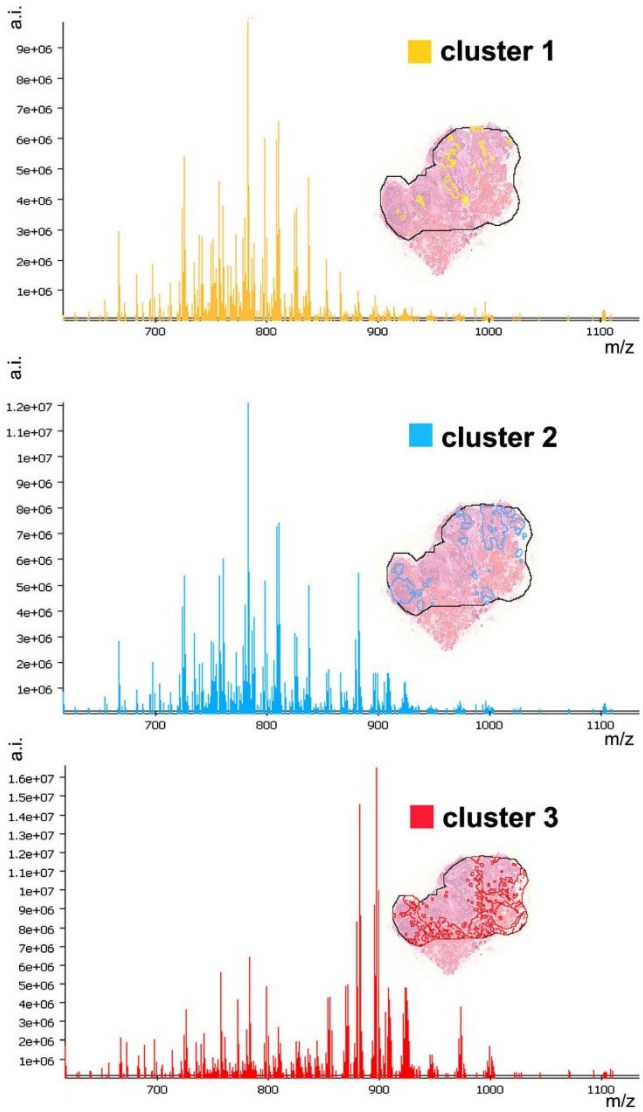

Figure 3. Comparison between the average spectra of selected clusters obtained by MALDI FT-ICR MSI in a HNSCC tissue section (first section in Figure 1). The regions of each cluster is shown as inserts

defined as in the first HNSCC sample, resulting in numerous tissue compartments comprised in one cluster. For example, the first cluster of the second HNSCC sample shown in blue in Figure 1 is defined by epithelial tumor components, but they are strongly keratinized. In the third tissue sample, the normal sample of parotid gland tissue, the first cluster shown in blue, includes mainly interstitial connective tissue but also fat tissue and parts of adjacent glandular parenchyma. Finally, the first cluster of the adenolymphoma section, also shown in blue, encloses epithelial parts, luminal parts, as well as lymphoid parts of the adenolymphoma. The latter parts are predominantly in this cluster.

The advantage of performing MALDI MSI measurements on an FT-ICR mass spectrometer is the high mass resolving power, which allowed us to make hypotheses on chemical formulas of numerous lipids. Figure 2 depicts the average mass spectrum obtained from the MALDI FT-ICR MSI analysis of the first HNSCC tissue (see Figure 1). The measured *m/z* values, which matched to possible lipid entities using the database LIPID MAPS within an allowable mass error of ±2 ppm, are marked with grey dots in Figure 2. It has to be kept in mind that the in situ analysis of intact lipids based on exact masses is often complicated by isomeric interferences. Hence, further confirmation by LC-ESI MS/MS from lipid extracts of the investigated tissue is ideal, which was, in our case, not possible because of the limited amount of available tissue. Hence, the received maximum number of lipid species based on exact mass measurements was 243 for the considered HNSCC tissue. Herewith, the categories glycerophospholipids [GP], glycerolipids [GL], and sphingolipids [SP] made up the majority. The complete list of the tentative lipid assigments of the evaluated HNSCC tissue can be found in the Supplementary Material.

In order to get a deeper knowledge about the complex lipidomic composition of the analyzed head and neck tissue in the different histomorphologic regions, the average spectrum of each cluster was created from the MALDI FT-ICR datasets using the software SCiLS Lab, which generates the region for each cluster and calculates the mean mass spectrum from the assigned spectra-group of this region. Figure 3 represents the average mass spectra for the first three clusters of the first HNSCC section (see Figure 1). This section has been chosen for in-depth analysis, since it showed the best accordance between segmentation results and histology.

In Figure 3, the area of each cluster within the HNSCC tissue is presented, using the same color scheme as in Figure 1. The first two clusters show high signals between *m/z* 700 and 800, which are characteristic for different phospholipid (PL) species. The strongest signal in both clusters is at *m/z* 782.567, which can be assigned to phosphatidylcholine (PC) as well as phosphatidylethanolamine(PE), which represent the most abundant PL classes in mammalian cell membranes [17]. It is comprehensible that the first two clusters share the same main lipid species, since they differ in their tumor environment only slightly; both consist mainly of epithelial tumor components. In contrast, the third cluster, which has a completely different morphology as revealed by the histologic examination (see Figure 1c). It consists mainly of fatty tissue. This morphologic difference is clearly reflected in the lipidomic profile, as shown in Figure 3 (bottom average spectrum in red). The average spectrum of this third cluster shows abundant signals between *m/z* 850 and 950, which are characteristic for triacylglycerols (TG). Since TGs represent the storage form for fatty acids in the human body, it is obvious that they are mainly localized in adipose tissue (fat tissue).

In order to identify differences in the lipid biochemistry within the HNSCC tissue according to the underlying morphology on the basis of a single lipid species, the Pearson correlation coefficient (PCC) between each tentative assigned lipid specie in the HNSCC tissue and the corresponding cluster was calculated (P value <0.05), using SCiLS Lab, as described in the Experimental section. The resulting PCC for each cluster (in total seven clusters, as shown in Figure 1) can be found in the Supplementary Material. Therein, it can be seen that PCC can vary between +1 and −1, whereas 1 is total positive correlation, 0 is no correlation, and −1 is total negative correlation, meaning that the specific signal is with high confidence in the remaning tissue region. Furthermore, a value between 0.5 to 1.0 indicates high correlation for the considered cluster, and a value between 0.3 to 0.5 a medium correlation. Subsequently, the tentative assigned lipid species with the highest PCC for the first three clusters are summarized in Table 1 with the corresponding elemental composition.

It should be noted that signals with a high signal intensity in a certain cluster are not necessarily suitable candidates to discriminate this tissue region from the surrounding area; e.g., the signal at *m/z* 782.567 (Table 1, first row) has a high signal intensity in the first cluster, as indicated in Figure 3 (first average spectrum in yellow); however, the PCC with 0.441 reveals only a medium association between the signal and the first cluster. In fact, this signal also has high signal intensities in the second cluster, as indicated in Figure 3 (second average

Table 1. Elemental Composition of the Compound with the Highest Pearson Correlation Coefficient (PCC) in the Considered Cluster in a HNSCC Tissue (First Section in Figure 1)

Cluster	PCC	Measured *m/z*	Calculated *m/z*	Lipid class	Molecular formula	Error (ppm)
1	0.441	782.567	782.567	PL	$C_{42}H_{82}NO_8P$ $[M+Na]^+$	0.2
2	0.672	788.616	788.616	PL	$C_{44}H_{86}NO_8P$ $[M+H]^+$	−0.1
3	0.624	871.716	871.715	TG	$C_{53}H_{100}O_6$ $[M+K]^+$	0.7

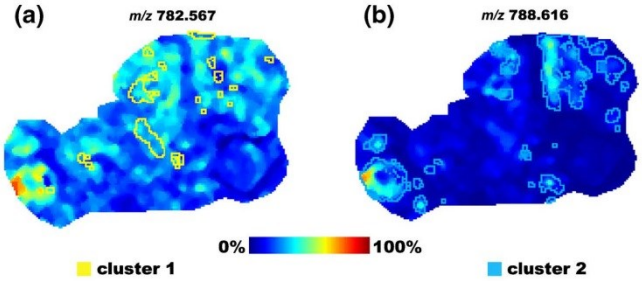

Figure 4. Extracted MALDI FT-ICR MSI ion images of PL species at **(a)** *m/z* 782.567, and **(b)** *m/z* 788.616. The region of the first cluster is outlined in yellow, the one of the second cluster in blue, respectively

spectrum in blue). This behavior is clearly shown in Figure 4a): high signal intensities of *m/z* 782.567 are observed in the constructed ion image outside the first cluster. For a better view, the regions of the first cluster are outlined in yellow.

Within the second and third clusters, several specific *m/z* values could be identified with high correlations (>0.6), which can be considered as suitable candidates to allow a discrimination between the considered cluster and the remaining tissue. The ion species with the highest PCC of the second cluster, *m/z* 788.616 (Table 1, second row), has been selected to demonstrate the discriminative potential. The extracted ion image of this signal, presented in Figure 4b), clearly illustrates an overexpression of the PL signal in the second cluster (outlined in blue), which consists mainly of ephithelial tumor parts, and little to no expression in the pre-existing tissue. From this it can be speculated that *m/z* 788.616 may function as a suitable candidate to define ephithelial tumor components. Of course

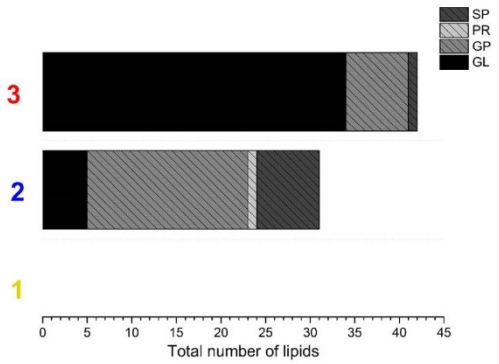

Figure 5. Graphical display of the tentative assigned lipids, divided into their categories, in the first three clusters in a HNSCC tissue section (first section in Figure 1). Each lipid species was allocated to the cluster with the highest PCC, provided the PCC was ≥0.5 to ensure a high correlation. No assigment was performed if the PCC was below 0.5. GL = glycerolipids; GP = glycerophospholipids; PR = prenol lipids; SP = sphingolipids

this finding is currently still a hypothesis and a comprehensive validation in a follow-up study is required, including MALDI FT-ICR MSI analysis of a statistically significant number of head and neck cancer samples with defined ephitelial tumor regions, followed by LC-ESI MS/MS assigment of the lipid signals as evidence. Related published work is in good agreement with our hypothesis by demonstrating the spatial confinement of PCs to specific cancer regions, such as the MALDI MSI study on colorectal cancer, which shows elevated levels of PC (16:0–18:1), LysoPC (16:0), and LysoPC (18:1) in the cancerous tissue [18], as well as the MALDI MSI study on breast tumor xyenographs, which shows elevated levels of PC (16:0/16:0), PC (16:0/18:1), PC (18:1/18:1), and PC (18:0/18:1) in the viable tumor regions [19]. Furthermore, the review article by Ridgway [20] proposes that PC contributes to proliferative growth and programmed cell death.

Finally, in order to identify the global lipidomic changes associated with the specific histopathologic entities in the first HNSCC tissue, the 243 tentatively assigned lipid species were arranged into the cluster with the highest PCC, given the PCC was ≥0.5; otherwise no assigment was performed. Using this approach, 73 tentatively assigned lipids could be categorized into the first three cluster, as shown in Figure 5. To simplify the interpretation, the lipid species were divided into their functional categories. Overall, it can be concluded that the first cluster cannot be differentiated from the second and the third cluster by a single lipid species. The second cluster contains all four categories, GL, GP, PR, and SP, highlighting the complexity of this tumor region. In the third cluster, the main category represents GLs, which certainly reflects the tissue morphology, mainly fat tissue, as discussed earlier in this paper.

Conclusion

In summary, the results indicate that the morphological changes observed in the investigated head and neck tumor samples are predominantly reflected in the MALDI FT-ICR MSI data. This gives hope that the developed approach will help in gaining further knowledge in the area of cancer research and

will allow a broader community to enable extracting useful information of huge high mass resolution MSI datasets. However, our experience shows the need to evaluate the spatial segmentation maps by an experienced pathologist.

Additionally, the matching of the discovered peaks against the lipidomics database LIPID MAPS provided hundreds hypotheses on the detected molecules providing valuable reduction from millions of original signals to possible candidates which can be validated by MS/MS using microdissection and "Folch" extraction [21] on fresh biopsy material.

Acknowledgments

The authors acknowledge the support from the Ministry of Education, Youth, and Sports of the Czech Republic (COST-CZ-LD13038). T.A. and D.T. acknowledge the funding from the European Union 7th Framework Programme (grant no. 305259). A.C.C. is grateful for the financial support of the short-term scientific mission (exchange visit in Prague) by COST (ECOST-STSM-BM1104-200513-028870). Professor Dr. U. S. Schubert is acknowledged for helpful support throughout the study and A. Urbanek for preparing the microscopic images of the H&E stained tissue sections.

References

1. Spengler, B., Hubert, M., Kaufmann, R.: MALDI ion imaging and biological ion imaging with a new scanning UV-laser microprobe. Proceedings of the 42nd Annual Conference on Mass Spectrometry and Allied Topics, pp. 1041, Chicago, IL (1994)
2. Caprioli, R.M., Farmer, T.B., Gile, J.: Molecular imaging of biological samples: localization of peptides and proteins using MALDI-TOF MS. Anal. Chem. **69**, 4751–4760 (1997)
3. Angel, P.M., Caprioli, R.M.: Matrix-assisted laser desorption ionization imaging mass spectrometry: in situ molecular mapping. Biochem. **52**, 3818–3828 (2013)
4. Gode, D., Volmer, D.A.: Lipid imaging by mass spectrometry—a review. Anal. **138**, 1289–1315 (2013)
5. Vidova, V., Pol, J., Volny, M., Novak, P., Havlicek, V., Wiedmer, S.K., Holopainen, J.M.: Visualizing spatial lipid distribution in porcine lens by MALDI imaging high-resolution mass spectrometry. J. Lipid Res. **51**, 2295–2302 (2010)
6. Sun, N., Ly, A., Meding, S., Witting, M., Hauck, S.M., Ueffing, M., Schmitt-Kopplin, P., Aichler, M., Walch, A.: High-resolution metabolite imaging of light and dark treated retina using MALDI- FTICR mass spectrometry. Proteomics **14**, 913–923 (2014)
7. Alexandrov, T., Becker, M., Deininger, S.O., Ernst, G., Wehder, L., Grasmair, M., von Eggeling, F., Thiele, H., Maass, P.: Spatial segmentation of imaging mass spectrometry data with edge-preserving image denoising and clustering. J. Proteome Res. **9**, 6535–6546 (2010)
8. Sobin, L., Gospodarowicz, M., Wittekind, C.: TNM Classification of Malignant Tumours (UICC International Union Against Cancer), 7th ed., pp. 23–39. Wiley-Blackwell:Oxford (2009)
9. Steinbach, M., Karypis, G., Kumar, V.: A comparison of document clustering techniques. University of Minnesota, Department of Computer Science and Engineering (2000)
10. Trede, D., Schiffler, S., Becker, M., Wirtz, S., Steinhorst, K., Strehlow, J., Aichler, M., Kobarg, J.H., Oetjen, J., Dyatlov, A., Heldmann, S., Walch, A., Thiele, H., Maass, P., Alexandrov, T.: Exploring three-dimensional matrix-assisted laser desorption/ionization imaging mass spectrometry data: three-dimensional spatial segmentation of mouse kidney. Anal. Chem. **84**, 6079–6087 (2012)
11. Strohalm, M., Kavan, D., Novak, P., Volny, M., Havlicek, V.: mMass 3: a cross-platform software environment for precise analysis of mass spectrometric data. Anal. Chem. **82**, 4648–4651 (2010)
12. Wehder, L., Ernst, G., Crecelius, A.C., Guntinas-Lichius, O., Melle, C., Schubert, U.S., von Eggeling, F.: Depicting the spatial distribution of proteins in human tumor tissue combining SELDI and MALDI imaging and immunohistochemistry. J. Histochem. Cytochem. **58**, 929–937 (2010)
13. Alexandrov, T., Becker, M., Guntinas-Lichius, O., Ernst, G., von Eggeling, F.: MALDI-imaging segmentation is a powerful tool for spatial functional proteomic analysis of human larynx carcinoma. J. Cancer Res. Clin. Oncol. **139**, 85–95 (2013)
14. Uchiyama, Y., Hayasaka, T., Masaki, N., Watanabe, Y., Masumoto, K., Nagata, T., Katou, F., Setou, M.: Imaging mass spectrometry distinguished the cancer and stromal regions of oral squamous cell carcinoma by visualizing phosphatidylcholine (16:0/16:1) and phosphatidylcholine (18:1/20:4). Anal. Bioanal. Chem. **406**, 1307–1316 (2014)
15. Goodwin, R.J., Dungworth, J.C., Cobb, S.R., Pitt, A.R.: Time-dependent evolution of tissue markers by MALDI-MS imaging. Proteomics **8**, 3801–3808 (2008)
16. Rompp, A., Spengler, B.: Mass spectrometry imaging with high resolution in mass and space. Histochem. Cell Biol. **139**, 759–783 (2013)
17. Horn, P.J., Korte, A.R., Neogi, P.B., Love, E., Fuchs, J., Strupat, K., Borisjuk, L., Shulaev, V., Lee, Y.J., Chapman, K.D.: Spatial mapping of lipids at cellular resolution in embryos of cotton. Plant Cell **24**, 622–636 (2012)
18. Mirnezami, R., Spagou, K., Vorkas, P.A., Lewis, M.R., Kinross, J., Want, E., Shion, H., Goldin, R.D., Darzi, A., Takats, Z., Holmes, E., Cloarec, O., Nicholson, J.K.: Chemical mapping of the colorectal cancer microenvironment via MALDI imaging mass spectrometry (MALDI-MSI) reveals novel cancer-associated field effects. Mol. Oncol. **8**, 39–49 (2014)
19. Chughtai, K., Jiang, L., Greenwood, T.R., Glunde, K., Heeren, R.M.: Mass spectrometry images acylcarnitines, phosphatidylcholines, and sphingomyelin in MDA-MB-231 breast tumor models. J. Lipid Res. **54**, 333–344 (2013)
20. Ridgway, N.D.: The role of phosphatidylcholine and choline metabolites to cell proliferation and survival. Crit. Rev. Biochem. Mol. **48**, 20–38 (2013)
21. Folch, J., Lees, M., Stanley, G.H.S.: A simple method for the isolation and purification of total lipides from animal tissues. J. Biol. Chem. **226**, 497–509 (1957)

5.3 Identification of proteomic marker in head and neck cancer using MALDI-MS Imaging, LC-MS/MS and Immunohistochemistry

Hoffmann F, Umbreit C, Krüger T, Pelzel D, Günther E, Kniemeyer O, Guntinas-Lichius O, Berndt A, von Eggeling F

Eingereicht am 13.03.2018 bei Proteomics – Clin. Appl., derzeit unter Begutachtung

Identification of proteomic markers in head and neck cancer using MALDI-MS Imaging, LC-MS/MS and Immunohistochemistry

Journal:	*Clinical Applications*
Manuscript ID	Draft
Wiley - Manuscript type:	Research Article
Date Submitted by the Author:	n/a
Complete List of Authors:	Hoffmann, Franziska; Universitatsklinikum Jena, ENT Department Umbreit, Claudia; Universitatsklinikum Jena, ENT Department Krüger, Thomas; Leibniz-Institut fur Naturstoff-Forschung und Infektionsbiologie eV Hans-Knoll-Institut, Department of Molecular and Applied Microbiology Pelzel, Daniela; Universitatsklinikum Jena, ENT Department Ernst, Günther; Universitatsklinikum Jena, ENT Department Kniemeyer, Olaf; Leibniz-Institut fur Naturstoff-Forschung und Infektionsbiologie eV Hans-Knoll-Institut, Department of Molecular and Applied Microbiology Guntinas-Lichius, Orlando; Universitatsklinikum Jena, ENT Department Berndt, Alexander; Universitatsklinikum Jena, Institute of Pathology von Eggeling, Ferdinand; Universitatsklinikum Jena, ENT Department; Friedrich Schiller Universitat Jena Physikalisch-Astronomische Fakultat, Institute of Physical Chemistry
Keywords:	FFPE, head and neck squamous cell carcinoma, MALDI MSI, LC-MS/MS, tumor marker

Identification of proteomic markers in head and neck cancer using MALDI-MS Imaging, LC-MS/MS and Immunohistochemistry

Franziska Hoffmann[1], Claudia Umbreit[1], Thomas Krüger[2], Daniela Pelzel[1], Günther Ernst[1], Olaf Kniemeyer[2], Orlando Guntinas-Lichius[1], Alexander Berndt[3], Ferdinand von Eggeling[1,4]

[1] Department of Otorhinolaryngology, Jena University Hospital, Germany

[2] Department of Molecular and Applied Microbiology, Leibniz Institute for Natural Product Research and Infection Biology, Hans Knöll Institute Jena, Germany

[3] Institute of Forensic Medicine, Jena University Hospital, Germany

[4] Institute of Physical Chemistry, Friedrich Schiller University Jena, Germany

Corresponding author:

Prof. Ferdinand von Eggeling

Stoystraße 3

07743 Jena

Germany

e-mail: feggeling@med.uni-jena.de

phone: 0049(0)3641/935526

List of abbreviations:

ACN	acetonitrile
CHCA	a-cyano-4-hydroxycinnamic acid
Da	dalton (molecular mass)
DHB	dihydroxybenzoic acid
EMT	Epithelial-mesenchymal transition
FFPE	formalin-fixed and paraffin-embedded
H&E	hematoxylin and eosin
HNC	head and neck cancer
HNSCC	head and neck squamous cell carcinoma
HPLC	high-performance liquid chromatography
HRP	horseradish peroxidase
HSP	heat shock protein
IHC	immunohistochemistry
ITO	Indium tin oxide
LC	liquid chromatography
MALDI-MS	matrix-assisted laser desorption/ionization-mass spectrometry
MS	mass spectrometry
MSI	Mass spectrometry imaging
MS/MS	tandem mass spectrometry
m/z	mass-to-charge ratio
PCA	principal components analysis
PGAM1	Phosphoglycerate mutase 1
pLSA	probalistic latent semantin analysis
TFA	trifluoroacetic acid
TIC	total ion current
TOF	time of flight

Keywords (max. 5): FFPE, head and neck squamous cell carcinoma, MALDI MSI, LC-MS/MS, tumor marker

Total number of words: 5031

Statement of Clinical Relevance

MALDI MSI can determine the spatial distribution of multiple compounds (lipids, peptides and proteins) in complex tissues in a single, label-free measurement. Especially in cancer research, spatial proteomic characterization of tissue and biomarker identification will lead to better diagnosis and individual predictive patterns of therapy response.

In this study, we used MALDI MSI to detect and locate proteomic markers for improved treatment of HNC patients. Among to the already used marker keratin 2 and vimentin, we identified other structural proteins (plakoglobin, desmoplakin and prelamin A/C). We also detected the drug target HSP 90 and two previously suggested candidate markers (PGAM1 and nucleolin). Therefore, our study both validates familiar markers and describes novel markers suitable for further evaluation in clinical studies. Our results show that MSI is a highly valuable tool for future pathological and clinical applications.

Abstract

Purpose

The heterogeneity of squamous cell carcinoma tissue greatly complicates diagnosis and individualized therapy. Therefore, characterizing the heterogeneity of tissue spatially and identifying appropriate biomarkers is crucial. MALDI imaging (MSI) is capable of analyzing spatially resolved tissue biopsies on a molecular level.

Experimental design

We used MALDI MSI on snap frozen and formalin-fixed and paraffin-embedded (FFPE) tissue samples from patients with head and neck cancer (HNC) to analyze *m/z* values localized in tumor and non-tumor regions. Peptide identification was performed using LC-MS/MS and immunohistochemistry (IHC).

Results

In both FFPE and frozen tissue specimens, we found eight characteristic masses of the tumor's epithelial region. Using LC-MS/MS, the peaks were identified as vimentin, keratin type II, nucleolin, heat shock protein 90, prelamin-A/C, junction plakoglobin and PGAM1. Lastly, vimentin, nucleolin and PGAM1 were verified with IHC.

Conclusions and Clinical Relevance

The combination of MALDI MSI, LC-MS/MS and subsequent IHC furnishes a tool suitable for characterizing the molecular heterogeneity of tissue. It is also suited for use in identifying new representative biomarkers to enable a more individualized therapy.

1. Introduction

Head and neck cancer (HNC) is one of the 10 most common cancer types worldwide with an increasing incidence. The 5 year survival rate is only 53% [1]. Early detection of HNC and prognostic evaluation of therapy response would improve patient clinical outcomes [2]. Most of the HNC are squamous cell carcinoma which developed as the result of field cancerization [3]. Those tissue specimens contain, besides the cancer tissue, a multitude of non-tumorous tissues such as different stages of dysplasia, well differentiated epithelium and tumor stroma [4]. In Germany, surgery is the primary treatment for most HNC cases. In 7.5% to 10% an R1 resection is done, with 50% needing a resurgery and/or radiotherapy [5]. The remaining 50% are unrecognized R1 resections. 75% of these suffer a relapse within two years. While the complete resection of the tumor is still investigated by histopathological evaluation, precancerous lesions are often overlooked or tumor borders are delimited inaccurately [6]. The spatial characterization of the different tumor parts is mainly investigated on the genetic level [7]. The main targets in therapy, however, will become proteins. Most proteomic techniques need *a priori* knowledge of the protein of interest and of the corresponding antibody's availability. Moreover, there is a strong need for detecting as many proteins as possible to describe the underlying molecular mechanisms. The approach suggested here is expected to contribute not only to a better understanding of carcinogenesis but also to diagnostic and therapeutic improvements.

In recent years, MALDI MSI has evolved into a powerful tool in cancer research [8-10]. The simultaneous, label-free detection of numerous biomolecules in intact tissue sections is an important advance over current histopathological techniques. MALDI MSI is particularly well-suited for studying molecular changes in tumor progression and for discovering new diagnostic and prognostic biomarkers.

Since MALDI MSI is still novel, besides our own studies [4, 11-13], there are only a few extant studies on using MSI for proteomic evaluation in HNC [14-17]. To date, no study has been published in which FFPE tissues of head and neck squamous cell carcinoma (HNSCC) were analyzed using MALDI MSI. FFPE tissues are readily available in large quantities from pathology archives where

they are easy and cost effective to store for long periods. Therefore, FFPE tumor samples are an ideal resource for MALDI MSI [18, 19].

In this study, we used MALDI MSI to investigate tumor tissue heterogeneity. We focused on searching for biomarkers that are useful for detecting malignant cells in squamous cell carcinoma. By using FFPE and fresh frozen tissue samples we were able to find 8 characteristic *m/z* values that let us distinguish between the tumor region and non-tumor regions. Serial sections were used to identify the peptides with LC-MS/MS after testing. The last step was to use IHC got verifying the results on tissue sections.

2. Material/ Methods

2.1 Tissue samples

Tissue samples from 13 patients with HNC were provided by the ENT Department of Jena University Hospital with Ethics Committee approval. The samples came from tumors in the oral cavity, oropharynx, laryngopharynx or nasopharynx. The primary tumors were classified as T2, T3 or T4 (Details Suppl. 1). Consecutive sections (6 µm thick from FFPE samples, 12 µm thick from snap frozen samples) were made with a microtome (RM 2265, Leica Biosystems) or a cryostat (CM3050S, Leica Biosystems), respectively. These slices were mounted on indium tin oxide slides.

2.2 Sample preparation

FFPE samples were prepared in the following sequence: (I) deparaffinization by incubation for 1h at 60 °C and washing with xylene (100%) three times for 220 sec each. (II) Rehydration in three baths of ethanol (100%, 95%, 70%) for 220 sec each. (III) pH-conditioning with 10 mM ammonium bicarbonate (AMBIC) buffer twice for 220 sec each. The (IV) antigen retrieval was performed for 30 min at 95°C in 10 mM pH6 citric acid monohydrate using a water bath. For on-tissue tryptic digestion, step (III) was repeated. Trypsin was applied with a solution of 2 µg/µl trypsin in 50 mM AMBIC buffer and 10% ACN. For trypsin deposition with the SunCollect (SunChrom) spraying system we used the following protocol: 8 layers; flow rate 10 µl/min; Speed x: low 7; Speed y: medium 1; vial

distance: 2 mm; Z position: 29 mm. The tryptic digestion was performed using the digestion chamber SunDigest (SunChrom) in "basic mode" for 2h, at 50 °C and 95% humidity. Fresh frozen tissue sections were prepared by following the same protocol but starting with step (III) after the antigen retrieval. Additionally, the digestion parameters were changed to "smart mode" using the following protocol: Number of steps: 2; Step 1: 900 sec, 0% fan speed, base temperature: 45 °C, cover temperature: 45°C; Step 2: 6,300 sec, 10% fan speed, base temperature: 45°C, cover temperature: 45 °C.

2.3 MALDI-TOF imaging experiments

The matrix used for FFPE tissue consisted of 10 mg/ml CHCA in 60% ACN and 0.2% TFA. For fresh frozen sections, it consisted of 30 mg/ml DHB in 50% ACN and 0.2% TFA. Matrix application was performed with the SunDigest (SunChrom). We used the same spraying protocol for both matrices, except that the number of layers differed, with 3 layers for CHCA and 5 layers for DHB. The other parameters were as follows: flow rate for layer 1 was 10 µl/min, for layers 2 to 3 or 5, respectively, 35 µl/min; speed x: low 3, speed y: medium 1; vial distance: 2 mm; Z position: 29 mm. MALDI-TOF MSI data acquisition was performed using the UltrafleXtreme mass spectrometer (Bruker Daltonik). Measurements were carried out in positive ion reflector mode. The spatial resolution was set to 50 µm with 300 shots per position. The mass range incorporates 500 to 4,000 *m/z*. The Bruker peptide calibration standard was used for external calibration. After MALDI MSI measurements, the sections were washed (80% ethanol) and H&E stained for histopathological annotation. An experienced pathologist (GE) annotated regions of squamous cell carcinoma, normal epithelium and other cell components.

2.4 MSI data and imaging analysis

For data and imaging analysis of the MSI experiments, the SCiLS Lab software, version 2017b Premium 3D (Bruker Daltonik) was used. For finding *m/z* values localized within tumor regions we used the unsupervised learning technique called probabilistic latent semantic analysis (pLSA) with a deterministic initialization. The analysis was performed on all individual spectra (aligned) without spatial denoising. The number of components was set from 5 to 7.

2.5 Protein isolation/ In-solution digest

FFPE tissue sections adjacent to sections used for MALDI Imaging measurements were utilized for protein isolation with the Qproteom FFPE tissue kit (Qiagen), in accord with the manufacturer's protocol. Samples were evaporated in a SpeedVac, resolubilized in 25 µL of 0.05% TFA in H_2O/ACN 98/2 (v/v) and filtered through Ultrafree-MC 0.2 µm PTFE membrane spin filters (Merck-Millipore). The filtrate was transferred to HPLC vials and injected into the LC-MS/MS instrument. Each sample was measured in duplicate (2 analytical replicates).

2.6 LC-MS/MS analysis

LC-MS/MS analysis was performed on an Ultimate 3000 nano RSLC system connected to a QExactive Plus mass spectrometer (both Thermo Fisher Scientific). Peptide trapping for 5 min on an Acclaim Pep Map 100 column (2 cm x 75 µm, 3 µm) at 5 µl/min was followed by separation on an analytical Acclaim Pep Map RSLC nano column (50 cm x 75 µm, 2µm). Mobile phase gradient elution of eluent A (0.1% (v/v) formic acid in water mixed with eluent B (0.1% (v/v) formic acid in 90/10 ACN/water) was performed as follows: 0-4 min at 4% B, 10 min at 7% B, 40 min at 10% B, 60 min at 15% B, 80 min at 25% B, 90 min at 30% B, 110 min at 50 % B, 115 min at 60% B, 120-125 min at 96% B, and 125.1-150 min at 4% B. Positively charged ions were generated at a spray voltage of 2.2 kV using a stainless steel emitter attached to the Nanospray Flex Ion Source (Thermo Fisher Scientific). The quadrupole/orbitrap instrument was operated in Full MS/data-dependent MS2 (Top10) mode. Precursor ions were monitored at *m/z* 300-1500 at a resolution of 70,000 full width at half maximum (FWHM) using a maximum injection time (ITmax) of 120 ms and an AGC (automatic gain control) target of 1e6. Precursor ions with a charge state of z=2-5 were filtered at an isolation width of *m/z* 1.6 amu for further HCD fragmentation at 30% normalized collision energy. MS2 ions were scanned at 17,500 FWHM (ITmax=120 ms, AGC= 2e5) using a fixed first mass of *m/z* 120 amu. Dynamic exclusion of precursor ions was set to 30 sec and the underfill ratio was set to 1.0%. The LC-MS/MS instrument was controlled by Chromeleon 7.2, QExactive HF Tune 2.8 and Xcalibur 4.0 software.

2.7 Protein database search

MAS/MS spectra were searched against the UniProt databases [20], using Proteome Discoverer (PD) 2.2 (Thermo) and the algorithms of Mascot 2.4 (Matrix Science), Sequest HT (version PD2.2) and MS Amanda 2.0. Two missed cleavages were allowed for the tryptic digestion. The precursor mass tolerance was set to 10 ppm and the fragment mass tolerance was set to 0.02 Da. Modifications were defined as dynamic methionin oxidation and protein N-term acetylation as well as static cys-carbamidomethylation. At least 2 peptides per protein and a strict FDR < 1% were required for positive protein hits. The percolator node of PD2.2 and a reverse decoy database were used for q-value validation of spectral matches. Only rank-1 proteins and peptides of the top scored proteins were counted.

2.8 Immunohistochemistry

For immunohistochemistry, frozen tissue sections were fixed with ice-cold methanol for 20 sec and acetone for 9 min. Primary antibodies for vimentin (V9 clone; monoclonal mouse anti vimentin, Dako; 1:200), nucleolin (NB600-241; polyclonal rabbit anti NB600-241; Novus Biologicals; 1:750) and PGAM1 (polyclonal rabbit anti PGAM1; SIGMA Life science; 1:20) were incubated at 4 °C overnight. Detection of antibodies was performed using the Dako REAL Detection System, AP/RED, Rabbit/Mouse (Agilent) following the manufacturer's guidelines. For negative control, the primary antibody was replaced by antibody dilution. The sections were counterstained with hematoxylin. The immunohistochemical expression of vimentin, nucleolin and PGAM1 was determined microscopically.

3. Results and Discussion

For MALDI MSI and the detection of *m/z* values characteristic of tumor regions we used tissue samples from 13 (7 FFPE, 6 fresh frozen) patients with HNSCC. After MALDI MSI measurements, the slices were H&E stained for histopathological annotation. A pathologist annotated regions of squamous cell carcinoma, normal epithelium and other tissue components (Fig. 1 A). These maps furnished the templates for further analysis. The FFPE sections were initially used for the discovery of *m/z* values which are either exclusively detectable in the tumor region or show significantly higher

intensities. Further, we investigated if these *m/z* values can also be found in the fresh frozen sections. FFPE sections consecutive to sections used for MSI measurements were employed for LC-MS/MS experiments to identify the characteristic *m/z* values. Finally, three of the discovered proteins were exemplary validated using IHC.

3.1 Unsupervised analysis of MALDI MSI data derived from FFPE samples

The unsupervised data analysis method of pLSA is an appropriate tool for studying tumor tissue heterogeneity [21]. For every tissue, one component could be found covering the manually annotated tumor region (Fig. 1B). With the help of loading plots, we utilized the most characteristic *m/z* values localized in the tumor components. Using this automated analysis algorithm, it was not possible to distinguish between epithelial tumor components and non-tumor epithelium (Fig. 1c). Therefore, single *m/z* values which were predominantly localized within the non-tumor regions were manually excluded from the lists. Based on this analyzing procedure, a peak list for every individual tissue section was generated. The final peak list which characterizes tumor tissue in FFPE sections contains 10 *m/z* values (Tab. 1, column 1). This list contains all *m/z* values which could be found in at least three tissue samples.

Given that the tumor cells develop from normal basal epithelial cells, tumor tissue is a complex mixture of epithelial subtypes. The tissue section shown in Fig. 1 contains dysplastic epithelium which could be precancerous. Therefore, this region shows proteomic features partly similar to those of tumor epithelium. Such tissue structures are often not strictly defined. To overcome these problems, a higher spatial resolution that allows depicting single cells will be helpful.

3.2 Detection of discriminating *m/z* values in fresh frozen tissue

After FFPE tissue samples, fresh frozen tissue samples are also of great interest for clinical applications, especially with respect to the diagnostically relevant instantaneous cryosections during surgery. Differing *m/z* values can be expected [22] for different treatments. Markers that are detectable in both FFPE and fresh frozen tissue therefore must be evaluated. Hence, we investigated whether the characteristic *m/z* values could also be found in fresh frozen sections.

Of the 10 *m/z* values detected in FFPE samples, 8 *m/z* values were also located in fresh frozen sections (Fig. 2). The *m/z* values are not homogeneously distributed within the tumor region. This reflects the above-mentioned tumor tissue heterogeneity. The bias in proteomic signatures between FFPE and fresh frozen tissue is a frequently debated topic and had already been demonstrated with MALDI MSI [23, 24]. Our findings could argue for supporting the use of both types of tissue specimen for biomarker discovery and translational research.

3.3 Identification of characteristic peptides with LC-MS/MS

For the identification we focused on *m/z* values found both in the fresh frozen and in the FFPE sections (Table 1). Because the fresh frozen tissues were strictly limited in size, only the FFPE tissues were used for the identification with LC-MS/MS. For each tumor sample, several hundred peptides could be identified (data not shown). As shown in Table 1, each *m/z* value could be correlated to a peptide. With MALDI, several adducts can arise (e. g. K^+, Na^+, HN_4^+). In contrast, during the sample processing for LC-MS/MS, all salts were eliminated (see chapter 2.6). For correlation, the measured MALDI *m/z* values must be corrected by the different ion masses of the above-mentioned adducts. Finally, these theoretical LC-MS/MS *m/z* values can be adjusted to the measured MALDI MSI *m/z* values. Since LC-MS/MS is more sensitive than MALDI, more peptides corresponding to the identified proteins could be detected with LC-MS/MS (Suppl. 2). The LC-MS/MS proteomics data have been deposited to the ProteomeXchange Consortium via the PRIDE partner repository with the dataset identifier PXD009144 [25].

Six *m/z* values could be assigned to the structural proteins keratin type II, vimentin, desmoplakin, junction plakoglobin and prelamin A/C (Tab. 1). Three were correlated with keratin type II, 858.658 *m/z* ($[M+2H]^{2+}$), 944.398 *m/z* ($[M+K]^+$) and 1198.690 *m/z* ($[M+Na]^+$).

For 944.398 *m/z* value, vimentin is also likely. Both proteins share the same peptide sequence. Therefore, a distinct identification using LC-MS/MS was not feasible. Regarding the biological function as part of intermediate filaments of either keratin type II or vimentin, both are equiprobable candidates located within tumor tissue. Keratin type II is known as tumor marker for epithelial cells [26]. Vimentin is used as a marker for mesenchymal cells in tumor stroma in HNC and other cancer

entities [27, 28]. The epithelial tumor regions were crossed by many tumor stroma cells. Given that MALDI MSI measurements were performed with a spatial resolution of 50 µm, these small structures could not be discriminated. For verification, IHC was performed subsequently (see chapter 3.4)

Desmoplakin (986.457 *m/z*, $[M+K]^+$, Tab. 1) is the major component of the desmosomes involved in processes during cancer development and progression [29]. For oral pharyngeal cancer, it has been reported to be correlated with the risk of metastasis formation [30].

Plakoglobin (998.689 *m/z*, $[M+H]^+$, Tab. 1) is also a component of the desmosomes. Its expression is regulated via the Wnt signaling pathway which is already described as key player in oral squamous cell carcinoma [31].

Prelamin A/C (1028.649 *m/z*, $[M+H]^+$, Tab. 1) is a structural protein located in the nucleus with organizing roles in coordinating transcription and replication. Lamin A/C deficiency, a post-translationally cleaved form of prelamin, is linked to the development of various tumors [32].

Heat shock protein 90 (901.452 *m/z*, $[M+H]^+$, Tab. 1) is a significant regulator of cellular proliferation and involved in cancer development and progression. Several inhibitors have been developed and are used in the clinical setting [33]. Additionally it is suggested as target for overcoming resistances resulting from traditional chemotherapy [34].

Nucleolin (957.511 *m/z*, $[M+NH_4]^+$ and 1095.550 *m/z*, $[M+K]^+$, Tab. 1) is located in the nucleolus and involved in polymerase I transcription whereby it could regulate cellular homeostasis. Therefore, it influences cell survival, proliferation and invasion. Its overexpression in different tumors is already known [35]. Additionally, nucleolin is used as receptor for *in vitro* targeted cancer therapy in head and neck cancer cell lines [36].

Phosphoglycerate mutase 1 (PGAM1) (1167.654 *m/z*, $[M+NH_4]^+$, Tab. 1) catalyzes the conversion of 3-phosphoglycerte into 2-phospoglycerate during glycolysis [37]. PGAM1 shows high expression in different cancer types, including lung cancer, liver cancer and colon cancer. Inhibiting PGAM1 activity induces reduced tumor growth and decreased apoptosis. Additionally, it is suggested as a poor

prognostic marker in OSCC [38]. Our detection of PGAM1 supports its role as potential marker for tumor growth.

3.4 IHC for validation of vimentin, PGAM1 and nucleolin

For exemplary validation of the correlated proteins we chose vimentin, PGAM1 and nucleolin. IHC was performed on fresh frozen sections since the FFPE sections were already used for LC-MS/MS.

Using IHC we could validate the MS data. The three proteins are located within the tumor region (Fig. 3). No expression could be seen in non-tumor regions. Nucleolin shows higher expression in moderately differentiated tumor regions whereby PGAM1 is higher expressed in well differentiated tumor regions.

4. Conclusion

In this study we used MALDI MSI and LC-MS/MS as tools for biomarker discovery in HNC. We found eight *m/z* values which discriminate tumor regions from non-tumor regions in FFPE and fresh frozen sections. On the one hand, the proteins identified were already known markers and drug targets like the structure proteins vimentin, keratin type II and HSP90. On the other hand, we could also identify new and previously suggested potential markers like prelamin-A/C and PGAM1.

Using the suggested approach, we could detect several discriminating structural proteins and investigate the epithelial-mesenchymal transition with the application of MALDI MSI [39]. Of course, higher spatial resolution is necessary to analyze these mechanisms in more detail. A higher spatial resolution will also be useful in overcoming the problem of discriminating between benign and cancerous epithelium and tumor stroma. In an earlier study, the same FFPE sample cohort was used in nonlinear-microscopy approaches, i.e., anti-stokes Raman scattering (CARS), two-photon excited fluorescence (TPEF) and second-harmonic generation (SHG) [40]. These techniques have cell resolving power and were able to discriminate small tumor structures.

Our results are the basis for further statistical validation of the found markers. By combining these findings with the new deep learning approach, a new classification model can be developed [41].

The bias problem between data from FFPE and fresh frozen tissue is an often-discussed issue. In our study, the absence of keratin type II peaks in fresh frozen tissue underlines the importance of using both kinds of tissues for marker discovery. Otherwise, the majority of peptides could be found in both. This demonstrates the reproducibility and reliability of MALDI MSI.

As far back as 2006, a study was published which analyzed oral squamous cell carcinoma with MALDI-TOF in lysed tissue. It detected 20 differently expressed proteins. Among these were an upregulation of PGAM1, keratin type II and downregulation of plakoglobin [42]. By upgrading the technique with the imaging process, we can now show the spatial distribution of these proteins.

In the context of precision medicine approaches for the treatment of HNC, MALDI MSI is capable of supporting the strategy of integrating molecular prognostic and predictive marker and cancer biology [43].

Our study reveals the potential MALDI MSI holds for clinical applications. In contrast to classical histopathological methods, it makes it possible to detect different markers in one tissue section and with a single measurement.

Furthermore, our results support the role of MALDI MSI for cancer research, especially in studying tumor progression and growth. It holds potential for the study of underlying molecular changes, which previously could not be detected with classical methods.

5. Acknowledgements

We acknowledge funding from the DFG (JBIL Core facility; EG 102/9-1) and the AiF (ZF4394901 MD7).

6. Conflict of Interest

The authors declare no conflict of interest.

7. References

[1] Parkin, D. M., Bray, F., Ferlay, J., Pisani, P., Global Cancer Statistics, 2002. *CA: A Cancer Journal for Clinicians* 2005, *55*, 74-108.

[2] Dissanayaka, W. L., Pitiyage, G., Kumarasiri, P. V. R., Liyanage, R. L. P. R., *et al.*, Clinical and histopathologic parameters in survival of oral squamous cell carcinoma. *Oral Surgery, Oral Medicine, Oral Pathology and Oral Radiology*, *113*, 518-525.

[3] Rivera, C., Essentials of oral cancer. *International Journal of Clinical and Experimental Pathology* 2015, *8*, 11884-11894.

[4] Lotz, J. M., Hoffmann, F., Lotz, J., Heldmann, S., *et al.*, Integration of 3D multimodal imaging data of a head and neck cancer and advanced feature recognition. *Biochimica et Biophysica Acta (BBA) - Proteins and Proteomics* 2017, *1865*, 946-956.

[5] Weijers, M., Snow, G. B., Bezemer, P. D., Van Der Wal, J. E., Van Der Waal, I., The clinical relevance of epithelial dysplasia in the surgical margins of tongue and floor of mouth squamous cell carcinoma: an analysis of 37 patients. *Journal of Oral Pathology & Medicine* 2002, *31*, 11-15.

[6] Sharma, S. J., Linke, J. J., Kroll, T., Klußmann, J. P., *et al.*, Praxis der Tumorendoskopie an deutschen HNO-Kliniken. *Laryngo-Rhino-Otol* 2013, *92*, 166-169.

[7] Swanton, C., Intratumour Heterogeneity: Evolution through Space and Time. *Cancer research* 2012, *72*, 4875-4882.

[8] Kunzke, T., Balluff, B., Feuchtinger, A., Buck, A., *et al.*, Native glycan fragments detected by MALDI-FT-ICR mass spectrometry imaging impact gastric cancer biology and patient outcome. *Oncotarget* 2017, *8*, 68012-68025.

[9] Alberts, D., Pottier, C., Smargiasso, N., Baiwir, D., *et al.*, MALDI Imaging-Guided Microproteomic Analyses of Heterogeneous Breast Tumors—A Pilot Study. *PROTEOMICS – Clinical Applications* 2018, *12*, 1700062-n/a.

[10] Delcourt, V., Franck, J., Leblanc, E., Narducci, F., *et al.*, Combined Mass Spectrometry Imaging and Top-down Microproteomics Reveals Evidence of a Hidden Proteome in Ovarian Cancer. *EBioMedicine* 2017, *21*, 55-64.

[11] Krasny, L., Hoffmann, F., Ernst, G., Trede, D., *et al.*, Spatial Segmentation of MALDI FT-ICR MSI Data: A Powerful Tool to Explore the Head and Neck Tumor In Situ Lipidome. *Journal of The American Society for Mass Spectrometry* 2015, *26*, 36-43.

[12] Ernst, G., Guntinas–Lichius, O., Hauberg–Lotte, L., Trede, D., *et al.*, Histomolecular interpretation of pleomorphic adenomas of the salivary gland by matrix-assisted laser desorption ionization imaging and spatial segmentation. *Head & Neck* 2015, *37*, 1014-1021.

[13] Alexandrov, T., Becker, M., Guntinas-Lichius, O., Ernst, G., von Eggeling, F., MALDI-imaging segmentation is a powerful tool for spatial functional proteomic analysis of human larynx carcinoma. *Journal of Cancer Research and Clinical Oncology* 2013, *139*, 85-95.

[14] Xie, X., Jiang, Y., Yuan, Y., Wang, P., *et al.*, MALDI imaging reveals NCOA7 as a potential biomarker in oral squamous cell carcinoma arising from oral submucous fibrosis. *Oncotarget* 2016, *7*, 59987-60004.

[15] Yuan, Y., Xie, X., Jiang, Y., Wei, Z., *et al.*, LRP6 is identified as a potential prognostic marker for oral squamous cell carcinoma via MALDI-IMS. *Cell Death & Disease* 2017, *8*, e3035.

[16] Chi, L.-H., Chang, W.-M., Chang, Y.-C., Chan, Y.-C., *et al.*, Global Proteomics-based Identification and Validation of Thymosin Beta-4 X-Linked as a Prognostic Marker for Head and Neck Squamous Cell Carcinoma. *Scientific Reports* 2017, *7*, 9031.

[17] Widlak, P., Mrukwa, G., Kalinowska, M., Pietrowska, M., *et al.*, Detection of molecular signatures of oral squamous cell carcinoma and normal epithelium – application of a novel methodology for unsupervised segmentation of imaging mass spectrometry data. *Proteomics* 2016, *16*, 1613-1621.

[18] Aichler, M., Walch, A., MALDI Imaging mass spectrometry: current frontiers and perspectives in pathology research and practice. *Laboratory Investigation* 2015, *95*, 422.

[19] Casadonte, R., Longuespée, R., Kriegsmann, J., Kriegsmann, M., in: Drake, R. R., McDonnell, L. A. (Eds.), *Advances in Cancer Research*, Academic Press 2017, pp. 173-200.

[20] *UniProt database (Homo sapiens)* http://www.uniprot.org/proteomes/UP000005640 *2017/10/23*.

[21] Jones, E. A., van Remoortere, A., van Zeijl, R. J. M., Hogendoorn, P. C. W., *et al.*, Multiple Statistical Analysis Techniques Corroborate Intratumor Heterogeneity in Imaging Mass Spectrometry Datasets of Myxofibrosarcoma. *PLOS ONE* 2011, *6*, e24913.

[22] Robert W. Sprung, J., Jonathan W. C. Brock‡§, Jarred P. Tanksley‡§, Ming Li ,Mary Kay Washington**, Robbert J. C. Slebos‡‡ ‡, and Daniel C. Liebler, Equivalence of Protein Inventories Obtained from Formalin-fixed Paraffin-embedded and Frozen Tissue in Multidimensional Liquid Chromatography-Tandem Mass Spectrometry Shotgun Proteomic Analysis. *Molecular and Cellular Proteomics* 2009, *8*, 1988-1998.

[23] Tanca, A., Pagnozzi, D., Burrai, G. P., Polinas, M., *et al.*, Comparability of differential proteomics data generated from paired archival fresh-frozen and formalin-fixed samples by GeLC–MS/MS and spectral counting. *Journal of Proteomics* 2012, *77*, 561-576.

[24] Ly, A., Buck, A., Balluff, B., Sun, N., *et al.*, High-mass-resolution MALDI mass spectrometry imaging of metabolites from formalin-fixed paraffin-embedded tissue. *Nature Protocols* 2016, *11*, 1428.

[25] Vizcaíno, J. A., Csordas, A., del-Toro, N., Dianes, J. A., *et al.*, 2016 update of the PRIDE database and its related tools. *Nucleic Acids Research* 2016, *44*, D447-D456.

[26] Karantza, V., Keratins in health and cancer: more than mere epithelial cell markers. *Oncogene* 2010, *30*, 127.

[27] Liu, P.-F., Kang, B.-H., Wu, Y.-M., Sun, J.-H., *et al.*, Vimentin is a potential prognostic factor for tongue squamous cell carcinoma among five epithelial–mesenchymal transition-related proteins. *PLoS ONE* 2017, *12*, e0178581.

[28] Mimeault, M., Batra, S. K., Molecular Biomarkers of Cancer Stem/Progenitor Cells Associated with Progression, Metastases, and Treatment Resistance of Aggressive Cancers. *Cancer Epidemiology Biomarkers & Prevention* 2014, *23*, 234-254.

[29] Huber, O., Petersen, I., 150th Anniversary Series: Desmosomes and the Hallmarks of Cancer. *Cell Communication & Adhesion* 2015, *22*, 15-28.

[30] Papagerakis, S., Shabana, A.-H., Pollock, B. H., Papagerakis, P., *et al.*, Altered desmoplakin expression at transcriptional and protein levels provides prognostic information in human oropharyngeal cancer. *Human Pathology*, *40*, 1320-1329.

[31] Shiah, S.-G., Shieh, Y.-S., Chang, J.-Y., The Role of Wnt Signaling in Squamous Cell Carcinoma. *Journal of Dental Research* 2016, *95*, 129-134.

[32] Chow, K.-H., Factor, R. E., Ullman, K. S., The nuclear envelope environment and its cancer connections. *Nature reviews. Cancer* 2012, *12*, 196-209.

[33] Chatterjee, S., Burns, T., Targeting Heat Shock Proteins in Cancer: A Promising Therapeutic Approach. *International Journal of Molecular Sciences* 2017, *18*, 1978.

[34] Subramanian, C., Kovatch, K. J., Sim, M. W., Wang, G., *et al.*, Novel C-Terminal Heat Shock Protein 90 Inhibitors (KU711 and Ku757) Are Effective in Targeting Head and Neck Squamous Cell Carcinoma Cancer Stem cells. *Neoplasia (New York, N.Y.)* 2017, *19*, 1003-1011.

[35] Berger, C. M., Gaume, X., Bouvet, P., The roles of nucleolin subcellular localization in cancer. *Biochimie* 2015, *113*, 78-85.

[36] Zhang, S., Gupta, S., Fitzgerald, T. J., Bogdanov, A. A., Jr., Dual radiosensitization and anti-STAT3 anti-proliferative strategy based on delivery of gold nanoparticle - oligonucleotide nanoconstructs to head and neck cancer cells. *Nanotheranostics* 2018, *2*, 1-11.

[37] Fothergill-Gilmore, L. A., Watson, H. C., The phosphoglycerate mutases. *Adv Enzymol Relat Areas Mol Biol* 1989, *62*, 227-313.

[38] Zhang, D., Wu, H., Zhang, X., Ding, X., *et al.*, Phosphoglycerate Mutase 1 Predicts the Poor Prognosis of Oral Squamous Cell Carcinoma and is Associated with Cell Migration. *Journal of Cancer* 2017, *8*, 1943-1951.

[39] Briest, F., Berndt, A., Clement, J., Junker, K., *et al.*, *Front Biosci (Elite Ed)* 2012, pp. 1871-1887.

[40] Heuke, S., Chernavskaia, O., Bocklitz, T., Legesse, F. B., *et al.*, Multimodal nonlinear microscopy of head and neck carcinoma — toward surgery assisting frozen section analysis. *Head & Neck* 2016, *38*, 1545-1552.

[41] Behrmann, J., Etmann, C., Boskamp, T., Casadonte, R., *et al.*, Deep learning for tumor classification in imaging mass spectrometry. *Bioinformatics* 2017, btx724-btx724.

[42] Turhani, D., Krapfenbauer, K., Thurnher, D., Langen, H., Fountoulakis, M., Identification of differentially expressed, tumor-associated proteins in oral squamous cell carcinoma by proteomic analysis. *ELECTROPHORESIS* 2006, *27*, 1417-1423.

[43] Monteiro de Oliveira Novaes, J. A., William, W. N., Prognostic factors, predictive markers and cancer biology: the triad for successful oral cancer chemoprevention. *Future Oncology* 2016, *12*, 2379-2386.

Fig. 1: Comparison of component analysis of MALDI MSI measurements on FFPE sections with pathohistological regions. One example of sample cohort is shown. A) H&E stained tissue section. B) Annotated regions, red: Squamous cell carcinoma, green: dysplastic epithelium, rest: non-tumor region, containing connective tissue with inflammatory infiltration and glandular regions (blue). C) Component which covers the tumor region, no spatial denoising was performed.

Fig. 2: Discriminating *m/z* values in fresh frozen sections. Comparison of component analysis of MALDI MSI measurements on FFPE sections with pathohistological regions. One example of sample cohort is shown. A) H&E stained tissue section. B) Annotated regions, red: tumor region, as diffuse infiltration in muscle tissue, rest: non-tumor region. C) *m/z* images of 8 *m/z* values which could be detected in fresh frozen sections, H&E-overlay, weak spatial denoising. D) Comparison of mean

spectra of tumor region (red) and non-tumor region (green), *m/z* axis incorporates all values shown in C (black arrows).

Fig. 3: Comparison of MALDI MSI *m/z* images with IHC of Vimentin, Nucleolin and PGAM1. A) H&E stained tissue section. B) Annotated regions, different tumor regions, light red: well differentiated tumor, dark red: moderately differentiated tumor with infiltrated tumor stroma, rest: non-tumor region. C) left: intensity maps of *m/z* values detected with MALDI MSI; middle: IHC stained tissue section with magnifications (upper boxes: 10x each, lower boxes 40x).

Tab. 1: Identified *m/z* values of characteristic HNC peaks with their corresponding peptides analyzed with LC-MS/MS. Column 1: monoisotopic *m/z* values (median) of peaks characteristic for the tumor regions in HNC, detected with MALDI MSI. Column 2: *m/z* values for $[M+H]^+$ measured with LC-MS/MS, correlated to MALDI MSI *m/z* value. Column 3: Deviation of MALDI MSI *m/z* value and corresponding LC-MS/MS *m/z* value. Column 4: theoretical *m/z* value of K^+, Na^+, NH_4^+ adducts of LC-MS/MS peaks. Columns 5-7: Identified Protein, Peptide sequence, Uniprot number with position of peptide in protein. Column 8: Sample types in which *m/z* value could be detected.

m/z value measured MSI	*m/z* value $[M+H]^+$ measured LC-MS/MS	Deviation	theor. *m/z* value of adduct	Protein name	Peptide sequence	Uniprot number [Position in Protein]	Sample type
858.658	1716.85112	0.7748386	$[M+2H]^{2+}$ 859.432836	Keratin type II cytoskeletal 1	[K].QISNLQQSISDAEQR.[G]	P04264 [418-432]	FFPE
901.451	901.52541	0.07441	[M+H]+	Heat shock protein HSP90	[K].TKPIWTR.[N]	P08238 [285-291]	Fresh frozen FFPE
944.398	906.46.796	0.025943	$[M+K]^+$ 944.423843	Vimentin Keratin type II cytoskeletal 78	[R].FLEQQNK.[IVM]	P08670 [123-129] Q8N1N4 [131-137]	Fresh frozen FFPE
957.511	940.51384	0.029389	$[M+NH_4]^+$ 957.540389	Nucleolin	[K].GIAYIEFK.[T]	P19338 [430-437]	Fresh frozen FFPE
986.457	948.50367	0.002553	$[M+K]^+$ 986.459553	Desmoplakin	[R].LPVEEAYK.[R]	P15924 [2310-2317]	Fresh frozen FFPE
998.689	998.58807	-0.10093	$[M+H]^+$	Junction plakoglobin	[R].LAEPSQLLK.[S]	P14923 [116-124]	Fresh frozen FFPE
1028.649	1028.57348	-0.07552	$[M+H]^+$	Prelamin-A/C	[R].LADALQELR.[A]	P02545 [241-249]	Fresh frozen FFPE
1095.555	1057.60406	0.004943	$[M+K]^+$ 1095.559943	Nucleolin	[K].VTLDWAKPK.[G]	P19338 [640-648]	Fresh frozen FFPE
1167.654	1150.66912	0.041669	$[M+NH_4]^+$ 1167.695669	Phosphoglycerate mutase 1	[R].VLIAAHGNSLR.[G]	P18669 [181-191]	Fresh frozen FFPE
1198.690	1176.55314	-0.155014	$[M+Na]^+$ 1198.534986	Keratin type II cytoskeletal 2	[K].EEAEALYHSK.[Y]	P35908 [365-274]	FFPE

Tab. 1: Identified *m/z* values of characteristic HNC peaks with their corresponding peptides analyzed with LC-MS/MS. Column 1: monoisotopic *m/z* values (median) of peaks characteristic for the tumor regions in HNC, detected with MALDI MSI. Column 2: *m/z* values for $[M+H]^+$ measured with LC-MS/MS, correlated to MALDI MSI *m/z* value. Column 3: Deviation of MALDI MSI *m/z* value and corresponding LC-MS/MS *m/z* value. Column 4: theoretical *m/z* value of K^+, Na^+, NH_4^+ adducts of LC-MS/MS peaks. Columns 5-7: Identified Protein, Peptide sequence, Uniprot number with position of peptide in protein. Column 8: Sample types in which *m/z* value could be detected.

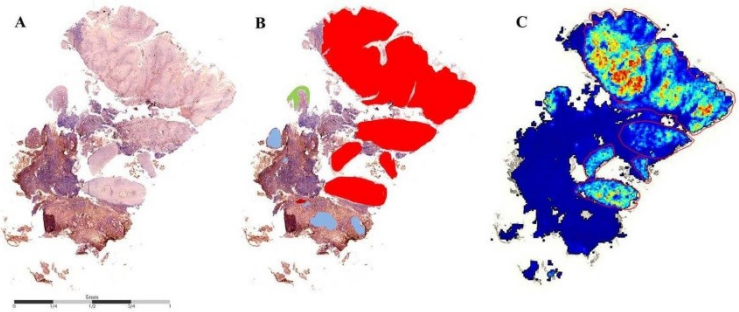

Fig. 1: Comparison of component analysis of MALDI MSI measurements on FFPE sections with pathohistological regions. One example of sample cohort is shown. A) H&E stained tissue section. B) Annotated regions, red: Squamous cell carcinoma, green: dysplastic epithelium, rest: non-tumor region, containing connective tissue with inflammatory infiltration and glandular regions (blue). C) Component which covers the tumor region, no spatial denoising was performed.

322x145mm (150 x 150 DPI)

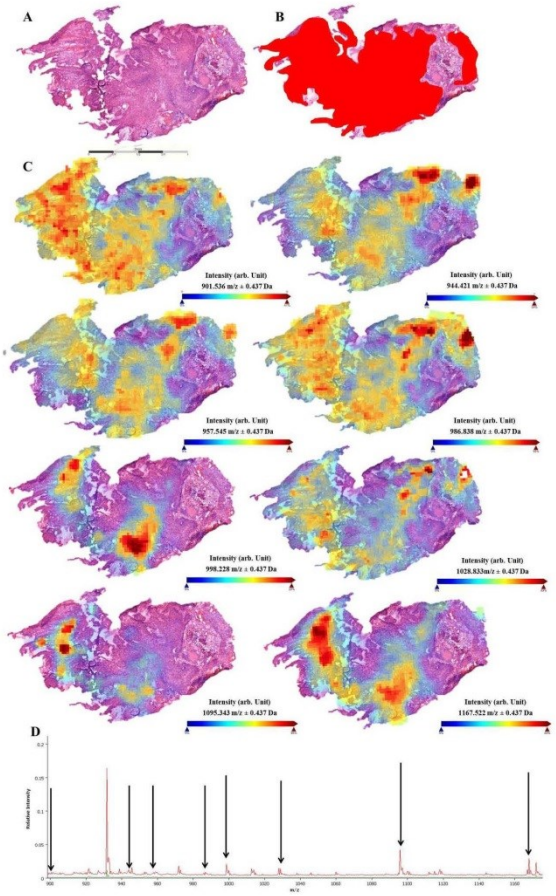

Fig. 2: Discriminating m/z values in fresh frozen sections. Comparison of component analysis of MALDI MSI measurements on FFPE sections with pathohistological regions. One example of sample cohort is shown. A) H&E stained tissue section. B) Annotated regions, red: tumor region, as diffuse infiltration in muscle tissue, rest: non-tumor region. C) m/z images of 8 m/z values which could be detected in fresh frozen sections, H&E-overlay, weak spatial denoising. D) Comparison of mean spectra of tumor region (red) and non-tumor region (green), m/z axis incorporates all values shown in C (black arrows).

283x457mm (150 x 150 DPI)

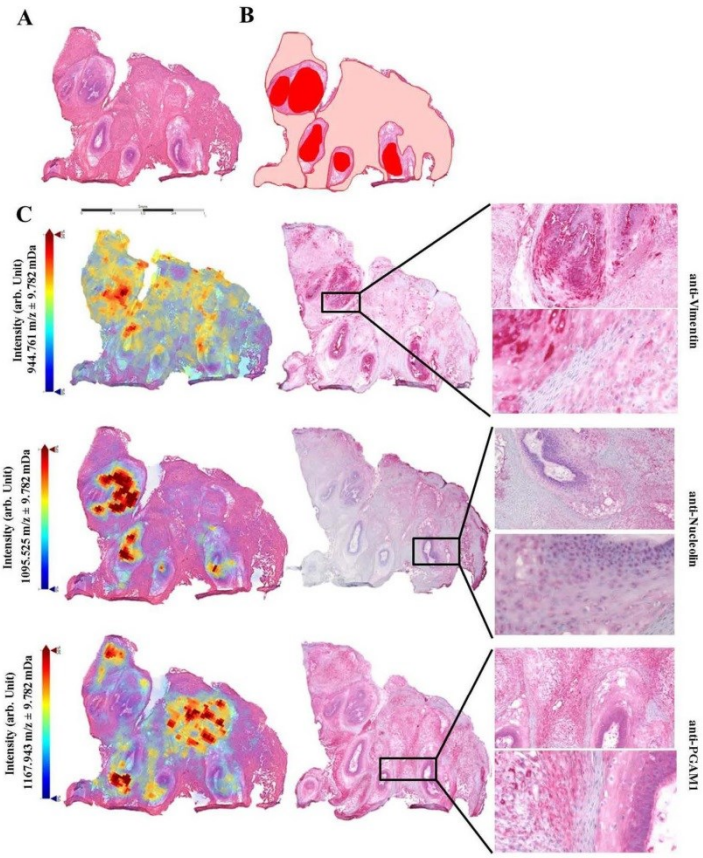

Fig. 3: Comparison of MALDI MSI m/z images with IHC of Vimentin, Nucleolin and PGAM1. A) H&E stained tissue section. B) Annotated regions, different tumor regions, light red: well differentiated tumor, dark red: moderately differentiated tumor with infiltrated tumor stroma, rest: non-tumor region. C) left: intensity maps of m/z values detected with MALDI MSI; middle: IHC stained tissue section with magnifications (upper boxes: 10x each, lower boxes 40x).

227x263mm (150 x 150 DPI)

6. Diskussion

In dieser Arbeit konnte gezeigt werden, dass MALDI-MS Imaging für die molekulare Charakterisierung von Kopf-Hals-Tumoren eingesetzt werden kann. Wie in Tabelle 1 dargestellt, war dies auf verschiedenen Ebenen möglich.

	Molekülklasse	*MALDI-MS Imaging-System*	*Gewebe*	*Kombinierte Methoden*
Lotz und Hoffmann et al.	Proteine	MALDI-TOF	Kryo	H&E IHC (anti-CD31)
Krasny et al.	Lipide	MALDI-FT-ICR	Kryo	H&E
Hoffmann et al.	Peptide (tryptisch verdaute Proteine)	MALDI-TOF	FFPE Kryo	H&E IHC (anti-Vimentin,-Nucleolin,-PGAM1) LC-MS/MS

Tabelle 1: Übersicht der in den Publikationen analysierten Moleküle, genutzten MALDI-MS-Systeme, Gewebearten und kombinierten Methoden.

Es konnten Methoden etabliert werden, welche die Lipidanalyse und deren Auswertung mittels hochauflösendem FT-ICR-MS-Imaging verbessert. Zudem konnte ein interaktives 3D-Modell eines Kopf-Hals-Tumors entwickelt werden, welches molekulare Informationen mit histologischen kombiniert. Die Verknüpfung von MALDI-MSI mit LC-MS/MS und IHC konnte genutzt werden um proteomische Marker zu finden und zu identifizieren, welche die Tumorregionen in Plattenepithelkarzinomen des Kopf-Hals- Bereiches charakterisieren.

6.1 MALDI-MS Imaging

MALDI-MS Imaging ist immer noch eine recht neue Methode, welche sehr komplex und interdisziplinär ist. Dies führt zu zahlreichen Herausforderungen, die gelöst werden müssen, bevor eine routinemäßige klinische Anwendung realisierbar ist. Beginnend mit der Probenvorbereitung, über die MALDI-MS-Messung, bis hin zur Datenauswertung und –interpretation ist eine Standardisierung notwendig.

6.1.1 Probenvorbereitung

Die Probenvorbereitung ist je nach Gewebetyp und der zu analysierenden Analyten unterschiedlich und essentiell für erfolgreiche MALDI-MSI-Experimente. Demnach ist

es notwendig, für jede Fragestellung spezifische Protokolle zu etablieren. Dies wurde innerhalb dieser Arbeit erfolgreich umgesetzt.

Vor allem das Nutzbarmachen von FFPE-Gewebe für MALDI-MS Imaging rückte in den letzten Jahren immer mehr in den Fokus, da weltweit große Archive von FFPE-Proben in den Pathologien existieren (Gorzolka und Walch 2014). Aufgrund der Konservierung bei gleichzeitiger Stabilisierung der Moleküle und der Morphologie des Gewebes sowie der unkomplizierten Langzeit-Lagerung bei Raumtemperatur hat es sich bereits Ende des 19. Jahrhunderts zum Goldstandard in den Pathologien entwickelt. Zudem ist das Gewebe durch die Einbettung sehr gut schneidbar, so dass Dünnschnitte bis zu 4 µm möglich sind. Bei einer Verwendung von FFPE-Gewebe können somit mehr Schnitte von einer Probe angefertigt werden als bei der Verwendung von Kryoproben. Durch die Formalinfixierung kommt es zu verschiedenen Modifikationen der Proteine, welche vor der MALDI-MS-Messung rückgängig gemacht werden müssen (Metz et al. 2004). Dies führt zu einem komplexen Arbeitsablauf, welcher im Vorfeld des allgemeinen Protokolls (Kapitel 3.2.1) das Deparaffinisieren, die Antigen-Demaskierung und eventuell einen enzymatischen Verdau für die Untersuchung von Proteinen beinhaltet. Jeder einzelne Schritt erfordert zahlreiche Handlungsabläufe, was zu einer hohen Variabilität führt.

Innerhalb der vorliegenden Arbeit wurde im Rahmen eines AIF Projektes (ZF4394901) ein Protokoll zur Erschließung von FFPE-Proben etabliert, welches für die Suche proteomischer Biomarker bei Kopf-Hals-Tumoren genutzt wurde (Kapitel 5.3/Hoffmann et al.). Dieses Protokoll beinhaltet qualitative Kontrollpunkte innerhalb des Arbeitsablaufes. Vor allem die Antigendemaskierung sowie der tryptische Verdau sollen dadurch objektiv evaluiert werden.

Für den 3D-Datensatz (Kapitel 5.1/Lotz und Hoffmann et al.) wurde Kryogewebe genutzt. Die Prozessierung von Gefrierschnitten für MALDI-MSI erfordert weniger Schritte, da die Moleküle in ihrem nativen Zustand erhalten bleiben. Das Rückgängigmachen der Modifikationen durch die Formalinfixierung ist nicht notwendig. Allerdings bestehen auch hier die Anforderungen an reproduzierbare Ergebnisse, da sich das Experiment aufgrund der Anzahl der Schnitte (n=58) über mehrere Wochen erstreckte. Alle Parameter wurden über diesen Zeitraum gleich gehalten und externe Kalibrierungsstandards vor jeder Messung genutzt. Allerdings fehlen bisher objektive Werte zur Qualitätsbewertung der Spektren, so dass ein

manueller Vergleich der Messungen über bekannte anatomische Strukturen und ihnen zugehörige *m/z*-Werte stattfand.
Für die Verwendung sowohl von Gefrierschnitten als auch von FFPE-Schnitten sind objektive Qualitätskontrollen unbedingt notwendig. Aktuelle Studien auf diesem Gebiet wurden bereits zusammengefasst (Erich et al. 2017). Zusätzlich werden dort quantitative Kennzahlen vorgestellt, deren Implementierung in die bestehenden Protokolle zukünftig von großer Bedeutung ist.
Ein anderer Aspekt der Probenvorbereitung betrifft das Auftragen der Matrix. Hierbei ist es besonders wichtig, eine homogene Schicht mit möglichst kleinen Kristallen zu erzeugen. Gleichzeitig muss eine gute Extraktion der Analyten erfolgen, was vor allem bei Proteinen und Peptiden eine gewisse Feuchtigkeit voraussetzt, die jedoch nicht zur Diffusion der Analyten führt. Generell dürfen durch das Auftragen der Matrix keine Artefakte entstehen, die in falschpositiven oder falschnegativen Signalen resultieren. Dafür wurden im Rahmen der Promotion die Eigenschaften (Homogenität, Kristallgröße) verschiedener Matrices mittels elektronen-mikroskopischer Messung analysiert und an Referenzgeweben (Maushirn, Mausleber) getestet. Darauf basierend konnten Protokolle für kommerziell erwerbbare Matrixsprayer entwickelt werden.

6.1.2 MALDI-MSI-Messung

Im Rahmen der Promotion war neben der Analyse von tryptisch verdauten Proteinen (Kapitel 5.3/Hoffmann et al.) auch die Analyse von intakten Proteinen im Tumorgewebe von Bedeutung. Hier konnten jedoch keine biologisch relevanten Ergebnisse produziert werden. Dies liegt unter anderem an Limitierungen, welche der Methodik von MALDI-MS Imaging inhärent sind (Stauber et al. 2010). Moleküle mit einer Größe von über 30 kDa sind nur schwer zu detektieren. Somit wird ein Großteil der Proteine von der Analyse ausgeschlossen. Für die Analyse kleinerer Moleküle wie Peptide und insbesondere Lipide ist MALDI-MSI jedoch besonders gut geeignet.
Weiterhin ist bei allen im Rahmen der Arbeit gemachten Studien zu beachten, dass es sich um eine sehr geringe Probenzahl handelt. Ein Grund dafür ist, dass die reine Messzeit mit ca. 12h pro 1 cm^2 Gewebe bereits sehr lang andauert. Schnellere Messungen sind bei einer geringeren räumlichen Auflösung möglich. Allerdings muss hinsichtlich der Fragestellung abgewogen werden welche räumliche Auflösung

zunächst geeignet und realisierbar ist. Für die feinstrukturierten Tumorgewebe war es notwendig, die höchstmögliche Auflösung zu nutzen. Um diese Daten in Zukunft an größeren Probenmengen zu validieren, kann nach der erfolgten Identifizierung der charakteristischen Proteine in den Plattenepithelkarzinomen die räumliche Auflösung auf 200 µm reduziert werden. Somit sind ein deutlich schnelleres Messen und ein höherer Probendurchsatz möglich.

6.1.3 Datenauswertung und –interpretation

Ein einziger MALDI-MSI-Datensatz besteht aus tausenden Spektren. Zuzüglich der hochaufgelösten Scans der histologischen Schnitte liegt das Speichervolumen pro Datensatz bei über 1 GB oder 100 GB bei FT-ICR-Datensätzen. Insbesondere bei der Erstellung und Auswertung des 3D-Datensatzes musste ein Kompromiss gefunden werden, um die produzierte Datenmenge möglichst gering zu halten und somit ein praktikables Werkzeug vorliegen zu haben. Daher wurden die Bilder der histologischen Färbungen nicht in der höchsten Auflösung verwendet, jedoch so gewählt, dass sie zu der 50 µm-Auflösung der MALDI-MSI-Messungen passen.
Darüber hinaus ist die Daten- und Bildauswertung solcher komplexen Datensätze nicht trivial und bedarf einer effizienten und geeigneten Analyse. Um diese Entwicklung voranzutreiben, wurde im Rahmen eines EU-Projektes (COMPUTIS, www.computis.org) ein einheitliches und frei verfügbares Datenformat namens imzML entwickelt (Schramm et al. 2012). Um eine erfolgreiche Weiterentwicklung und um einen Austausch zu gewährleisten, wurden die Rohdaten des 3D-Datensatzes in diesem Format zur freien Verfügung veröffentlicht (Oetjen et al. 2015). Damit sollen Impulse für neue und innovative bioinformatische Entwicklungen gesetzt werden.
Für die Visualisierung und Untersuchung der heterogenen Gewebsstruktur der Proben wurden die Segmentierung und die pLSA genutzt. Dabei konnten gute Übereinstimmungen der spektralen Daten mit den pathohistologischen Annotationen festgestellt werden. Jedoch gab es Areale, welche keine Übereinstimmung zeigten (Kapitel 5.2/ Krasny et al.). Die mittels MALDI-MSI detektierten molekularen Veränderungen sind auch dann nachweisbar, wenn die Regionen noch keine morphologisch sichtbaren Veränderungen zeigen. Dieser eigentliche Vorteil erschwert jedoch die Datenauswertung. Die manuellen pathologischen Annotationen

beruhen auf den sichtbaren Veränderungen der Gewebe- und Zellstruktur. Ob es sich um tatsächliche Abweichungen oder um Artefakte handelt, lässt sich nur schwer feststellen.

Großes Potential liegt in der Multimodalität. Hierbei kann MALDI-MS Imaging mit weiteren analytischen Methoden ergänzend kombiniert werden. Daher wurde in einem weiteren Projekt ein neuer Workflow entwickelt, bei dem Raman-Spektroskopie-Imaging mit MALDI-MS Imaging verknüpft wurden (Bocklitz et al. 2015). Raman-Spektroskopie ist nicht destruktiv, so dass es vor MALDI-MS Imaging für eine objektive Annotation verschiedener Gewebetypen genutzt werden kann. Anschließend können deren detaillierten molekularen Eigenschaften mit MALDI-MS Imaging analysiert werden.

6.2 Identifizierung von *m/z*-Werten

Ein weiterer Aspekt, der in Zusammenhang mit der Biomarkersuche diskutiert werden muss, ist die Identifizierung von *m/z*-Werten. Aufgrund der komplexen Gewebsstruktur und der damit verbundenen Vielzahl an Molekülen, welche detektiert werden, ist dies eine große Herausforderung. In diesem Zusammenhang spielt die Massengenauigkeit und Massenauflösung eine entscheidende Rolle. Für die Analyse von kleinen Molekülen steht eine Vielzahl an Massenspektrometern zur Verfügung, welche verschiedene Vor- und Nachteile haben. Für die Lipidanalyse in der vorliegenden Arbeit wurde MALDI-FT-ICR MSI genutzt (Kapitel 5.2/Krasny et al.). Dieses Konzept wurde erstmalig in der Arbeitsgruppe von Ron Heeren vorgestellt (Taban et al. 2007). Die in dem Tumorbereich auffälligen *m/z*-Werte wurden mit der LIPID MAPS Datenbank verglichen (www.lipidmaps.org). Aufgrund der hohen Massenauflösung konnten die Lipidgruppen identifiziert werden. Allerdings bedarf es für die konkrete Aussage, um welche Lipide es sich handelt weiterer Methoden wie LC-ESI-MS/MS der Lipidextrakte.

Für die Proteinidentifizierung wurden zum einen ein tryptischer Verdau direkt auf dem Gewebeschnitt und zum anderen die Korrelation mit LC-MS/MS-Daten durchgeführt, welche von lysierten Schnitten der gleichen Proben generiert wurden (Kapitel 5.3/Hoffmann et al.). Der Ionenspiegel des Massenspektrometers steigert zwar die Auflösung, allerdings reicht sie nicht für eine Identifizierung. Ein weiteres Problem liegt darin, dass die detektierten charakteristischen Massen in nicht ausreichender

Konzentration im Gewebe vorlagen, so dass auch der Einsatz von MS/MS-Analysen direkt von den Gewebeschnitten nicht möglich war. Zukünftig müssen weitere technische Entwicklungen Abhilfe schaffen, um eine Identifizierung leichter zu ermöglichen.

Die oben genannten Probleme machen eine Validierung der identifizierten Lipide und Proteine mittels anderer Methoden notwendig. Für die Proteinmarker wurden daher immunhistochemische Färbungen mit den entsprechenden Antikörpern eingesetzt. Es konnten die massenspektrometrischen Daten bestätigt werden. Diese Form der Validierung steht jedoch nicht für Lipide zur Verfügung. Daher muss nach Methoden gesucht werden, welche dies gestatten. Vielversprechende Entwicklungen gibt es hier in dem Bereich der nichtlinearen Raman-Spektroskopie und der Sekundärionen-Massenspektrometrie (Daemen et al. 2016).

Alle in den Kapiteln 6.1 und 6.2 diskutierten Aspekte lassen sich kombiniert auf eine Fragestellung reduzieren: Wie können spektrale Daten in molekulares Wissen übersetzt werden? Es zeigt sich, dass die Bioinformatik dabei eine übergeordnete Rolle spielt, indem sie als Hilfsmittel in allen genannten Bereichen fungiert. Das große Potential dieser Technik zeigt sich in aktuellen Konzepten wie METASPACE (Palmer et al. 2016). In diesem Projekt werden Datenbanken hochauflösender MS-Imaging-Messungen angelegt, um effiziente Algorithmen zu entwickeln die aus den komplexen spektralen Daten molekulare Annotationen und biologische Interpretationen liefern sollen.

6.3 Tumorheterogenität

Tumore entstehen durch Akkumulation genetischer und epigenetischer Veränderungen. Bei Plattenepithelkarzinomen des Kopf-Hals-Bereiches kommt es im Vorfeld zu einer wachsenden Gruppierung von Zellen mit tumor-assoziierten genetischen Veränderungen in der Schleimhaut. Dies kann an mehreren Stellen geschehen, welche jedoch häufig histologisch unauffällig sind. Dieser Vorgang wird als Feldkanzerisierung bezeichnet. Nach Entfernung des Primärtumors können diese Areale unbemerkt im Gewebe verbleiben und werden daher als eine Ursache für die hohe Rezidivrate angesehen (Leemans et al. 2011).

Dieser Vorgang kann zu einer intratumoralen Heterogenität führen. Dies ist von großer Bedeutung, da diese Veränderungen zusammen mit der Existenz spezifischer

Zellpopulationen, die Stammzelleigenschaften aufweisen (Prince et al. 2007), dazu beitragen, dass es innerhalb des Tumors Zellen gibt, welche auf Radio- und Chemotherapie ansprechen, während andere Bereiche resistent sind.

Diese genetischen Veränderungen konnten bereits vielfach gezeigt werden (Leemans et al. 2018). Projekte wie *The Cancer Genome Atlas* (TCGA) und *International Cancer Genome Consortium* (ICGC) konnten zahlreiche neue Erkenntnisse zur Tumor-Genomik liefern und die pathologische Forschung und Arbeit maßgeblich beeinflussen (Cooper et al. 2018). Jedoch ist der Einfluss der genetischen Veränderungen auf Proteinebene noch nicht ausreichend untersucht. Somit stellt diese Arbeit einen wichtigen Schritt in Richtung Aufklärung der Pathogenese von Kopf-Hals-Tumoren dar.

Die Untersuchung der geweblichen Heterogenität auf histologischer Ebene war ein Schwerpunkt dieser Arbeit. In allen Publikationen konnte gezeigt werden, dass mittels MALDI-MS Imaging die molekulare Heterogenität der Gewebeproben visualisiert werden kann. Die verschiedenen Datenanalysen - Segmentierung und pLSA - reflektieren die heterogene Zusammensetzung sowohl auf Protein- als auch auf Lipidebene. Dies konnte bereits für zahlreiche andere Tumore gezeigt werden (Rodrigo et al. 2014, Balluff et al. 2015). Dies gelang ebenso bei Kopf-Hals-Tumoren, jedoch nicht unter Verwendung von FFPE-Gewebe (Widlak et al. 2016).

Die Unterscheidung von feinen histologischen Strukturen wie der Stromabereiche des Tumors war nicht möglich. Da es sich teilweise um wenige Zellen oder nur einer Zellreihe handelt, konnten diese mit einer räumlichen Auflösung von 50 µm nicht voneinander getrennt werden. Für die Analyse von kleinen Molekülen sind in den letzten Jahren Methoden und Instrumente entwickelt worden, die eine räumliche Auflösung von 5 bis 10 µm gewährleisten (Rompp und Spengler 2013). Für die Detektion enzymatisch verdauter Proteine liegt der Standard jedoch noch immer bei 50 µm. An einer Verbesserung auf diesem Feld wird ebenfalls innerhalb des bereits erwähnten AIF-Projektes (Kapitel 4) gearbeitet.

Die identifizierten Proteine sind vorwiegend Strukturproteine (Kapitel 5.3/Hoffmann et al.). Diese sind in die epitheliale-mesenchymale Transition (EMT) involviert (Thiery 2002). Dieser Prozess wird mit Tumorinvasion und Metastasierung in Zusammenhang gebracht. Indem ihre Verteilung innerhalb des Tumorgewebes dargestellt werden kann, ist auch die Aufklärung der Prozesse an der Infiltrationszone möglich.

Neben der Bedeutung des Einsatzes der Proteomik für ein besseres Verständnis der Tumorbiologie stellen Proteine geeignete Biomarker dar. Für Plattenepithelkarzinome wurden bereits zahlreiche proteomische Marker vorgeschlagen (Malik et al. 2016). Diese Arbeit reiht sich somit in das aktuelle Forschungsfeld ein. Zukünftig müssen all diese potentiellen Marker validiert werden, indem diese in groß angelegten zentralen Probensammlungen studiert werden. Ebenso ist eine striktere Fokussierung der Biomarkersuche nötig, bei der konkrete klinische Fragestellungen mit geeignetem und zuvor entsprechend ausgewähltem Probenmaterial bearbeitet werden. Dies macht den Einsatz von FFPE-Gewebe zwingend notwendig, da nur so ausreichend Material zur Verfügung stehen wird. Hier kann die Arbeit durch das Etablieren eines Protokolls für die Verwendung von FFPE-Gewebe für MALDI-MSI dazu beigetragen.

Lipide spielen eine entscheidende Rolle in zellulären Prozessen, welche in die Karzinogese involviert sind wie der Proliferation, dem Zelltod und dem Zellüberleben. Es konnte bereits mehrfach gezeigt werden, dass es tumorspezifische Lipidveränderungen gibt (Zhao et al. 2015). Dies führte dazu, dass in den letzten Jahren das Feld der Lipidomik in der Tumorforschung als vielversprechende Erweiterung neben der Genomik und Proteomik etabliert wird (Perrotti et al. 2016).

Innerhalb dieser Arbeit konnte gezeigt werden, dass Kopf-Hals-Tumore auch hinsichtlich ihrer Lipidzusammensetzung heterogen sind. Insbesondere die Klasse der Phosphatidylcholine konnte in der epithelialen Tumorkomponente nachgewiesen werden. Das diagnostische Potential dieser Lipide konnte bereits in Studien gezeigt werden, welche in Lungen- und Brustkarzinomen höhere Level nachwiesen als in gesunden Kontrollen (Perrotti et al. 2016). Dies unterstützt das Potential von MALDI-MSI für zukünftige diagnostische Anwendungen.

7. Schlussfolgerungen

Mit jeder Veröffentlichung im Rahmen der Promotion konnten neue Aspekte der molekularen Charakterisierung von Kopf-Hals-Tumoren gezeigt werden: (I) Zum einen die Untersuchung von Lipiden mittels MALDI-MS Imaging bei hoher Massenauflösung, (II) zum anderen eine komplexe 3D-Darstellung der molekularen Informationen in Kombination mit (immun-)histochemischen Informationen, sowie (III) die Anwendung von MALDI-MSI zum Auffinden neuer und bereits bekannter Biomarker.

Mittels MALDI-MS Imaging ist es möglich, bisher unbekannte Veränderungen in der Protein- und Lipidzusammensetzung von Kopf-Hals-Tumoren zu detektieren und somit die genetische Tumorheterogenität auf molekularer Ebene zu untersuchen. Zudem können bereits bekannte Marker in die Analysen einbezogen und visualisiert werden. Darüber hinaus können diese Daten mit bereits etablierten histologischen Methoden korreliert werden. Um die gefundenen Signaturen zu bestätigen, müssen diese zukünftig an einer großen Probenanzahl getestet werden.

Für ein besseres Verständnis der Biologie von Kopf-Hals-Tumoren kann MALDI-MSI eingesetzt werden. Im speziellen können die aktuellen Fragestellungen wie die der Tumorstammzellen, die Immuncheckpoint-Inhibitoren oder die Charakterisierung von Patientenuntergruppen bearbeitet werden.

Die Gesamtheit der Arbeit unterstützt die Hypothese, dass MALDI-MS Imaging ein Werkzeug ist, welches sich für die Tumorforschung etabliert hat und darüber hinaus durch Weiterentwicklung das Potential hat in die klinische Routine zu gelangen. Vielversprechend ist hierbei das Konzept, MALDI-MSI in ein Sortiment aus sich ergänzenden Techniken einzubinden. Die Verbesserung der Standardisierung der Methode und die Weiterentwicklung geeigneter bioinformatischer Hilfsmittel sind dabei zwingende Voraussetzungen.

Die in dieser Arbeit entwickelten Konzepte werden in einem neuen aktuellen SFB-TransRegio-Projekt (FungiNet - Pathogenic fungi and their host: Networks of interaction) für die Untersuchung von Wirts-Pathogen-Interaktionen bei Pilzinfektionen genutzt und optimiert.

Zusammenfassend zeigt sich, dass MALDI-MS Imaging ein vielversprechendes Werkzeug für die Tumorforschung ist. Eine weitere Optimierung der Methode, vor allem der Standardisierung im Bereich der Probenvorbereitung sowie der Daten- und

Bildauswertung ist notwendig, um MALDI-MS Imaging zukünftig für diagnostische Zwecke zur Verfügung zu stellen.

8. Literatur- und Quellenverzeichnis

Alberts D, Pottier C, Smargiasso N, Baiwir D, Mazzucchelli G, Delvenne P, Kriegsmann M, Kazdal D, Warth A, De Pauw E, Longuespée R. 2018. MALDI Imaging-Guided Microproteomic Analyses of Heterogeneous Breast Tumors—A Pilot Study. PROTEOMICS – Clinical Applications, 12 (1):1700062-n/a.

Alexandrov T, Becker M, Guntinas-Lichius O, Ernst G, von Eggeling F. 2013. MALDI-imaging segmentation is a powerful tool for spatial functional proteomic analysis of human larynx carcinoma. Journal of Cancer Research and Clinical Oncology, 139 (1):85-95.

Balluff B, Frese CK, Maier SK, Schone C, Kuster B, Schmitt M, Aubele M, Hofler H, Deelder AM, Heck A, Jr., Hogendoorn PC, Morreau J, Maarten Altelaar AF, Walch A, McDonnell LA. 2015. De novo discovery of phenotypic intratumour heterogeneity using imaging mass spectrometry. J Pathol, 235 (1):3-13.

Bauer JA, Chakravarthy AB, Rosenbluth JM, Mi D, Seeley EH, De Matos Granja-Ingram N, Olivares MG, Kelley MC, Mayer IA, Meszoely IM, Means-Powell JA, Johnson KN, Tsai CJ, Ayers GD, Sanders ME, Schneider RJ, Formenti SC, Caprioli RM, Pietenpol JA. 2010. Identification of Markers of Taxane Sensitivity Using Proteomic and Genomic Analyses of Breast Tumors from Patients Receiving Neoadjuvant Paclitaxel and Radiation. Clinical cancer research : an official journal of the American Association for Cancer Research, 16 (2):681-690.

Bocklitz T, Brautigam K, Urbanek A, Hoffmann F, von Eggeling F, Ernst G, Schmitt M, Schubert U, Guntinas-Lichius O, Popp J. 2015. Novel workflow for combining Raman spectroscopy and MALDI-MSI for tissue based studies. Anal Bioanal Chem, 407 (26):7865-7873.

Bonner JA, Harari PM, Giralt J, Azarnia N, Shin DM, Cohen RB, Jones CU, Sur R, Raben D, Jassem J, Ove R, Kies MS, Baselga J, Youssoufian H, Amellal N, Rowinsky EK, Ang KK. 2006. Radiotherapy plus Cetuximab for Squamous-Cell Carcinoma of the Head and Neck. New England Journal of Medicine, 354 (6):567-578.

Braakhuis BJM, Leemans CR, Visser O. 2014. Incidence and survival trends of head and neck squamous cell carcinoma in the Netherlands between 1989 and 2011. Oral Oncology, 50 (7):670-675.

Caprioli RM, Farmer TB, Gile J. 1997. Molecular Imaging of Biological Samples: Localization of Peptides and Proteins Using MALDI-TOF MS. Analytical Chemistry, 69 (23):4751-4760.

Cooper LA, Demicco EG, Saltz JH, Powell RT, Rao A, Lazar AJ. 2018. PanCancer insights from The Cancer Genome Atlas: the pathologist's perspective. J Pathol, 244 (5):512-524.

Daemen S, van Zandvoort MAMJ, Parekh SH, Hesselink MKC. 2016. Microscopy tools for the investigation of intracellular lipid storage and dynamics. Molecular Metabolism, 5 (3):153-163.

Erich K, Sammour DA, Marx A, Hopf C. 2017. Scores for standardization of on-tissue digestion of formalin-fixed paraffin-embedded tissue in MALDI-MS imaging. Biochimica et Biophysica Acta (BBA) - Proteins and Proteomics, 1865 (7):907-915.

Ernst G, Guntinas–Lichius O, Hauberg–Lotte L, Trede D, Becker M, Alexandrov T, von Eggeling F. 2015. Histomolecular interpretation of pleomorphic adenomas of the salivary gland by matrix-assisted laser desorption ionization imaging and spatial segmentation. Head & Neck, 37 (7):1014-1021.

Ferlay J, Soerjomataram I, Dikshit R, Eser S, Mathers C, Rebelo M, Parkin DM, Forman D, Bray F. 2015. Cancer incidence and mortality worldwide: Sources, methods and major patterns in GLOBOCAN 2012. International Journal of Cancer, 136 (5):E359-E386.

Friedrich DT, Scheithauer MO, Greve J, Hoffmann TK, Schuler PJ. 2017. Recent advances in robot-assisted head and neck surgery. The International Journal of Medical Robotics and Computer Assisted Surgery, 13 (2):e1744.

Glish GL, Vachet RW. 2003. The basics of mass spectrometry in the twenty-first century. Nature Reviews Drug Discovery, 2:140.

Gorzolka K, Walch A. 2014. MALDI mass spectrometry imaging of formalin-fixed paraffin-embedded tissues in clinical research. Histol Histopathol, 29 (11):1365-1376.

Grégoire V, Lefebvre JL, Licitra L, Felip E, On behalf of the EEEGWG. 2010. Squamous cell carcinoma of the head and neck: EHNS–ESMO–ESTRO Clinical Practice Guidelines for diagnosis, treatment and follow-up. Annals of Oncology, 21 (suppl_5):v184-v186.

Kriegsmann J, Kriegsmann M, Casadonte R. 2015. MALDI TOF imaging mass spectrometry in clinical pathology: a valuable tool for cancer diagnostics (review). Int J Oncol, 46 (3):893-906.

Leemans CR, Braakhuis BJ, Brakenhoff RH. 2011. The molecular biology of head and neck cancer. Nat Rev Cancer, 11 (1):9-22.

Leemans CR, Snijders PJF, Brakenhoff RH. 2018. The molecular landscape of head and neck cancer. Nat Rev Cancer, 18 (5):269-282.

Malik UU, Zarina S, Pennington SR. 2016. Oral squamous cell carcinoma: Key clinical questions, biomarker discovery, and the role of proteomics. Arch Oral Biol, 63:53-65.

Metz B, Kersten GF, Hoogerhout P, Brugghe HF, Timmermans HA, de Jong A, Meiring H, ten Hove J, Hennink WE, Crommelin DJ, Jiskoot W. 2004. Identification of formaldehyde-induced modifications in proteins: reactions with model peptides. J Biol Chem, 279 (8):6235-6243.

Moskovitz J, Moy J, Ferris RL. 2018. Immunotherapy for Head and Neck Squamous Cell Carcinoma. Current Oncology Reports, 20 (2):22.

Oetjen J, Veselkov K, Watrous J, McKenzie JS, Becker M, Hauberg-Lotte L, Kobarg JH, Strittmatter N, Mróz AK, Hoffmann F, Trede D, Palmer A, Schiffler S, Steinhorst K, Aichler M, Goldin R, Guntinas-Lichius O, von Eggeling F, Thiele H, Maedler K, Walch A, Maass P, Dorrestein PC, Takats Z, Alexandrov T. 2015. Benchmark datasets for 3D MALDI- and DESI-imaging mass spectrometry. GigaScience, 4:20.

Palmer A, Trede D, Alexandrov T. 2016. Where imaging mass spectrometry stands: here are the numbers. Metabolomics, 12 (6):107.

Perrotti F, Rosa C, Cicalini I, Sacchetta P, Del Boccio P, Genovesi D, Pieragostino D. 2016. Advances in Lipidomics for Cancer Biomarkers Discovery. International Journal of Molecular Sciences, 17 (12):1992.

Prince ME, Sivanandan R, Kaczorowski A, Wolf GT, Kaplan MJ, Dalerba P, Weissman IL, Clarke MF, Ailles LE. 2007. Identification of a subpopulation of cells with cancer stem cell properties in head and neck squamous cell carcinoma. Proc Natl Acad Sci U S A, 104 (3):973-978.

Rodrigo MA, Zitka O, Krizkova S, Moulick A, Adam V, Kizek R. 2014. MALDI-TOF MS as evolving cancer diagnostic tool: a review. J Pharm Biomed Anal, 95:245-255.

Rompp A, Spengler B. 2013. Mass spectrometry imaging with high resolution in mass and space. Histochem Cell Biol, 139 (6):759-783.

Schramm T, Hester A, Klinkert I, Both JP, Heeren RM, Brunelle A, Laprevote O, Desbenoit N, Robbe MF, Stoeckli M, Spengler B, Rompp A. 2012. imzML--a common data format for the flexible exchange and processing of mass spectrometry imaging data. J Proteomics, 75 (16):5106-5110.

Schwamborn K, Caprioli RM. 2010. MALDI Imaging Mass Spectrometry – Painting Molecular Pictures. Molecular Oncology, 4 (6):529-538.

Stauber J, Ayed ME, Wisztorski M, Salzet M, Fournier I. 2010. Specific MALDI-MSI: Tag-Mass. Methods Mol Biol, 656:339-361.

Taban IM, Altelaar AF, van der Burgt YE, McDonnell LA, Heeren RM, Fuchser J, Baykut G. 2007. Imaging of peptides in the rat brain using MALDI-FTICR mass spectrometry. J Am Soc Mass Spectrom, 18 (1):145-151.

Thiery JP. 2002. Epithelial-mesenchymal transitions in tumour progression. Nat Rev Cancer, 2 (6):442-454.

Trim PJ, Snel MF. 2016. Small molecule MALDI MS imaging: Current technologies and future challenges. Methods, 104:127-141.

Weijers M, Snow GB, Bezemer PD, Wal JEVD, Waal IVD. 2002. The clinical relevance of epithelial dysplasia in the surgical margins of tongue and floor of mouth squamous cell carcinoma: an analysis of 37 patients. Journal of Oral Pathology & Medicine, 31 (1):11-15.

Widlak P, Mrukwa G, Kalinowska M, Pietrowska M, Chekan M, Wierzgon J, Gawin M, Drazek G, Polanska J. 2016. Detection of molecular signatures of oral squamous cell carcinoma and normal epithelium – application of a novel methodology for unsupervised segmentation of imaging mass spectrometry data. Proteomics, 16 (11-12):1613-1621.

Zhao Y-Y, Miao H, Cheng X-L, Wei F. 2015. Lipidomics: Novel insight into the biochemical mechanism of lipid metabolism and dysregulation-associated disease. Chemico-Biological Interactions, 240:220-238.

9. Anhang

9.1 Danksagung

Ich möchte mich an dieser Stelle bei allen Menschen bedanken die mich während der Arbeit begleitet und unterstützt haben. Es war eine ungemein spannende und aufregende Zeit für mich.

Im besonderen Maße möchte ich mich bei meinem Doktorvater Prof. Ferdinand von Eggeling für die ausgezeichnete und fürsorgliche Betreuung bedanken. Mit seiner unermüdlichen Unterstützung konnte ich dieses spannende Projekt mit der perfekten Balance zwischen kreativer Freiheit und Führung bearbeiten.

Einen großen Dank möchte ich ebenfalls „unserem“ Pathologen Dr. Günther Ernst aussprechen. Nicht nur für die pathohistologischen Beurteilungen sondern auch dafür, dass er mit seiner stets diskussionsfreudigen Art und seinen klaren Standpunkten wesentlich zum Gelingen der Arbeit beigetragen hat.

Ich danke Herrn Prof. Orlando Guntinas-Lichius dafür, dass ich meine Arbeit an der Klinik für Hals-, Nasen- und Ohrenheilkunde anfertigen konnte.

Herrn Prof. Jürgen Popp danke ich für die Bereiterklärung die vorliegende Arbeit zu begutachten.

Bei Dr. Dennis Trede und Dr. Jan Hendrik Kobarg von der Firma Scils möchte ich mich dafür bedanken, dass sie mich bei der Datenauswertung unterstützten und für Anregungen immer ein offenes Ohr hatten.

Mein besonderer Dank gilt meinen Kolleginnen Daniela Pelzel und Annett Urbanek. Diese haben mich nicht nur bei den Laborarbeiten tatkräftig unterstützt, sondern ertrugen auch die Hochs und Tiefs des Labor- und Büroalltags mit mir und sind mittlerweile mehr als Kollegen für mich geworden.

Auch wenn er eigentlich unerwähnt bleiben wollte, danke ich meinem Mann Martin der immer für mich da war und mit seiner übermenschlichen Unterstützung mir auch in schwierigen Situationen Halt gegeben hat.

9.2 Ehrenwörtliche Erklärung

Hiermit erkläre ich, dass mir die Promotionsordnung der Medizinischen Fakultät der Friedrich-Schiller-Universität bekannt ist,

ich die Dissertation selbst angefertigt habe und alle von mir benutzten Hilfsmittel, persönlichen Mitteilungen und Quellen in meiner Arbeit angegeben sind,

mich folgende Personen bei der Auswahl und Auswertung des Materials sowie bei der Herstellung des Manuskripts unterstützt haben: Prof. Dr. Ferdinand von Eggeling, Dr. Günther Ernst,

die Hilfe eines Promotionsberaters nicht in Anspruch genommen wurde und dass Dritte weder unmittelbar noch mittelbar geldwerte Leistungen von mir für Arbeiten erhalten haben, die im Zusammenhang mit dem Inhalt der vorgelegten Dissertation stehen,

dass mein Anteil an der geteilten Erstautorenschaft sich klar von dem von Frau Judith Lotz abtrennt,

dass ich die Dissertation noch nicht als Prüfungsarbeit für eine staatliche oder andere wissenschaftliche Prüfung eingereicht habe und

dass ich die gleiche, eine in wesentlichen Teilen ähnliche oder eine andere Abhandlung nicht bei einer anderen Hochschule als Dissertation eingereicht habe.

Ort, Datum Unterschrift des Verfassers